AD-A045 324 RENSSELAER POLYTECHNIC INST TROY NY MICROWAVE ACOUST--ETC F/G 20/12
NONDESTRUCTIVE EVALUATION OF ELECTRICAL PROPERTIES OF SEMICONDU--ETC(U)
JUL 77 H GILBOA, P DAS N00014-75-C-0772
UNCLASSIFIED RPI-MA-ONR-15 NL

1 OF 3
AD
A045 324

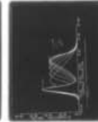

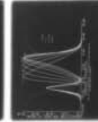

ADA045324

(12)

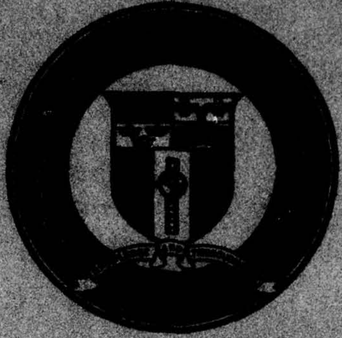

Rensselaer Polytechnic Institute
Troy, New York 12181

NONDESTRUCTIVE EVALUATION OF ELECTRICAL PROPERTIES OF SEMICONDUCTORS USING SAW

by

H. Gilboa and P. Das

DDC
RECEIVED
OCT 14 1977
C

Office of Naval Research
Contract N00014-75-C-0772
Project NR 009-017
Technical Report MA-ONR-15

July 2, 1977

DISTRIBUTION STATEMENT A
Approved for public release;
Distribution Unlimited

AD No. ____
DDC FILE COPY

Distribution of this document is unlimited. Reproduction in whole or in part is permitted for any purpose of the United States Government.

UNCLASSIFIED

SECURITY CLASSIFICATION OF THIS PAGE (When Data Entered)

REPORT DOCUMENTATION PAGE

READ INSTRUCTIONS BEFORE COMPLETING FORM

Field	Entry
1. Report Number	RPI MA-ONR-15
2. Govt Accession No.	
3. Recipient's Catalog Number	
4. Title (and Subtitle)	NONDESTRUCTIVE EVALUATION OF ELECTRICAL PROPERTIES OF SEMICONDUCTORS USING SAW.
5. Type of Report & Period Covered	Technical Report.
6. Performing Org. Report Number	
7. Author(s)	H. Gilboa and P. Das
8. Contract or Grant Number(s)	N00014-75-C-0772, NSF-ENG-074-22688
9. Performing Organization Name and Address	Electrical and Systems Engineering Department, Rensselaer Polytechnic Institute, Troy, NY 12181
10. Program Element, Project, Task Area & Work Unit Numbers	NR009-017
11. Controlling Office Name and Address	Office of Naval Research, Code 427, Washington, DC 20360
12. Report Date	July 1977
13. Number of Pages	187
14. Monitoring Agency Name & Address (if different from Controlling Office)	205p.
15. Security Class. (of this report)	
15a. Declassification/Downgrading Schedule	
16. Distribution Statement (of this Report)	Distribution of this document is unlimited.
17. Distribution Statement (of the abstract entered in Block 20, if different from Report)	
18. Supplementary Notes	
19. Key Words (Continue on reverse side if necessary and identify by block number)	surface waves, semiconductor surface, acousto-electric interaction, surface states, non-destructive testing

20. ABSTRACT (Continue on reverse side if necessary and identify by block number)

This work presents a study of the electrical properties of semiconductors using the interaction between surface acoustic waves and a semiconductor in the separated medium configuration (the SAW convolver). This study has been conducted towards developing a new technique for nondestructive evaluation of semiconductor surfaces using surface acoustic waves. The semiconductor is placed a small distance above the delay line, with a uniform airgap between the two media. Although there is no mechanical contact between the two media, the electric fields associated with the surface acoustic waves penetrate into the

DD FORM 1 JAN 73 1473 EDITION OF 1 NOV 65 IS OBSOLETE

S/N 0102-014-6601

UNCLASSIFIED

SECURITY CLASSIFICATION OF THIS PAGE (When Data Entered)

410 427

20. Abstract (continued from front)

semiconductor and interact with the free carriers. As a result of this non-linear interaction, the SAW is attenuated, there is a change in the SAW velocity, and dc acousto-electric voltages are developed across the semiconductor. In the case of two oppositely propagating surface waves, voltage proportional to the convolution of the two input voltages is also generated.

A theory for the SAW-semiconductor interaction in flat-band condition, taking into account both majority and minority carriers, surface recombination velocity, and the free carriers lifetime is presented. For the infinite semiconductor thickness approximation, simple analytical expressions are obtained for the propagation loss, dc acousto-electric voltages, and convolution voltages. For finite semiconductor thickness, numerical solution is used to obtain these quantities. For the off flat-band condition, the bulk conductivity is replaced by an effective surface conductivity. The effective surface conductivity is related to the semiconductor surface potential through the excess charge density, in the space charge region, and the surface mobility of the carriers.

The semiconductor on lithium niobate structure (the SAW convolver) is used to determine the distribution of surface states, and majority carriers capture cross section in the energy gap. This nondestructive testing is done by observing the transient response of the attenuated delay line output during and after a high voltage dc pulse is applied across the semiconductor-delay line structure.

Photoconductivity response time for various semiconductors is obtained by observing the transient response of the attenuated delay line output after a pulse of light is applied to the semiconductor.

The SAW convolver is used to determine the absor[illegible] edge and the location of surface states in the energy gap. The spectral response of the delay line attenuation and the dc transverse acousto-electric voltage are used to monitor changes in the semiconductor conductivity, and the charge trapped in the surface states due to optical excitation. Transverse acoustoelectric voltage inversion is observed in the spectral response of the dc acousto-electric voltage for high resistivity semiconductor, which improves the sensitivity of the technique.

CONTENTS

		Page
	PREFACE	v
	ABSTRACT	vi
	LIST OF FIGURES	viii
	LIST OF TABLES	xiii
	LIST OF SYMBOLS	xiv
I.	INTRODUCTION	1
II.	SURFACE ACOUSTIC WAVE-SEMICONDUCTOR INTERACTION IN THE SEPARATED MEDIUM STRUCTURE	8
	2.1 Basic SAW-Semiconductor Interaction Mechanism	8
	2.1.1 Propagation Loss	12
	2.1.2 The Acoustoelectric Voltages	16
	2.1.3 The Convolution Voltages	18
	2.2 SAW-Semiconductor Two-Carrier Interaction, Near Flat-band Condition	21
	2.2.1 Introcution	21
	2.2.2 The rf Electric Potential in the Semiconductor	23
	2.2.3 Semi-infinite Semiconductor Approximation	25
	2.2.4 Finite Semiconductor Thickness	35
	2.3 The Effective Surface Conductivity Approximation for the Off Flat-band Condition	47
	2.3.1 SAW-Semiconductor Interaction in the Off Flat-band Condition	47
	2.3.2 The Space Charge Region	52
	2.3.3 The Effective Surface Conductivity	55
	2.3.4 SAW-Semiconductor Interaction Dependence on the Semiconductor Surface Potential	59
	2.3.5 The Exact Solution for the Off Flat-band Condition	65

ACCESSION for
NTIS White Section
DDC Buff Section
UNANNOUNCED
JUSTIFICATION
BY
DISTRIBUTION/AVAILABILITY CODES
Dist. SPECIAL
A

Page

	Page
III. SEMICONDUCTOR SURFACE EVALUATION USING THE SAW CONVOLVER	69
3.1 Introduction	69
3.1.1 Experimental Procedure	69
3.1.2 The Propagation Loss, Transverse Acousto-electric Voltage, and Convolution Voltage	73
3.2 Transient Response of the SAW Propagation Loss	78
3.2.1 Pulsed Field Effect on SAW Attenuation	78
3.2.2 Dynamics of Surface States-The Schockley Read Model	83
3.2.3 Free Carrier Density at the Semiconductor Surface	90
3.2.4 Energy and Capture Cross Section Distribution of Fast Surface States	91
3.2.5 Slow Surface States	104
3.3 Transverse Acoustoelectric Voltate Inversion	108
3.4 Photoconductivity Study using SAW Convolver	116
3.5 Semiconductor Surface Study using SAW Velocity Change	133
IV. SEMICONDUCTOR SURFACE SPECTROSCOPY USING THE SAW CONVOLVER	140
4.1 Absorption Process in Semiconductors	140
4.2 Transverse Acoustoelectric Voltage Inversion and Its Application to Semiconductor Surface Study: CdS	142
4.3 Determination of Absorption Edge, and Surface State Locations in GaAs using the SAW Convolver	159
4.4 Semiconductor Spectroscopy using the Transient Delay Line Attenuation	166
4.5 The Spectral Response of the Convolution Voltage	170
V. SUMMARY	176
VI. REFERENCES	181

Preface

This technical report was prepared by the Microwave Acoustics Laboratory, Electrical and Systems Engineering Department of Rensselaer Polytechnic Institute, Troy, New York. The partial supports for this work came from National Science Foundation grant no. Eng. 074-22688 (Dr. [illegible] H. Harris, project monitor) and Office of Naval Research contract no. N00014-75-0772 (Dr. D. K. Ferry, project monitor).

This report summarizes the work related to determination of electrical properties of Semiconductors using SAW. Part of this work has already been published (References 55, 61-70) and other parts will be published in the near future. The objective of this report is to present all the information in one place coherently.

Dr. M. E. Motamedi and Mr. R. T. Webster have contributed significantly as co-authors of many papers included in this report. Mr. H. Estrada-Vasquez, Mr. Collin Lanzl and other students in the laboratory have provided help in experimental set-up from time to time. Finally, a major part of this report forms the Ph.D. Thesis of Mr. H. Gilboa.

ABSTRACT

This work presents a study of the electrical properties of semiconductors using the interaction between surface acoustic waves and a semiconductor in the separated medium configuration (the SAW convolver). This study has been conducted towards developing a new technique for nondestructive evaluation of semiconductor surfaces using surface acoustic waves. The semiconductor is placed a small distance above the delay line, with a uniform airgap between the two media. Although there is no mechanical contact between the two media, the electric fields associated with the surface acoustic waves penetrate into the semiconductor and interact with the free carriers. As a result of this nonlinear interaction, the SAW is attenuated, there is a change in the SAW velocity, and dc acousto-electric voltages are developed across the semiconductor. In the case of two oppositely propagating surface waves, voltage proportional to the convolution of the two input voltages is also generated.

A theory for the SAW-semiconductor interaction in flat-band condition, taking into account both majority and minority carriers, surface recombination velocity, and the free carriers life-time is presented. For the infinite semiconductor thickness approximation, simple analytical expressions are obtained for the propagation loss, dc acoustoelectric voltages, and convolution voltages. For finite semiconductor thickness, numerical solution is used to obtain

these quantities. For the off flat-band condition, the bulk conductivity is replaced by an effective surface conductivity. The effective surface conductivity is related to the semiconductor surface potential through the excess charge density, in the space charge region, and the surface mobility of the carriers.

The semiconductor on lithium niobate structure (the SAW convolver) is used to determine the distribution of surface states, and majority carriers capture cross section in the energy gap. This nondestructive testing is done by observing the transient response of the attenuated delay line output during and after a high voltage dc pulse is applied across the semiconductor-delay line structure.

Photoconductivity response time for various semiconductors is obtained by observing the transient response of the attenuated delay line output after a pulse of light is applied to the semiconductor.

The SAW convolver is used to determine the absorption edge and the location of surface states in the energy gap. The spectral response of the delay line attenuation and the dc transverse acoustoelectric voltage are used to monitor changes in the semiconductor conductivity, and the charge trapped in the surface states due to optical excitation. Transverse acoustoelectric voltage inversion is observed in the spectral response of the dc acoustoelectric voltage for high resistivity semiconductor, which improves the sensitivity of the technique.

LIST OF FIGURES

		Page
Fig. 2.1	The SAW Convolver Structure	9
Fig. 2.2	Propagation Loss vs. Conductivity with Frequency as a Parameter	30
Fig. 2.3	Transverse Acoustoelectric Voltage vs. Conductivity with Frequency as a Parameter	31
Fig. 2.4	Longitudinal Acoustoelectric Voltage vs. Conductivity with Frequency as a Parameter	32
Fig. 2.5	Convolution Voltage vs. Conductivity with the Frequency as a Parameter	36
Fig. 2.6	Propagation Loss vs. Conductivity with the Frequency as a Parameter (Log scale)	40
Fig. [illegible]	Propagation Loss vs. Conductivity with the Frequency as a Parameter (Log scale)	41
Fig. 2.8	Transverse Acoustoelectric Voltage vs. Conductivity with Frequency as a Parameter (Log scale)	42
Fig. 2.9	Transverse Acoustoelectric Voltage vs. Conductivity with Frequency as a Parameter (Log scale)	43
Fig. 2.10	Longitudinal Acoustoelectric Voltage vs. Conductivity with Frequency as a Parameter (Log scale)	44
Fig. 2.11	Longitudinal Acoustoelectric Voltage vs. Conductivity with Frequency as a Parameter (Log scale)	45
Fig. 2.12	SAW Velocity Change vs. Semiconductor Conductivity	46
Fig. 2.13	Propagation Loss vs. Surface Recombination Velocity with Bulk Conductivity as a Parameter	48
Fig. 2.14	Transverse Acoustoelectric Voltage vs. Surface Recombination Velocity with Bulk Conductivity as a Parameter	49
Fig. 2.15	Energy Band Diagram	51

Page

Fig. 2.16 Propagation Loss vs. Semiconductor Surface Potential with Bulk Resistivity as a Parameter .. 60

Fig. 2.17 Transverse Acoustoelectric Voltage vs. Semiconductor Surface Potential with Bulk Resistivity as a Parameter 61

Fig. 2.18 Longitudinal Acoustoelectric Voltage vs. Semiconductor Surface Potential with Bulk Resistivity as a Parameter 62

Fig. 2.19 Convolution Voltage vs. Semiconductor Surface Potential with Bulk Resistivity as a Parameter .. 63

Fig. 2.20 SAW Velocity Change vs. Surface Potential 64

Fig. 3.1 Schematic of the Experimental Set-up 71

Fig. 3.2 (a) rf Input Pulse to the Delay Line 76
(b) Attenuated and Delayed Output 76
(c) Transverse Acoustoelectric Voltage 76
(d) rf Output Pulse from the Delay Line 76

Fig. 3.3 Auto-convolution of Two rf Pulses 77

Fig. 3.4 Attenuated rf Pulse while an External dc Pulse is Applied Across the Semiconductor Delay Line Structure 79

Fig. 3.5 Dynamics of Surface States in Accumulation 84

Fig. 3.6 Dynamics of Surface States in Depletion 85

Fig. 3.7 Steady State Propagation Loss vs. External dc Bias 92

Fig. 3.8 Propagation Loss Relaxation During Depletion Bias 95

Fig. 3.9 Propagation Loss Time Constant After the Negative dc Bias is Removed 98

Fig. 3.10 Capture Cross Section vs. the Change in Semiconductor Surface Potential 100

Fig. 3.11 Density of Surface States vs. the Change in Semiconductor Surface Potential 101

Page

Fig. 3.12 Transient Response of the SAW Propagation Loss for 10 ohm-cm n-type Si with High Density of Surface States 103

Fig. 3.13a Transient Response of the Delay Line Attenuation Dominated by Slow Surface States 105

Fig. 3.13b Time Constant of the Delay Line Attenuation vs. Light Intensity 107

Fig. 3.14 Transverse Acoustoelectric Voltage Inversion 109

Fig. 3.15 Peak Transverse Acoustoelectric Voltage at the Beginning of the rf Pulse and the Difference Between the Two Peaks vs. Light Intensity 111

Fig. 3.16 Peak Transverse Acoustoelectric Voltage vs. Input Voltage to the Interdigital Transducer 113

Fig. 3.17 Peak Transverse Acoustoelectric Voltage vs. Light Intensity for Silicon, 10 ohm-cm, n-type, and GaAs, 0.7 ohm-cm n-type 115

Fig. 3.18 Block Diagram for the Photoconductivity Study using the SAW Convolver 119

Fig. 3.19 Photodiode Response to the Pulse of Light 121

Fig. 3.20 Photoconductivity Decay as Observed by the Delay Line Output of Grade A CdS 122

Fig. 3.21 Photoconductivity Decay vs. Time for Si 10 ohm-cm n-type 123

Fig. 3.22 Logarithm of the Delay Line Attenuation vs. Time for Si 10 ohm-cm n-type 125

Fig. 3.23 Logarithm of the Delay Line Attenuation vs. Time for CdS Grade A 10^8 ohm-cm n-type 126

Fig. 3.24 Logarithm of the Delay Line Attenuation vs. Time for GaAs 0.7 ohm-cm n-type 127

Fig. 3.25 Photoconductivity Decay while an External dc Bias is Applied 132

Page

Fig. 3.26 Experimental Arrangement for Observing SAW Velocity Change 134

Fig. 3.27 Multiexposure Photograph Showing the Variation of Mixer Output as a Function of Frequency 136

Fig. 3.28 SAW Velocity Disturbed by an Externally Applied dc Bias 137

Fig. 4.1 Equivalent Circuit for the Transverse Acousto-electric Voltage 143

Fig. 4.2 Transverse Acoustoelectric Voltage 145

Fig. 4.3 Plot of Peak Transverse Acoustoelectric Voltage as a Function of the Input rf Voltage 147

Fig. 4.4 Transverse Acoustoelectric Voltage for Various Wavelengths of Light for Grade A CdS 148

Fig. 4.5 The Spectral Response of the Peak Transverse Acoustoelectric Voltage, Measured at the Beginning of the rf Pulse in Grade A CdS 149

Fig. 4.6 The Spectral Response of the Peak Transverse Acoustoelectric Voltage Measured at the Beginning of the rf Pulse in UHP CdS 151

Fig. 4.7 Photoconductivity and Transmission Spectrum for Grade A and UHP CdS 153

Fig. 4.8 Acoustoelectric Voltage for Various Wavelengths of Light for n-type GaAs 161

Fig. 4.9 Plot of Peak Acoustoelectric Voltage as a Function of the Wavelength of Light 162

Fig. 4.10 Plot of Delay Line Attenuation as a Function of Wavelength of the Light 164

Fig. 4.11 Attenuated Delay Line Output for n on n^+ GaAs, when an External dc Voltage is Applied Across the Semiconductor and $LiNbO_3$ such that the Semiconductor Surface is Depleted 168

Fig. 4.12 Plot of the Attenuation of Delay Line Output for n on n^+ GaAs, as a Function of the Wavelength of Light 169

Page

Fig. 4.13 Attenuated Delay Line Output for n on n^+ GaAs, when External dc Voltage is Applied Across the Semiconductor and $LiNbO_3$ such that the Semiconductor Surface is Accumulated 171

Fig. 4.14 Plot of the Time Constant Associated with the Return to Steady State in Delay Line Output for n on n^+ GaAs, as a Function of the Wavelength of Light 172

Fig. 4.15 Experimental Arrangement for Measuring the SAW Convolution, Transverse Acoustoelectric Voltage and Attenuation 174

Fig. 4.16 The Spectral Response of (a) the Convolution Voltage, and SAW Attenuation; (b) the Peak Transverse Acoustoelectric Voltage 175

LIST OF TABLES

Page

Table 3.1 Excess Trapped Carriers in Surface States, Filling Time Constant and Emission Time Constant for Various Changes in Surface Potential 99

Table 3.2 Photoconductivity Response Time for Various Materials 128

Table 4.1 Wavelength (in nm) in which Peak Transverse Acoustoelectric Voltage Transistion or Maxima is Observed in CdS 152

Table 4.2 Observed Surface States, Absorption Edge and Surface Absorption in CdS 159

LIST OF SYMBOLS

D	displacement field
H	magnetic field
E	electric field
E_1	rf electric field
$J(2\omega)$	nonlinear current density
S_Z	SAW power/width
E_{ae}	acoustoelectric field
V_{con}	convolution voltage/unit SAW power input
V_G	gate voltage
v_s	SAW velocity
d_p	piezoelectric substrate thickness
ν	SAW frequency
λ	SAW wavelength
g	optical generation
u_i	mechanical displacement
ω	angular frequency
k	SAW wave number
Z_A	surface impedance
Z_S	semiconductor surface impedance
α	attenuation constant
ϵ_s	semiconductor permittivity
ϵ_p	effective piezoelectric permittivity
ϵ_O	vacuum permittivity
q	electronic charge
k_B	Boltzman constant

σ conductivity

μ mobility (also with subscripts n (electron), p (hole))

D diffusion constant (only with subscripts n and p)

ω_C dielectric relaxation frequency (also with subscripts n and p)

ω_D diffusion frequency (also with subscripts n and p)

n_i intrinsic carrier density

n electron density

n_b bulk electron density

n_1 excess rf electron density

E_c conduction band

E_F Fermi level

E_t surface state level

ϕ_O dc potential

ϕ_B bulk potential

u_O reduced notation for the potential

u_B reduced notation for bulk potential

τ_O photoconductivity response time

τ_{O1} recombination time constant

τ_{O2} trapping time constant

p hole density

p_b bulk hole density

p_1 excess rf hole density

J current density (also with subscripts n and p)

ρ charge density

ρ_1	excess rf charge density
L	semiconductor length
d	semiconductor thickness
τ	carrier lifetime (also with subscripts n and p)
L_{Di}	intrinsic Debye length
L_D	extrinsic Debye length
n_t	density of trapped electron in surface states
N_t	total density of surface states
n_s	density of free electrons on the semiconductor surface
c_n	electron capture probability
e_n	electron emission probability
v_t	thermal velocity
σ_n	capture cross section
τ_e	surface states emission time constant
τ_f	surface states filling time constant
u_s	reduced notation for surface potential
U_s	surface bending potential
μ_{ns}	electron surface mobility
μ_{ps}	hole surface mobility
s	surface recombination velocity

CHAPTER I

INTRODUCTION

This work is concerned with the application of surface acoustic waves (SAW) to nondestructive evaluation of semiconductor surfaces. A separeted medium convolver is used in this study. In this device surface acoustic waves propagating on a piezoelectric substrate interact with carriers in a neighboring semiconductor. The piezoelectric and the semiconducting media have their surfaces mechanically isolated from one another due to the presence of an air gap. The acoustoelectric coupling is achieved through the electric fields which accompany the surface waves. These electric fields also exist outside the piezoelectric substrate and can penetrate into the semiconductor.

Coupling of the acoustic wave to mobile charge carriers was first reported by Nine[1] who observed that the attenuation of bulk acoustic waves in photoconductive CdS varied with illumination. Hutson, et al.,[2,3] demonstrated that ultrasonic wave amplification could be obtained when the mobile carrier drift velocity was greater than that of the sound. A detailed theory of bulk ultrasonic amplification is given by White.[4]

The introduction of the interdigital transducer,[5] gave way to an efficient method for the excitation of surface acoustic waves, and hence, the interaction phenomena between acoustic waves and free carriers was extended to surface waves.

In the SAW interaction with free carriers the semiconductor medium can be either separated from the piezoelectric substrate (separated medium) or directly deposited on it, thus forming a monolithic structure.[6-8] There is also a third family of devices which employ piezoelectric semiconductors such as GaAs[9,10] (combined medium).

The theory for efficient excitation of surface acoustic waves on a piezoelectric substrate was first developed by Campbell and Jones.[11] Ingebrigtsen[12,13] used these results to develop the theory for the propagation loss of SAW due to various electromagnetic boundary conditions, especially the interaction of SAW with carriers in a semiconducting film on the piezoelectric substrate. The amplification of SAW in the composite structure consisting of a semiconductor spaced a small distance away from the piezoelectric was first reported by Lakin and Shaw.[14] Several authors published theories on the interaction of SAW with free carriers in a semiconductor,[14-19] however, they only covered the flat band case of a highly extrinsic semiconductor with perfect surfaces. Lately[20,21] some work has been done to extend these theories to high resistivity materials, and off flat-band condition. The work by Takada et al., assumes near flat-band condition and infinite semiconductor thickness. The work by Gautier et al., assumes an extrinsic semiconductor such that the SAW losses can be ignored.

The interaction of SAW with free carriers in a semiconductor is particularly interesting for VHF signal processing and optical imaging. Linear interaction gives rise to surface acoustic wave amplifiers.[14] Based on the nonlinear interaction, parametric signal

processing using SAW has been developed over the last few years. Under the label of 'parametric' we include all the techniques by which, from two input signals, one can generate a third one at the sum or difference frequency. A parametric processor must, therefore, include a nonlinear mechanism responsible for the coupling between the waves. Of such, there are two major nonlinear mechanisms. The first is the acoustic nonlinearity of the acoustic medium itself through which the acoustic waves propagate. In the second mechanism, the electric field associated with the acoustic waves interacts with charge carriers in a semiconductor; and wave-wave coupling is achieved through the space charge nonlinearity. The piezoelectric nonlinearity is limited and the device efficiency is very low. On the other hand, the separated medium nonlinearity can be very strong, much more than the combined medium nonlinearity, but correspondingly the technology is harder to implement. Real-time signal processing systems and devices for convolution, correlation, Fourier transformation, inverse Fourier transformation, pulse compression, match filtering, time inversion and ambiguity function generation have been built and these functions demonstrated (see J. D. Maines, et al., and R. M. Hays, et al., Review Papers).[22,23]

Optical signal processing and imaging[24] using the nonlinear interaction of SAW and free carriers in the separated medium structure are based on the fact that the coupling between these two media depends on the electronic properties of the semiconductor surface; specifically the surface conductivity and the surface state charge

density. The surface conductivity and surface potential both determine the propagation loss and the interaction strength. Due to the photoconductivity of the semiconductor, these surface parameters vary locally according to the intensity of the light illuminating the semiconductor surface. Thus, the interaction of SAW and a semiconductor can be used as an optical image sensor, and if scanning mechanism is desired, one can use for example, a short SAW pulse. When this pulse moves along the semiconductor the acoustoelectric voltage or the convolution voltage, record the surface condition along the semiconductor.

Acoustic memory devices have recently become of more interest. In general, the physical phenomenon underlying the memory effect is charging of the surface or volume traps,[25,26] or charging of capacitors associated with diode arrays.[27] The parametric interaction of two acoustic waves of angular frequency ω and wave number k, gives rise to a dc electric field in the form of a spatially periodic array with wave number 2k. This dc term generates a dc electron current which produces a trapped charge grating. The return to equilibrium can be very slow in special cases. Both combined media and separated media semiconductor convolvers have been utilized to form these memory devices.

Determination of the electrical properties of semiconductors using the SAW was first reported by A. Bers et al.[28] They determined the surface mobility of electrons in the accumulation layer by measuring the dc acoustoelectric current for different external dc biases.

Bierbaum[29] determined the electron mobilities in thin metal films deposited directly on the surface of the delay line, by measuring the propagation loss. T. C. Lim et al,[30,31] observed the wavelength dependence of the photoenhancement convolution on piezoelectric ZnO corresponding to the exciton transitions. The same experiment on GaAs was reported by K. Hah et al.,[32] and on CdS by Zueda et al.[33] The application of surface acoustic waves to the study of semiconductor surface states in Ge using the separated medium longitudinal acoustoelectric effect was reported first by T. Shiosaki et al.[34] They observed the transient to steady state in the acoustoelectric voltage after applying an external high voltage dc pulse across the semiconductor delay line structure. The well known pulsed field effect surface conductance relaxation processes[35] can be observed using the acoustoelectric voltage as a sensor.

Nondestructive evaluation of semiconductor surfaces using the separated medium convolver, was first proposed by P. Das et al.,[61-71] In this work the propagation loss, the transverse acoustoelectric voltage, the convolution voltage, and the change in SAW velocity, (which we refer in this work as the SAW-semiconductor interaction parameters) are used to monitor changes in the semiconductor conductance, and charge trapped in the surface states, due to an external disturbance. The external disturbance can be either an external dc bias applied across the semiconductor delay line structure, or an optical excitation. The main advantage of this new technique is that it requires no contact to the semiconductor surface, and

hence, it it truely a nondestructive method for study of electrical properties of semiconductors.

Nondestructive evaluation of semiconductor surfaces is of great interest since one can perform evaluation of the semiconductor surface during different stages of the device processing, and later on, a device can be built on the same substrate. The SAW convolver may be used for nondestructive evaluation of semiconductor surfaces. To achieve that, a study of the SAW-semiconductor interaction has been conducted, and electrical properties of semiconductors have been determined in this work.

This work is concerned mainly with the study of semiconductor surface states using the SAW-semiconductor interaction. Surface states are localized states in the energy gap at the semiconductor surface, due to the termination of the lattice periodicity or due to surface contamination. While considered theoretically much earlier, surface states first became of practical significance when Bardeen[36] proposed that it was these states, and not the metal work-function, which determined the height of a Schottky barrier. A review of earlier work on surface states can be found in the book by Many et al.[35] The statistics of the recombination of holes and electrons occurring through a deep trap level as was developed by Shockley and Read[37] can be used also for surface states trapping by using sheet carrier density on the surface instead of volume carrier density in the bulk.

The most detailed data available on surface state characteristics has been obtained by the MOS conductance and capacitance

techniques, which yield the surface state density and capture cross section as functions of energy. The results of various studies[38-40] reveal that the surface state densities are relatively constant near the mid gap, and rise toward the band edges. Capture cross sections are constant near midgap and drop exponentially toward the band edges. Typical surface state densities range from 10^{10} to $10^{13}/cm^2$-eV, while capture cross sections range from 10^{-13} to 10^{-15} cm^2. Recently a new technique, deep level transient spectroscopy (DLTS) has been developed by Lang.[41] This is a high frequency capacitance transient thermal scanning method useful for observing a wide variety of traps in semiconductors. This technique is superior to all other capacitance techniques such as thermally stimulated capacitance,[42,43] admittance spectroscopy,[44] and photocapacitance.[45] The main advantages of the DLTS technique are (i) no need for analysis of optical cross sections; (ii) much greater sensitivity; (iii) greater range of observable trap depths; and (iv) much more convenient to use and interpret.

In Chapter II we develop a theory for the SAW-semiconductor interaction. The theory includes majority and minority carrier interaction, and also semiconductor parameters such as lifetime and surface recombination velocity. SAW-semiconductor interaction parameters for high resistivity materials are calculated for the finite semiconductor thickness and for the case of infinite thickness approximation. For semiconductor surfaces in accumulation, depletion and inversion condition, we introduce the effective surface conductivity

interaction approach. The interaction parameters for various semiconductor surface potentials are numerically calculated using a digital computer. In Chapter III experimental results are presented for surface states and capture cross section evaluation using the propagation loss as a sensor, while an external dc bias is used to vary the semiconductor surface potential. The response time of photoconductivity decay is observed by the transient response of the delay line attenuation while an externally dc bias is applied to the semiconductor. In this Chapter we also present the use of other SAW-semiconductor interaction parameters, such as the dc acoustoelectric voltage, and the change in SAW velocity to obtain electrical properties of a semiconductor. In Chapter IV a semiconductor spectroscopy using the SAW convolver as a sensor is presented. Valuable information such as the position of surface states in the energy gap, and the photon energy for total surface absorption can be obtained using this technique. The sensitivity of the technique is yet to be improved, but the basic information for using the SAW convolver for nondestructive evaluation of semiconductor is presented in this thesis.

CHAPTER II

SURFACE ACOUSTIC WAVE-SEMICONDUCTOR INTERACTION IN THE SEPARATED MEDIUM STRUCTURE

2.1 Basic SAW-Semiconductor Interaction Mechanism

In this Chapter we shall give the theory for the interaction of surface acoustic waves propagating on a piezoelectric substrate with the free carriers in a semiconductor placed above the delay line with a uniform air gap between them. The structure to which all the work reported here applies, is shown in Fig. 2.1. The SAW is excited by an interdigital transducer fabricated directly on the surface of the piezoelectric crystal. Although several types of surface waves may exist, we are only concerned with those called Rayleigh waves.[46,47] The SAW propagates in the vicinity of the piezoelectric crystal surface with a constant velocity slightly lower than the bulk shear wave velocity of the crystal. The mechanical motions are confined to the surface of the crystal decaying exponentially within the crystal away from the surface. The SAW is accompanied by propagating electric fields. Though these electric fields are also confined to the surface they exist both inside and outside the crystal. The decay constant of the electric fields outside the surface is of the order of the SAW wavelength.

When a semiconductor sample is placed near the SAW delay line, these electric fields peentrate into the semiconductor. It will be shown that inside the semiconductor the electric fields decay within a Debye length from the surface. For an n-type silicon with

carrier density of 10^{15}-10^{17} cm^{-3} the interaction between the rf fields and the free carriers, takes place 1.5-0.2 μm away from the semiconductor surface. The rf acoustic fields modulate the carrier density inside the semiconductor, hence, rf components of the carrier density appear near the semiconductor surface. for an extrinsic semiconductor the rf acoustic fields result in a depletion layer on the semiconductor surface, since the Debye length decreases in the half cycle that tends to accumulate majority carriers, whereas the E-fields penetrate further into the semiconductor in the half cycle that tends to deplete the surface.

As the surface waves propagate under the semiconductor, the longitudinal and the transverse components of their E-fields interact with the carriers causing a current density J, which depends on the semiconductor conductivity. There is power absorbed from the acoustic waves, which are, therefore, attenuated. This attenuation constant is directly related to the conductivity of the semiconductor. In addition, the larger the air gap, the smaller the acoustoelectric coupling to the semiconductor, and hence, the smaller the attenuation.

The interaction of the rf acoustic fields with the free carriers in the semiconductor (both time-varying and time-independent) results in ac and dc currents inside the semiconductor. As a result of these currents, transverse and longitudinal voltages appear across the semiconductor. In the case of two oppositely propagating surface waves at the same frequency, a spatially uniform potential is generated at the double frequency and, as a function of time, it

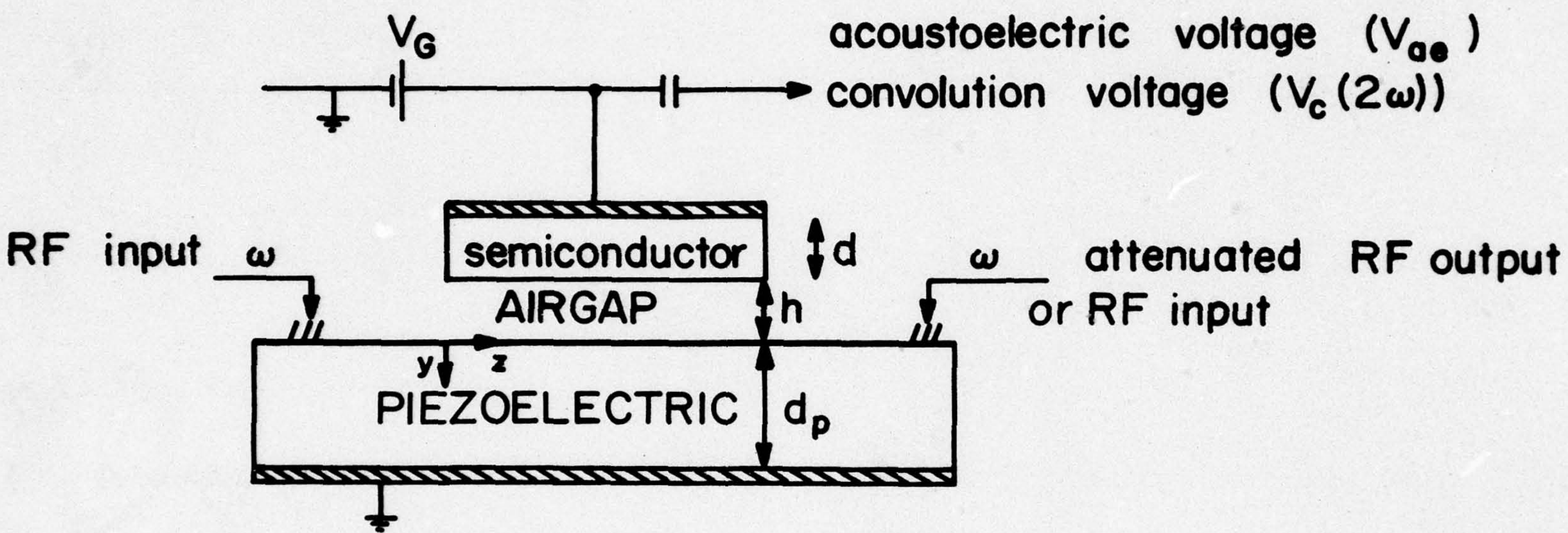

Fig. 2.1 The SAW Convolver Structure

represents the convolution of the modulation of the input signals. The nonlinear interaction which results in the dc voltages (the acoustoelectric voltages), and the ac voltages (the convolution voltages), is the basis for the parametric coupling and mixing of acoustic waves.

Several theories have been published[14-21] for the SAW-semiconductor interaction. They are very useful for the design of the convolver operating under normal conditions. Thus, they assume constant carrier density near flat band condition, a highly extrinsic semiconductor (hence, only majority carrier interaction is considered), and an ideal semiconductor surface (thus, neglecting surface recombination). Only the works by Takada et al.[20] and Gautier[21] considered non-uniform carrier density (off flat-band condition). It was shown that for highly extrinsic semiconductors, a varactor-like approach can be considered. The varactor-like approach is based on the assumption that for the high conductivity semiconductor and an acoustic wavelength long compared to the Debye length, the nonlinear interaction can be analyzed in terms of the transverse electric displacement field which accompanies the acoustic waves. A normal component of electric displacement at the semiconductor surface creates a potential which is proportional to the square of the electric field. This is the mechanism that takes place in a varactor; but whereas a varactor is generally voltage-driven, the semiconductor convolver is displacement current or E-field driven. However, for nondestructive evaluation of a semiconductor surface, the exact

solution has to be considered.

2.1.1 Propagation Loss

The general solution to surface acoustic waves propagating on a semi-infinite medium have been given by Campbell and Jones[11] in the form of a linear combination of these terms

$$u = U_i \exp(-\alpha_i ky) \exp[j(\omega t - kz)]$$
$$\phi = \phi_i \exp(-\alpha_i ky) \exp[j(\omega t - kz)] \quad (2.1\text{-}1)$$

where u is the mechanical displacement, ϕ is the electric potential, ω is the angular frequency, and k is the wave number. Particular values of U_i, ϕ_i and α_i are obtained by solving the wave equation for the acoustic waves, subject to the boundary conditions. In establishing these boundary conditions it is assumed that the surface is mechanically free although the adjoining medium is not necessarily a vacuum. Thus, a uniform air gap is assumed between the piezo-electric substrate and the adjoining medium.

The electrical boundary condition on the surface of the delay line may be represented by the TM wave impedance,

$$Z_A = \frac{E_z}{H_x} = -j \frac{k}{v_s} \frac{\phi_{y=0}}{D_{y_{y=0}}} \quad (2.1\text{-}2)$$

where D_y is the displacement field, ϕ is the electric potential, and v_s is the SAW velocity.

Since the electric boundary conditions require ϕ and D_y to be continuous across the substrate surface, the impedance will be continuous. An electrical boundary condition is, therefore, $Z_P = Z_A$, where Z_P is the TM wave impedance defined right on the surface of the piezoelectric substrate. Since Z_P is purely imaginary when v_s is real, we will obtain real solutions for only when Z_A is purely imaginary. This is the case when the adjoining medium is lossless. When Z_A has a non zero real part we find solutions for the complex value of v_s which corresponds to damped waves. Furthermore, the change in the SAW velocity due to the adjoining medium is obtained by the perturbation theory to be

$$\frac{v_s - v_O}{v_O} = \frac{\Delta v}{v_O} = \frac{K^2}{2} \frac{\epsilon_p v_s Z_A}{\epsilon_p v_s Z_A + j} \qquad (2.1\text{-}3)$$

K is the coupling coefficient for the piezoelectric substrate and is defined by $K^2/2 = \Delta v_\infty / v_O$. The quantity $\Delta v_\infty / v_O$ is the percentage difference in the velocity between a free surface* and a surface coated by an infinitesimally thin perfect conductor. This quantity has been shown[13] to be a direct estimate of the surface-wave coupling to interdigital transducers. ϵ_p is the piezoelectric permittivity, and v_O is the SAW velocity for a metallized piezoelectric surface.

---

*A free surface is defined by an infinite external impedance, Z_A on the piezoelectric surface. Whenever the piezoelectric material has a large dielectric constant, the vacuum boundary condition approximates the ideal free surface.

The change in SAW velocity can be written as $\Delta v/v_O = -\Delta k/k_O$, where $\Delta k = k - k_O = \Delta\beta + j\alpha(\alpha < 0)$. Substituting this into Equation (2.1-3) we obtain

$$\alpha = -\frac{K^2}{2} k \ \mathrm{Im}\left(\frac{\epsilon_p v_s Z_A}{\epsilon_p v_s Z_A + j}\right) \qquad (2.1\text{-}4)$$

This equation describes the SAW propagation loss due to any electrical load of an adjoining medium. The only parameter needed to be known for a given substrate is the surface impedance, Z_A. The surface impedance is given by

$$Z_A = \frac{Z_S + j/v_s\epsilon_O \tanh(kh)}{1 - j\, v_s\epsilon_O Z_S \tanh(kh)} \qquad (2.1\text{-}5)$$

where Z_S is the semiconductor surface impedance viewed through a lossy transmission line with a characteristic impedance $j/v_s\epsilon_O$.

The semiconductor surface impedance is related to the potential inside the semiconductor. A perturbation analysis of the SAW convolver has predicted the results of various experiments over a wide range of parameters. The traveling acoustic waves produce excess free carriers in the semiconductor. The first-order perturbation calculation gives the electrons and holes excess concentration (n_1 and p_1), and the rf acoustic potential inside the semiconductor. This is done through the weak coupling approximation, by assuming that the acoustic wave at a point is unperturbed by the interaction at that point. This approximation is valid because the coupling between the acoustic and electric fields is given by a small parameter K^2, which is of the order of 1%. The small signal equations

(subtracting the equilibrium terms from the exact equations and dropping second-order terms) are:

$$J_n = \sigma E_1 - D_n \nabla \rho_1 \tag{2.1-6}$$

$$\nabla J_n + \frac{\partial \rho_1}{\partial t} = 0 \tag{2.1-7}$$

$$\nabla^2 \phi = -q\rho_1/\epsilon_s \tag{2.1-8}$$

where ρ_1 is the excess charge density due to the rf acoustic fields. For an extrinsic n-type semiconductor $\rho_1 = -qn_1$, where n_1 is the excess electron density due to the rf acoustic field. Assuming that the rf acoustic potential has the form $\phi(y,z,t) = \phi_1(y)e^{j(\omega t - kz)}$, and an extrinsic n-type semiconductor, substituting Equations (2.1-6) and (2.1-8) into Equation (2.1-7) results in a fourth order differential equation for the rf acoustic potential $\phi_1(y)$.

$$\phi_1'''' - k^2(1 + \gamma^2)\phi_1'' + k^4 \gamma^2 \phi_1 = 0 \tag{2.1-9}$$

where $\gamma^2 = 1 + \omega_c\omega_D/\omega^2 + j\,\omega_D/\omega$

$\omega_c = \sigma/\epsilon_s$ dielectric relaxation frequency

$\omega_D = v_s{}^2/D_n$ diffusion frequency.

The general solution to Equation (2.1-9) is

$$\phi_1(y) = \sum_{i=1}^{4} A_i e^{\alpha_i ky} \tag{2.1-10}$$

where $\alpha_i = 1, -1, \gamma, -\gamma.$

The amplitude coefficients in (2.1-10) are quite complicated and can be obtained from the boundary conditions. However, they can be very much simplified if the semiconductor thickness is much larger than the SAW wavelength (for 100 MHz the SAW wavelength is 34 μm). In this case, only the positive exponential (y is the negative) will contribute to the solution (2.1-10). Equations (2.1-4) and (2.1-5) describe the propagation loss of the SAW due to an electrical load separated a distance h from the piezoelectric crystal. For an extrinsic semiconductor $\gamma \gg 1$, hence the rf electric field decays inside the semiconductor exponentially with a decay constant of the order of $(\gamma k)^{-1}$ which is equal to the extrinsic Debye length.

2.1.2 The Acoustoelectric Voltages

The acoustoelectric voltage is the dc voltage developed inside the semiconductor due to the nonlinear interaction between the electric fields accompanying the SAW and the free carriers inside the semiconductor. The free carriers concentrations are given by the sum of the equilibrium and the rf carrier densities, where the electric fields inside the semiconductor are given by the derivatives of the electric potential, Equation (2.1-10). Using Poisson's equation the excess charge density is

$$\rho_1(y) = -\epsilon_s \sum_{i=1}^{4} k^2(\alpha_i^2 - 1)A_i e^{\alpha_i ky} \qquad (2.1\text{-}11)$$

The transverse and longitudinal electric fields are

$$E_y(y) = -\frac{\partial\phi}{\partial y} = -\sum_{j=1}^{4} \alpha_j k A_j e^{\alpha_j ky} \quad (2.1\text{-}12)$$

$$E_z(y) = -\frac{\partial\phi}{\partial z} = jk \sum_{j=1}^{4} A_j e^{\alpha_j ky} \quad (2.1\text{-}13)$$

The transverse acoustoelectric field is by definition the average field resulting from the nonlinear current developed inside the semiconductor, thus the transverse and longitudinal acoustoelectric fields are

$$E_{aey} = \frac{1}{\sigma}\,\frac{1}{2}\,\mathrm{Re}(\sigma_1 E_y^{*}(y)) \quad (2.1\text{-}14)$$

$$E_{aez} = \frac{1}{\sigma}\,\frac{1}{2}\,\mathrm{Re}(\sigma_1 E_z^{*}(y)) \quad (2.1\text{-}15)$$

where $\sigma_1 = q\mu_n n_1 + q\mu_p p_1$. (2.1-16)

Substituting from (2.1-11)-(2.1-13) into Equations (2.1-14), (2.1-15), the acoustoelectric fields for extrinsic material is given by

$$E_{aey} = \pm \frac{\epsilon_s \mu k^3}{2\sigma} \mathrm{Re}\left[\sum_{i=1}^{4}\sum_{j=1}^{4} (\alpha_i^2 - 1)\,\alpha_j^{*} A_i A_j^{*}\, e^{(\alpha_i+\alpha_j^{*})ky'}\right] \quad (2.1\text{-}17)$$

$$E_{aez} = \mp \frac{\epsilon_s \mu k^3}{2\sigma} \mathrm{Re}\left[\sum_{i=1}^{4}\sum_{j=1}^{4} j(\alpha_i^2 - 1)\, A_i A_j^{*}\, e^{(\alpha_i+\alpha_j^{*})ky'}\right] \quad (2.1\text{-}18)$$

where y' = y - h. The transverse field is positive for p-type and negative for an n-type material. The longitudinal is negative for p-type and positive for n-type material.

2.1.3 The Convolution Voltages

When the device is operated as a convolver, two waves are launched at frequencies ω_1 and ω_2 respectively and in opposite directions. If we take the center of the semiconductor as the origin $z = 0$, and neglect the propagation loss, these waves have fields that vary as

$$f_1(t - \frac{z}{v}) \exp\ [j\omega_1(t - \frac{z}{v})] \quad \text{and} \quad f_2(t + \frac{z}{v}) \exp\ [j\omega_2(t + \frac{z}{v})]$$

respectively, where we have neglected a small phase correction of $\exp\ (jkl/2)$, in each term. v is the surface wave velocity and f_1 and f_2 are the modulations of the input signals. Each electric field will generate an excess carrier density with the same time and space variation. The nonlinear interaction produces the following three signals for a second order nonlinearity:

i. $$K_c f_1^2(t - \frac{z}{v}) \exp\ [2j\omega_1(t - \frac{z}{v})]$$

ii. $$K_c f_2^2(t + \frac{z}{v}) \exp\ [2j\omega_2(t + \frac{z}{v})]$$

iii. $$K_c f_1(t - \frac{z}{v})\ f_2(t + \frac{z}{v}) \exp\ \{j\ [(\omega_1 + \omega_2)t - (\omega_1 - \omega_2)\frac{z}{v}]\}$$

where K_c is a constant representing the strength of the nonlinearity. The first two terms represent second harmonic generation. The third term contains the product of the two envelope functions, and is the term of interest. In the degenerate case, the two input signals are at the same frequency $\omega = \omega_1 = \omega_2$; thus, all three signals are at a frequency 2ω; however, the first two have phase variation with respect

to space whereas the last one is space independent. If we integrate all three terms with respect to z, the first two do not increase at all, while the third increases monotonically with the length of integration, L.

For large values of L, say $L > 10\lambda$ where λ is the SAW wavelength, the third term is the only important one. In this case, the open circuit output signal detected between a metal plane electrode on the top surface of the semiconductor and the lower surface of the delay line, takes the form

$$V_{op} = K_c \exp(j2\omega t) \int_{-L/2}^{+L/2} f_1(t - \frac{z}{v})\, f_2(t + \frac{z}{v})dz$$

If the modulated signals exist for time shorter than the acoustic delay along the semiconductor, we can take the limit of integration to infinity; and with the change of variable $\tau = t - \frac{z}{v}$, the output signal takes on the final form

$$V_{op} = K_c v \exp(j2\omega t) \int_{-\infty}^{+\infty} f_1(\tau)\, f_2(2t - \tau)d\tau \qquad (2.1\text{-}19)$$

The output is seen to be the true convolution of the modulated signals, compressed by a factor of 2.

The electric potential accompanying the two signals propagating in opposite directions for the degenerate case are

$$\phi^+ = e^{j(\omega t - kz)} \sum_{i=1}^{4} A_i e^{\alpha_i k y'}$$
$$\phi^- = e^{j(\omega t + kz)} \sum_{j=1}^{4} B_j e^{\beta_j k y'} \qquad (2.1\text{-}20)$$

where $y' = y - h$.

When no external dc bias is applied to the semiconductor, $\alpha_i = \beta_j$, $A_i = A_j$, and only the normal component of the electric field (along y) will contribute to the convolved signal ($J_z(2\omega) = 0$).

The transverse electric fields are given by $E_y = -\frac{\partial\phi}{\partial y}$, hence,

$$E_y^+ = -e^{j(\omega t - kz)} \quad k \sum_{i=1}^{4} \alpha_i A_i e^{\alpha_i k y'}$$

$$E_y^- = -e^{j(\omega t + kz)} \quad k \sum_{j=1}^{4} \alpha_j A_j e^{\alpha_j k y'} \tag{2.1-21}$$

The corresponding excess charge density is given by Poisson's Equation

$$\rho_1 = -\epsilon_s \nabla^2\phi.$$

$$\rho_1^+ = -e^{j(\omega t - kz)} \quad \epsilon_s k^2 \sum_{i=1}^{4} (\alpha_i^2 - 1) A_i e^{\alpha_i k y'}$$

$$\rho_1^- = -e^{j(\omega t + kz)} \quad \epsilon_s k^2 \sum_{i=j}^{4} (\alpha_j^2 - 1) A_j e^{\alpha_j k y'} \tag{2.1-22}$$

The second order current density is given by

$$J_y(2\omega) = \sigma_1^+ E_y^- + \sigma_1^- E_y^+ \tag{2.1-23}$$

Substituting Equations (2.1-21) and (2.1-22) into (2.1-23), the second order current density for an extrinsic semiconductor is given by

$$J_y(2\omega) = \pm \frac{1}{2} \mu \epsilon_s k^3 \sum_{i=1}^{4} \sum_{j=1}^{4} A_i A_j (\alpha_i + \alpha_j)(\alpha_i \alpha_j - 1) e^{(\alpha_i + \alpha_j) k y'} \quad (2.1\text{-}24)$$

where the positive sign is for p-type and the negative for n-type material.

The relation between the open circuit convolution voltage and the current density Equation (2.1-24) will be developed in the next section for the general case of two carrier interactions.

2.2 SAW-Semiconductor Two Carrier Interaction Near Flat-band Condition

2.2.1 Introduction

Otto[19] has shown that in order to maximize the output power or a SAW convolver one must simultaneously minimize the transducer conversion loss, eliminate the output circuit parasitics, and achieve an optimal balance between the coupling and propagation loss. The optimal value of the convolution voltage is achieved for $\alpha L = 1$ or 8.7 dB, where α is the propagation loss and L is the semiconductor length. For most delay line substrates and semiconductors, these conditions require an extrinsic semiconductor. For Si 10 ohm-cm, the dielectric relaxation time is $\epsilon_s/\sigma = 1.04 \times 10^{-11}$ sec. Therefore, as long as the SAW frequency is such that the transient time duration is much shorter than 10^{-11} sec $(f < \sigma/\epsilon_s)$, the charge neutrality condition can be considered. More important

is the fact that for extrinsic semiconductors near the flat-band condition a small signal perturbation is assumed, thus, the thermal equilibrium condition specified by the flat-band distribution is used in order to solve for the various parameters of the SAW convolver.

Nondestructive evaluation of semiconductor surfaces using the SAW convolver structure requires the removal of several assumptions used in the previous theories.[12-21] We would like to use high-resistivity materials as well as low resistivity materials and in addition, to use an external dc bias to accumulate or deplete the semiconductor surfaces. Thus, majority and minority carrier interaction is considered. For materials such as GaAs with very low lifetime of the free carriers (nsec), and very high surface recombination velocity, the theory should include these semiconductor parameters. In order to keep the small signal analysis valid, very low SAW power input should be used for high resistivity materials.

The evaluation of electrical properties of bulk semiconductors using the SAW convolver is a study of an active region extending a few μm away from the surface. This region can be further reduced by accumulating the semiconductor surface such that the effective Debye length will be of the order of several hundred angstroms. For epitaxial layers it is important to use SAW frequencies such that the infinite semiconductor approximation is valid, hence $d > \lambda$ (d = epitaxial thickness, λ = SAW wavelength).

2.2.2 The rf Electric Potential in the Semiconductor

In this section we shall put all the quantities that vary with space and time in the form $f(y)e^{j\omega t - kz)}$. The current equations are (neglecting second order)

$$J_{pz} = q\mu_p \, p \, E_z + jk \, qD_p \, p_1$$
$$J_{py} = q\mu_p \, p \, E_y - q \, D_p \frac{\partial p_1}{\partial y} \qquad (2.2\text{-}1)$$

for holes and

$$J_{nz} = q\mu_n \, n \, E_z - jk \, qD_n \, n_1$$
$$J_{ny} = q\mu_n \, n \, E_y + qD_n \frac{\partial n_1}{\partial y} \qquad (2.2\text{-}2)$$

for electrons. Here p and n are the total time and space independent carrier densities of holes and electrons respectively, p_1 and n_1 are the excess carrier densities caused by the electric fields accompanying the surface waves.

The continuity equations are

$$j\omega q p_1 = jk \, J_{pz} - \frac{\partial J_{py}}{\partial y} + qg_p - \frac{qp + qp_1}{\tau p}$$
$$j\omega q n_1 = -jk \, J_{nz} + \frac{\partial J_{ny}}{\partial y} + qg_n - \frac{qn + qn_1}{\tau_n} \qquad (2.2\text{-}3)$$

and the Poisson's equation is

$$\nabla^2 \phi = -q(p_1 - n_1)/\epsilon_s \qquad (2.2\text{-}4)$$

The time and space independent carrier density is assumed to be in the steady state even if external generation (like light) exists, and they are given by $p = g_p\tau_p$; $n = g_n\tau_n$ as can be seen from Equation (2.2-3). Assuming that all the time and space varying functions decay inside the semiconductor in a form $e^{-\gamma ky}$, we obtain from (2.2-1)-(2.2-4) the following equation for the decay constant:

$$(\gamma^2 - 1)^2 \left[\frac{\omega_{Cp}}{D_p(\gamma^2 - k^2) - (1/\tau_n + j\omega)} + \frac{\omega_{Cn}}{D_n(\gamma^2 - k^2) - (1/\tau_p + j\omega)} - 1 \right] = 0 \qquad (2.2\text{-}5a)$$

where $\omega_{Cp} = \frac{q\mu_p p}{\epsilon_s}$, and $\omega_{Cn} = \frac{q\mu_n n}{\epsilon_s}$.

The roots to Equation (2.2-5) are

$$\gamma_1^2 = 1$$

$$\gamma_2^2 = 1 + \frac{\omega_{Cn}\omega_{Dn} + \omega_{Cp}\omega_{Dp}}{\omega^2} + \frac{\omega_{Cn}\omega_{Dn}^2(1/\tau_n + j\omega) + \omega_{Cp}\omega_{Dp}^2(1/\tau_p + j\omega)}{\omega^2(\omega_{Cn}\omega_{Dn} + \omega_{Cp}\omega_{Dp})} \qquad (2.2\text{-}5b)$$

$$\gamma_3^2 = 1 + \frac{\omega_{Cn}\omega_{Dn}\omega_{Dp}(1/\tau_n + j\omega) + \omega_{Cp}\omega_{Dp}\omega_{Dn}(1/\tau_p + j\omega)}{\omega^2(\omega_{Cn}\omega_{Dn} + \omega_{Cp}\omega_{Dp})}$$

where $\omega_{Dp} = v_s^2/D_p$ and $\omega_{Dn} = v_s^2/D_n$, v_s is the SAW velocity.

In most cases of interest the third root will be identical to the first one as the condition $\omega^2 >> \omega_{Dp}(\frac{1}{\tau_p} + j\omega)$, $\omega_{Dn}(\frac{1}{\tau_n} + j\omega)$ is always satisfied. For semiconductors with very short lifetimes (nsec), SAW frequency in the GHz range has to be used in order to keep this assumption valid. For highly extrinsic semiconductors (n-type), $\omega_{Cp} << \omega_{Cn}$, hence $\gamma_3^2 = \gamma_1^2$, and $\gamma_2^2 = \gamma$, where γ is the electric potential decay constant for one carrier interaction, Equation (2.1-9). In the next section we shall use the above solution for the potential decay inside the semiconductor to obtain the interaction parameters for the two cases a) the semiconductor thickness is larger compared to the SAW wavelength and b) the semiconductor thickness is of the same order as the SAW wavelength.

2.2.3 Semi-infinite Semiconductor Approximation

For a semiconductor, such that $d >> \lambda$, where d is the thickness of the semiconductor, and λ is the SAW wavelength, the potential decays inside the semiconductor mainly due to the two terms with a negative exponent. If, in addition, the carriers lifetime is much smaller than the SAW period (frequency^{-1}), and $\omega >> \omega_{Dp}$, ω_{Dn} or ω_{Cn}, $\omega_{Cp} >> \omega$, the third mode of decay is equal to the first one, and the second mode can be considered as a real quantity. Under these conditions the potential inside the semiconductor is

$$\phi = (A_1 e^{ky} + A_2 e^{\gamma ky}) e^{j(\omega t - kz)} \qquad (2.2\text{-}6)$$

where

$$\gamma = 1 + \frac{\omega_{Cn}\omega_{Dn} + \omega_{Cp}\omega_{Dp}}{\omega^2}$$

The boundary conditions

$$J_{py} = qsp_1$$

$$J_{ny} = -qsn_1$$

at $y = 0$ determine A_1/A_2, where s is the surface recombination velocity.

$$A_1/A_2 = R_1 + j\omega R_2 \qquad (2.2\text{-}7)$$

where

$$R_1 = \frac{\omega_{Cn}\omega_{Dn}^2/\tau_n + \omega_{Cp}\omega_{Dp}^2/\tau_p}{(\omega_{Cn}\omega_{Dn} + \omega_{Cp}\omega_{Dp})^2} \left[\gamma + \frac{s}{k}\,\frac{\omega_{Cn}\omega_{Dn}/D_n + \omega_{Cp}\omega_{Dp}/D_p}{\omega_{Cn}\omega_{Dn} + \omega_{Cp}\omega_{Dp}}\right] + \frac{s}{k}\,\frac{\omega_{Cn}\omega_{Dn}/D_n + \omega_{Cp}\omega_{Dp}/D_p}{\omega_{Cn}\omega_{Dn} + \omega_{Cp}\omega_{Dp}}$$

and

$$R_2 = \frac{\omega_{Cn}\omega_{Dn}^2 + \omega_{Cp}\omega_{Dp}^2}{(\omega_{Cn}\omega_{Dn} + \omega_{Cp}\omega_{Dp})^2} \left[\gamma + \frac{s}{k}\,\frac{\omega_{Cn}\omega_{Dn}/D_n + \omega_{Cp}\omega_{Dp}/D_p}{\omega_{Cn}\omega_{Dn} + \omega_{Cp}\omega_{Dp}}\right]$$

Using Equations (2.2-6)-(2.2-7) the semiconductor surface impedance is given by

$$Z_s = \frac{1}{v_s}\,\frac{E_z}{D_y} = \frac{j}{\epsilon_s v_s}\;\frac{1 + R_1 + j\omega R_2}{\gamma + R_1 + j\omega R_2} \qquad (2.2\text{-}8)$$

Substituting Equation (2.2-8) into Equations (2.1-4) and (2.1-5), results in the propagation loss of the SAW due to an infinite semiconductor. For zero spacing between the semiconductor and the delay line, α is obtained as

$$\alpha = -\frac{K^2}{2} k\epsilon_p/\epsilon_s \frac{\omega R_2(\gamma - 1)}{\omega^2 R_2^{\,2}(1 + \epsilon_p/\epsilon_s)^2 + [\gamma + R_1 + \epsilon_p/\epsilon_s(1 + R_1)]^2} \tag{2.2-9}$$

The power flux penetrating inside the semiconductor is

$$S_y = -1/2 \, \mathrm{Re}(E_z H_x^*) = \frac{k^2}{2} |\phi'_{y=0}|^2 \, \mathrm{Re}(\frac{1}{Z_A^*}) \tag{2.2-10}$$

where $\phi'_{y=0}$ is the perturbed potential on the surface of the substrate, and we have used the surface impedance $Z_A = E_z/H_x$ to substitute for $E_z H_x^*$. Assuming that the power loss of the SAW is mainly due to the acoustoelectric coupling to the semiconductor, we can write

$$S_y = -2\alpha S_z \tag{2.2-11}$$

where α is the propagation loss (α is a negative quantity according to our definition), and S_z is the power flux per unit length in the direction of propagation. From (2.2-10) and (2.2-11) the perturbed potential on the substrate surface is given by

$$\phi'_{y=0} = (\frac{4\alpha S_z}{k^2 \mathrm{Re}(1/Z_A^*)})^{1/2} \tag{2.2-12}$$

The perturbed potential $\phi'(y)$ satisfies Laplace's equation in the air gap, hence the potential and displacement fields in the air gap are given by

$$\phi'(y) = Ae^{ky} + Be^{-ky}$$

and (2.2-12)

$$D'(y) = -\epsilon_0 k(Ae^{ky} - Be^{-ky})$$

for the region $0 < y < -h$. The constants A and B are found from the boundary condition at the substrate surface, Equation (2.2-12) and the definition of the surface impedance, Equation (2.1-2).

$$\phi'(y) = \frac{\phi'_{y=0}}{2}\left(1 + \frac{j}{V_s \epsilon_0 Z_A}\right)e^{-ky} + \frac{\phi'_{y=0}}{2}\left(1 - \frac{j}{V_s \epsilon_0 Z_A}\right)e^{ky} \quad (2.2\text{-}13)$$

The excess rf carrier densities qn_1 and qp_1 are determined by solving Poisson's equation and the continuity equation. This results in

$$qn_1 = \epsilon_s \nabla^2 \phi \frac{\omega_{Cn}\omega_{Dn}}{\omega_{Cn}\omega_{Dn} + \omega_{Cp}\omega_{Dp}} \quad (2.2\text{-}14)$$

$$qp_1 = -\epsilon_s \nabla^2 \phi \frac{\omega_{Cp}\omega_{Dp}}{\omega_{Cn}\omega_{Dn} + \omega_{Cp}\omega_{Dp}}$$

The acoustoelectric fields in the semiconductor are given by Equations (2.2-14) and (2.2-15). Substituting from Equations (2.2-6)-(2.2-14) results in

$$E_{aey} = - \frac{\epsilon_s k^3}{2} \frac{\mu_n \omega_{Cn} \omega_{Dn} - \mu_p \omega_{Cp} \omega_{Dp}}{\omega^2} \frac{|\phi'_{y=-h}|^2}{(1 + R_1)^2 + \omega^2 R_2^2}$$

$$(R_1 e^{(\gamma + 1)ky} + \gamma R_2 e^{2\gamma ky}) \quad (2.2\text{-}15)$$

for the transverse field and

$$E_{aez} = \frac{\epsilon_s k^3}{2} \frac{\mu_n \omega_{Cn} \omega_{Dn} - \mu_p \omega_{Cp} \omega_{Dp}}{\omega} \frac{|\phi'_{y=-h}|^2}{(1 + R_1)^2 + \omega^2 R_2^2} R_2 e^{(\gamma + 1)ky}$$

for the longitudinal field.

Figures 2.2-2.4 are plots of the propagation loss, transverse acoustoelectric voltage, and the longitudinal acoustoelectric voltage, as a function of the semiconductor conductivity. The SAW frequency is used as the parameter and s = 0, h = 0 are used. The following values for constants are used.

$\epsilon_p = 50.2$; $\epsilon_s = 11.7$; $\mu_n = 1350\ cm^2/V\ sec$;

$\mu_p = 480\ cm^2/V\ sec$

$v_s = 3.488\ 10^5$ cm/sec $\qquad \frac{K^2}{2} = 2.4\ 10^{-2}$

$\tau_n = \tau_p = 10^{-6}$ sec $\qquad s = 0$ cm/sec

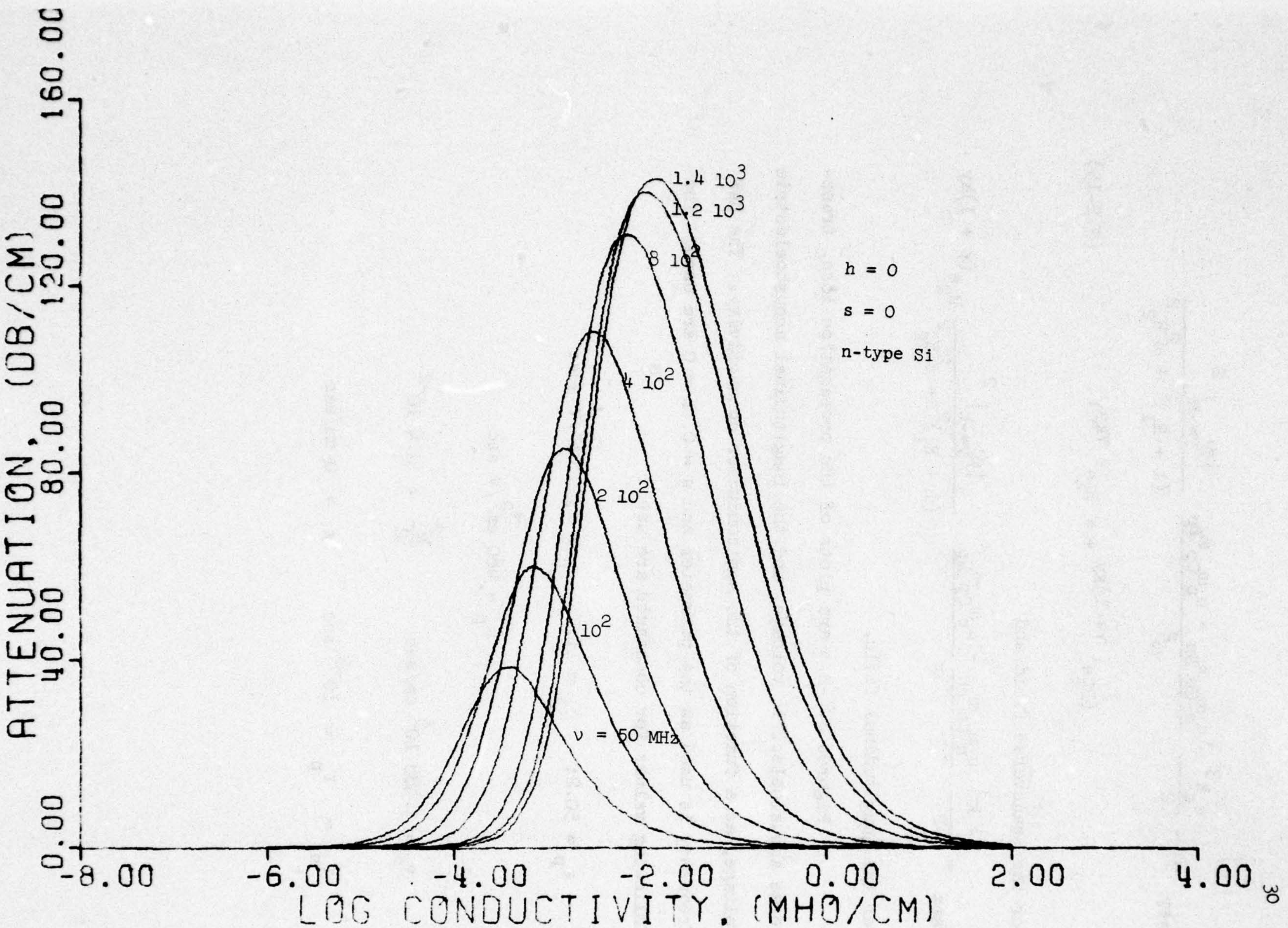

Fig. 2.2 Propagation Loss vs. Conductivity with Frequency as a Parameter

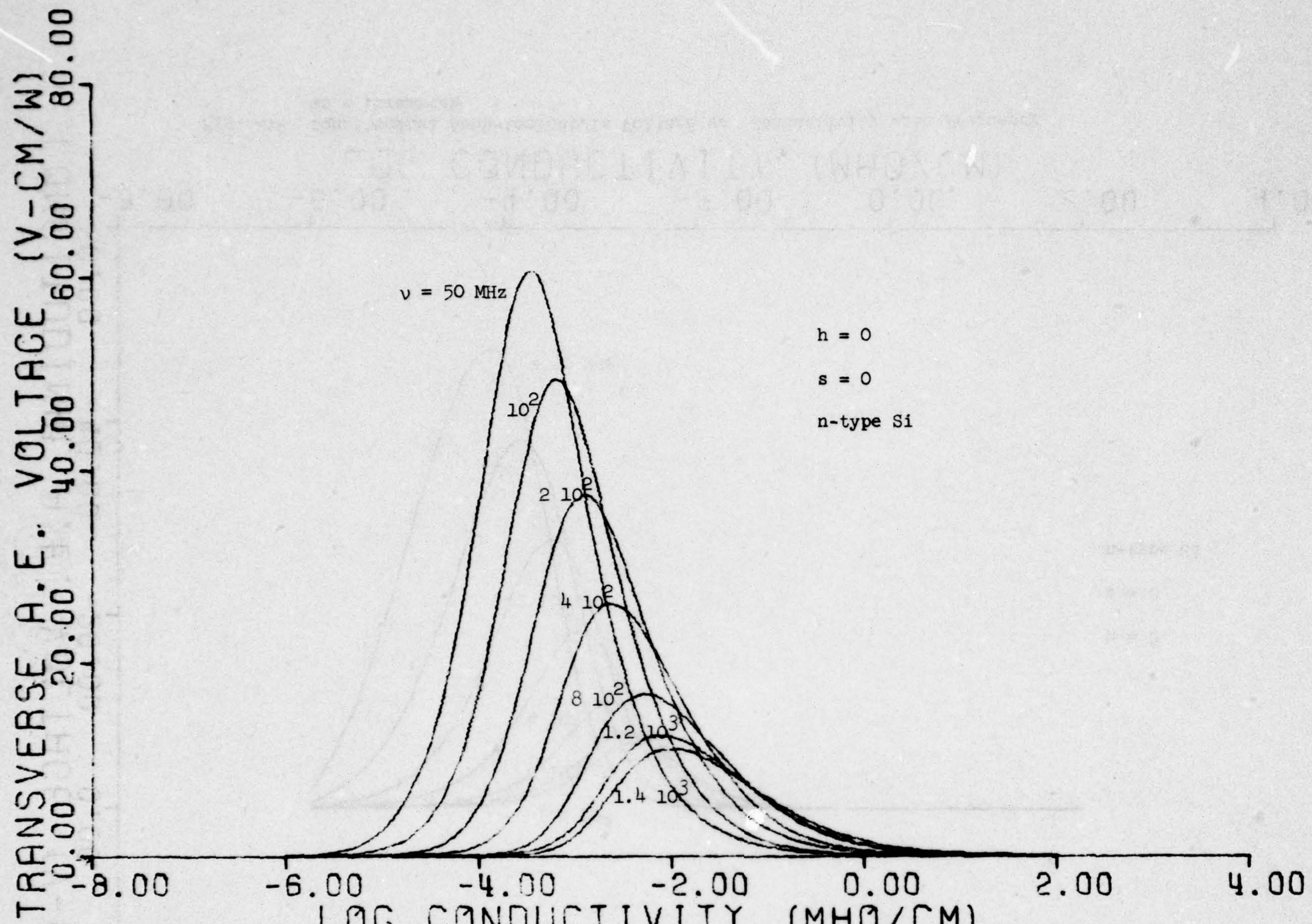

Fig. 2.3 Transverse Acoustoelectric Voltage vs. Conductivity with Frequency as a Parameter

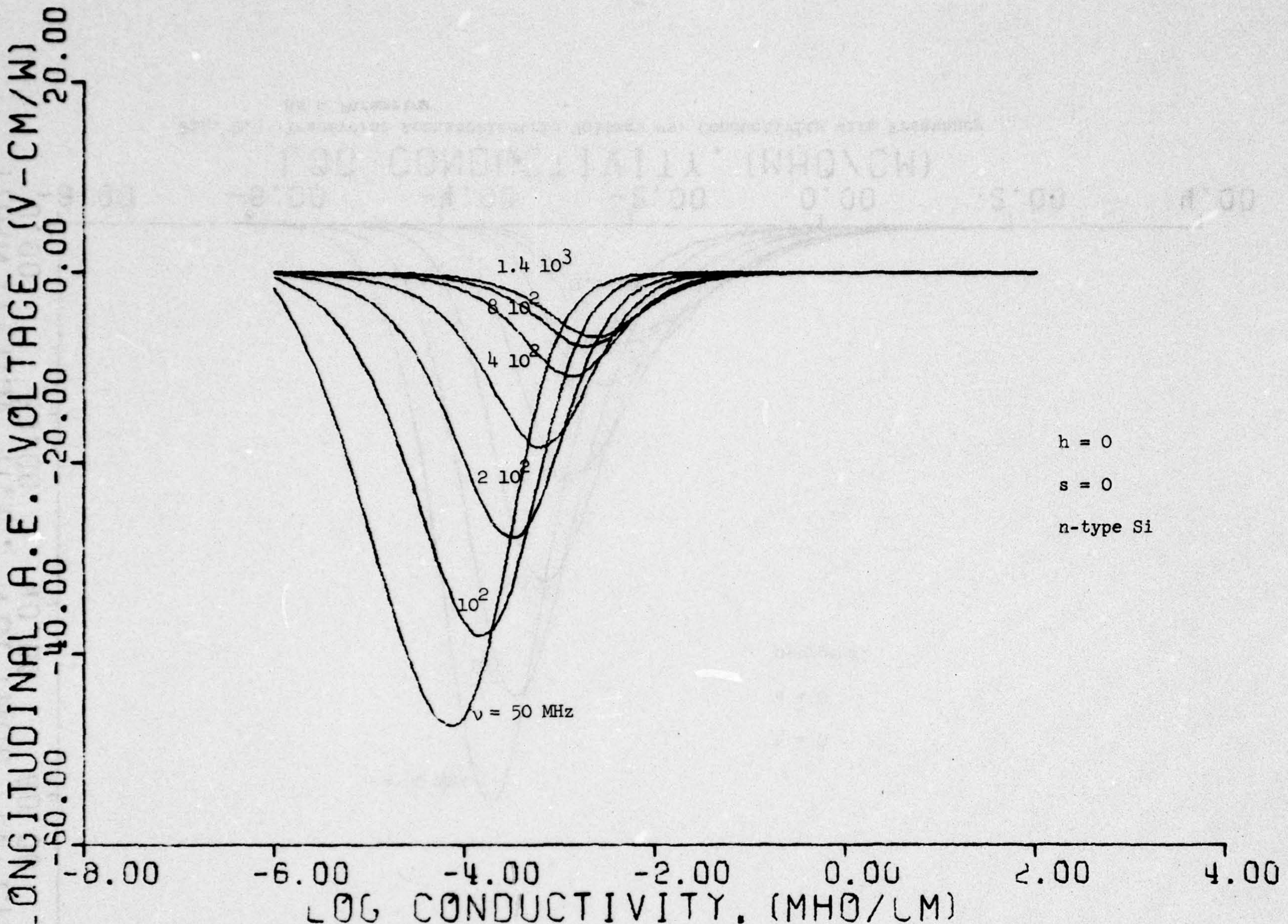

Fig. 2.4 Longitudinal Acoustoelectric Voltage vs. Conductivity with Frequency as a Parameter

The open circuit convolution voltage is related to the second order current density, equation (2.1-24). The total second-order current developed in the semiconductor is given by

$$J_{ny} = (\sigma_n + j\omega\epsilon_s)E_2(2\omega) + J_{ny}(2\omega) + qD_n \frac{\partial n_2}{\partial y}$$

$$J_{py} = (\sigma_p + j\omega\epsilon_s)E_2(2\omega) + J_{py}(2\omega) - qD_p \frac{\partial p_2}{\partial y} \qquad (2.2\text{-}15)$$

where $J_{ny}(2\omega)$, $J_{py}(2\omega)$ are given by Equation (2.1-24) and n_2, p_2 are the second order carrier density in the semiconductor. Dividing each equation by the diffusion constant and adding these two equations results in

$$J_y = [\frac{\sigma_n}{D_n} + \frac{\sigma_p}{D_p} + 2j\omega\epsilon_s (\frac{1}{D_n} + \frac{1}{D_p})] E_2 + \frac{J_{ny}(2\omega)}{D_n} + \frac{J_{np}(2\omega)}{D_p} + \frac{\partial}{\partial y}(qn_2 - qp_2) \qquad (2.2\text{-}16)$$

The second-order potential developed in the semiconductor is uniform along the direction of propagation. Hence, using Poisson's equation the second order charge density is given by

$$\rho = q(p_2 - n_2) = -\epsilon_s \nabla^2 \phi = \epsilon_s \frac{\partial^2 E_2}{\partial y^2} \qquad (2.2\text{-}17)$$

Substituting Equation (2.2-17) into (2.2-16) results in a differential equation for the second-order electric field. For an open circuit condition $J_y = 0$, hence,

$$\frac{\partial^2 E_2}{\partial y^2} - [\frac{\sigma_n}{\epsilon_s D_n} + \frac{\sigma_p}{\epsilon_s D_p} + 2j\omega(\frac{1}{D_n} + \frac{1}{D_p})] E_2 = \frac{J_{ny}(2\omega)}{\epsilon_s D_n} + \frac{J_{py}(2\omega)}{\epsilon_s D_p} \qquad (2.2\text{-}18)$$

The right-hand side of Equation (2.2-18) is given by substituting qn_1 and qp_1 from Equation (2.2-13) into Equation (2.1-23). This results in

$$\frac{J_{ny}(2\omega)J_{py}(2\omega)}{\epsilon D_n} + \frac{}{\epsilon_s D_p} = \frac{k^3}{2}\left(\frac{\mu_p A_p}{D_p} - \frac{\mu_n A_n}{D_n}\right) \sum_{i=1}^{4} \sum_{j=1}^{4} A_i A_j \,(\alpha_i + \alpha_j)(\alpha_i \alpha_j - 1)\, e^{(\alpha_i + \alpha_j)ky^1}$$

where

$$A_p = \frac{\omega_{Cp}\omega_{Dp}}{\omega_{Cn}\omega_{Dn} + \omega_{Cp}\omega_{Dp}}$$

$$A_n = \frac{\omega_{Cn}\omega_{Dn}}{\omega_{Cn}\omega_{Dn} + \omega_{Cp}\omega_{Dp}}$$

The general solution to Equation (2.2-18) is

$$E_2 = A_0 + A_1 e^{Ny} + A_2 e^{-Ny} + E_p \qquad (2.2\text{-}19)$$

where

$$N^2 = \frac{\sigma_n}{\epsilon_s D_n} + \frac{\sigma_p}{\epsilon_s D_p} + 2j\omega\left(\frac{1}{D_n} + \frac{1}{D_p}\right)$$

$$E_p = \sum_{i=1}^{4} \sum_{j=1}^{4} A_{ij}\, e^{(\alpha_i + \alpha_j)ky'}$$

$$A_{ij} = \frac{k^3}{2}\left(\frac{A_p \mu_p}{D_p} - \frac{A_n \mu_n}{D_n}\right) \frac{A_i A_j (\alpha_i + \alpha_j)(\alpha_i \alpha_j - 1)}{(\alpha_i + \alpha_j)^2 k^2 - N}$$

E_2 is zero as $y \to -\infty$, hence, $A_2 = 0$, and $A_0 = 0$. From the boundary condition $E_2 = 0$ at $y = 0$ we obtain the constant A_1. Thus, the general solution to the second order electric field is

$$E_2 = \sum_{i=1}^{4} \sum_{j=1}^{4} A_{ij}\left(e^{(\alpha_i + \alpha_j)ky'} - e^{Ny'}\right) \qquad (2.2\text{-}20)$$

Integrating Equation (2.2-20) results in the open circuit convolution voltage

$$V_{con} = e^{j2\omega t} \frac{k^3}{2} \left(\frac{A_p\mu_p}{D_p} - \frac{A_n\mu_n}{D_n}\right) \sum_{i=1}^{4} \sum_{j=1}^{4} \frac{A_iA_j(\alpha_i + \alpha_j)(\alpha_i\alpha_j - 1)}{(\alpha_i + \alpha_j)^2k^2 - N^2} \left[\frac{e^{-(\alpha_i + \alpha_j)kd} - 1}{(\alpha_i + \alpha_j)k} - \frac{e^{-Nd} - 1}{N}\right] \qquad (2.2\text{-}21)$$

for a unit SAW power input. Equation (2.2-21) reduces to the equation developed by M. E. Nokali[72] for semi-infinite thickness, and one carrier interaction ($d >> \lambda$, N and $A_p << A_n$)

For semi-infinite semiconductor using Equation (2.2-7) the convolution voltage for a unit SAW power input is given by

$$V_{con} = \frac{k^2}{2N} \frac{(\phi'_{y=-h})^2}{(1+R_1+j\omega R_2)^2} \left(\frac{A_p\mu_p}{D_p} - \frac{A_n\mu_n}{D_n}\right) \left[\frac{2(1+R_1+j\omega R_2)(\gamma_2-1)}{(1+\gamma)k + N} - \frac{\gamma^2 - 1}{2\gamma k + N}\right] e^{j2\omega t} \qquad (2.2\text{-}22)$$

Figure 2.5 is a plot of the convolution voltage vs. the semiconductor conductivity with the frequency as a parameter.

2.2.4 Finite Semiconductor Thickness

In order to compare the infinite semiconductor approximation to a more exact solution of the SAW interaction, with a finite semiconductor, we shall assume that the condition $\omega^2 >> \omega_{Dp}(\frac{1}{\tau_p} + j\omega)$,

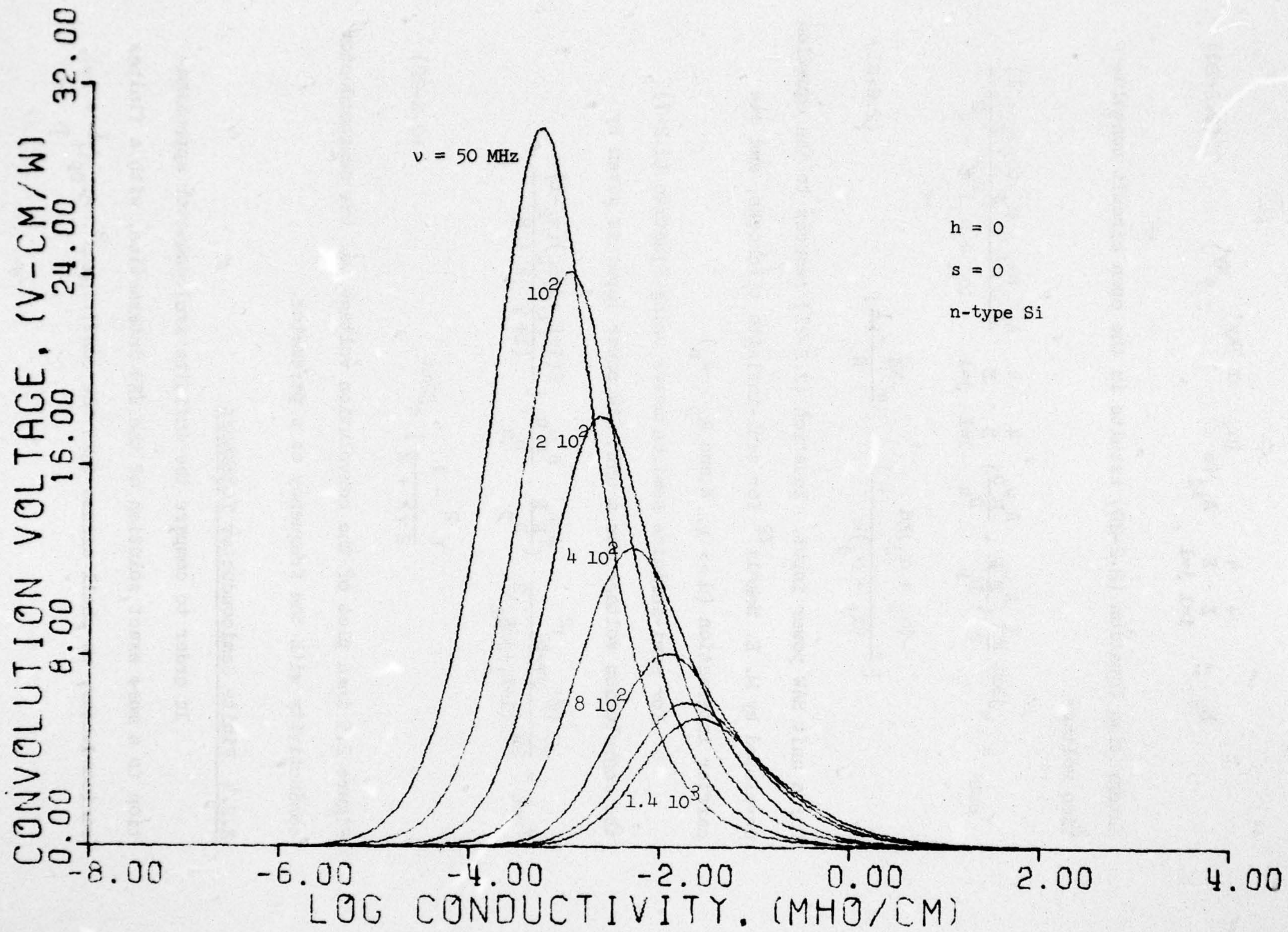

Fig. 2.5 Convolution Voltage vs. Conductivity with the Frequency as a Parameter

$\omega_{Dn}(\frac{1}{\tau_n} + j\omega)$ is satisfied. Thus, only the first two modes of the decay will be considered. The general solution to the electric potential is

$$\phi = e^{j(\omega t - kz)} \sum_{i=1}^{4} A_i e^{\alpha_i k y'} \qquad (2.2\text{-}23a)$$

where $y' = y + h$ and $\alpha_i = 1, -1, \gamma, -\gamma$. is defined in Equation (2.2-5b). The amplitude coefficients A_i are determined from the boundary conditions[14]

(i) the potential and normal component of the electric displacement are continuous at $y' = -d$

(ii) the normal component of the current is zero at $y' = -d$, and

(iii) the normal component of the current at the semiconductor surface is determined by the surface recombination velocity.

The fourth coefficient is related to the input acoustic power. After applying the boundary conditions one obtains:

$$A_1, A_2, A_3 = \frac{D_1}{D} A_4, \frac{D_2}{D} A_4, \frac{D_3}{D} A_4 \qquad (2.2\text{-}23b)$$

where

$$D = ce^{-\gamma\theta}(\epsilon' \cosh\theta + \sinh\theta) - c_1\epsilon' + e^{-\gamma\theta}(\epsilon' - \gamma)\sinh\theta$$

$$D_1 = \frac{e^{\theta}}{2}[\epsilon'(c_1 e^{\gamma\theta} + c_2 e^{-\gamma\theta}) + (c_1 e^{\gamma\theta} - c_2 e^{-\gamma\theta})] -$$

$$-\epsilon' c - \frac{ce^{\theta}}{2}(c_1 e^{\gamma\theta} - c^2 e^{-\gamma\theta})(\epsilon' + 1)$$

$$D_2 = \frac{e^{-\Theta}}{2}[\epsilon'(c_1 e^{\gamma\Theta} + c_2 e^{-\gamma\Theta}) + (c_1 e^{\gamma\Theta} - c_2 e^{-\gamma\Theta})] -$$

$$-\epsilon' c + \frac{ce^{-\Theta}}{2}(c_1 e^{\gamma\Theta} - c_2 e^{-\gamma\Theta})(\epsilon' - 1)$$

$$D_3 = ce^{\Theta}(\epsilon' \cosh\Theta + \sinh\Theta) - c_2\epsilon' - e^{\Theta}(\epsilon' + \gamma)\sinh\Theta$$

$$\epsilon' = \frac{\epsilon_d}{\epsilon_s} \qquad \epsilon_d = \text{dielectric constant of insulating layer.}$$

(In case of metal $\epsilon' \to \infty$).

$$c = j\gamma\omega \frac{\omega_{Cn}\omega_{Dn}^2 + \omega_{Cp}\omega_{Dp}^2}{(\omega_{Cn}\omega_{Dn} + \omega_{Cp}\omega_{Dp})^2}$$

$$c_1 = c - \frac{s}{2k}(1/D_n + 1/D_p)(1 + j\omega \frac{\omega_{Cn}\omega_{Dn}^2 + \omega_{Cp}\omega_{Dp}^2}{(\omega_{Cn}\omega_{Dn} + \omega_{Cp}\omega_{Dp})^2})$$

$$c_2 = c + \frac{s}{2k}(1/D_n + 1/D_p)(1 + j\omega \frac{\omega_{Cn}\omega_{Dn}^2 + \omega_{Cp}\omega_{Dp}^2}{(\omega_{Cn}\omega_{Dn} + \omega_{Cp}\omega_{Dp})^2})$$

$$\Theta = kd$$

The coefficient A_4 is related to the acoustic power flux S_z and can be found using Equation (2.2-13)

$$A_4 = \phi'_{y=-h} \frac{D}{D_1 + D_2 + D_3} \qquad (2.2\text{-}24)$$

Using Equations (2.2-23) and (2.2-24) in Equations (2.1-4), (2.1-17), (2.1-18), and (2.1-24), the propagation loss, transverse acousto-electric voltage and the change in SAW velocity can be found for semiconductors of finite thickness. Figures 2.6-2.12 are numerical plots for n- and p-type silicon. All the constants values are the same as in the semiconductor plots for infinitely thick semiconductors, except the thickness of the semiconductor which is 200 μm. For epitaxial layer the finite semiconductor solution has to be used.

A comparison between the plots of the SAW-semiconductor parameters for the infinite thickness approximation, Figs. 2.2-2.5, and the finite thickness case, Figs. 2.6-2.11, show that the delay line attenuation is very similar for frequencies lower than 200 MHz. For the acoustoelectric voltages there are some differences also in this range of frequencies, especially for semiconductor conductivity lower than 10^{-3} mho/cm. The reason for that difference is not the finite thickness of the semiconductor, but rather the assumption that γ is a real quantity. This assumption is not valid for frequencies above 200 MHz and very low conductivities as the real part of γ becomes very small and one cannot neglect the imaginary part of γ . Hence, the simple analytical expression derived for the infinite semiconductor can be used whenever the semiconductor thickness is larger than the wavelength (even smaller but the same order of magnitude) but only when the semiconductor conductivity is larger than 10^{-2} mho/cm. Thus, for deep depletion the exact theory should be used, whereas for shallow depletion or accumulation condition on the semiconductor surface the simplified theory can be used.

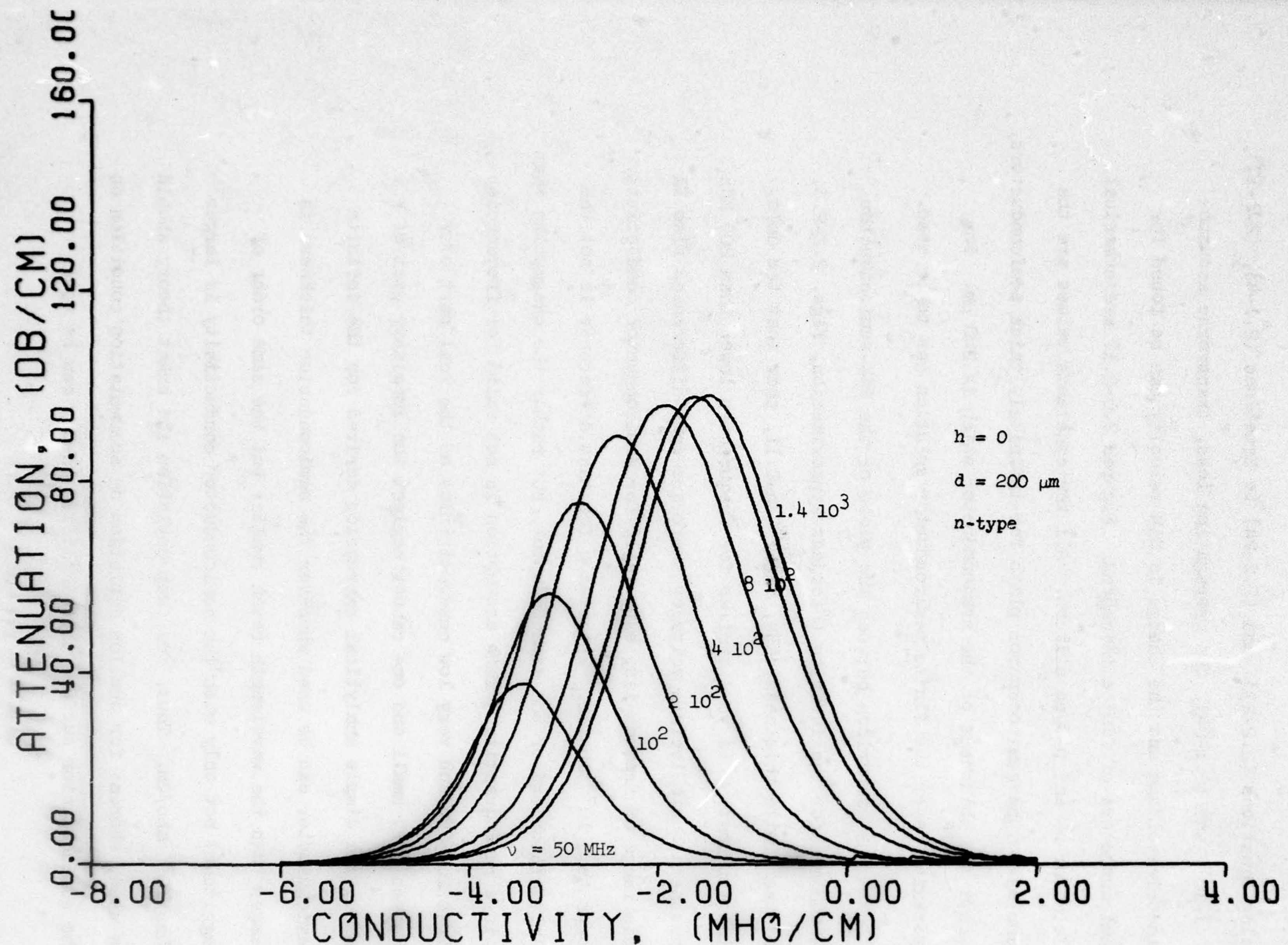

Fig. 2.6 Propagation Loss vs. Conductivity with the Frequency as a Parameter (Log scale)

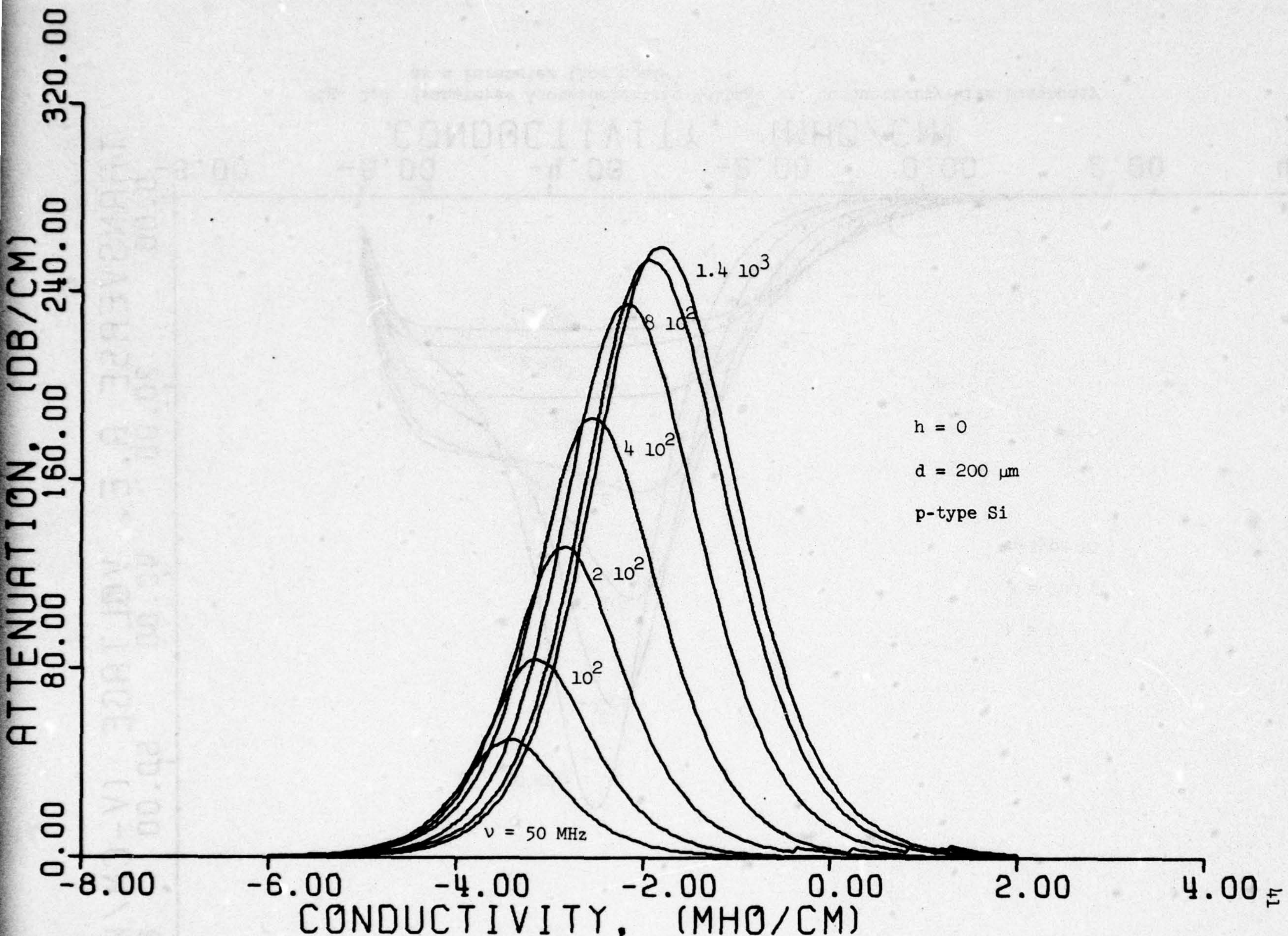

Fig. 2.7 Propagation Loss vs. Conductivity with the Frequency as a Parameter (Log scale)

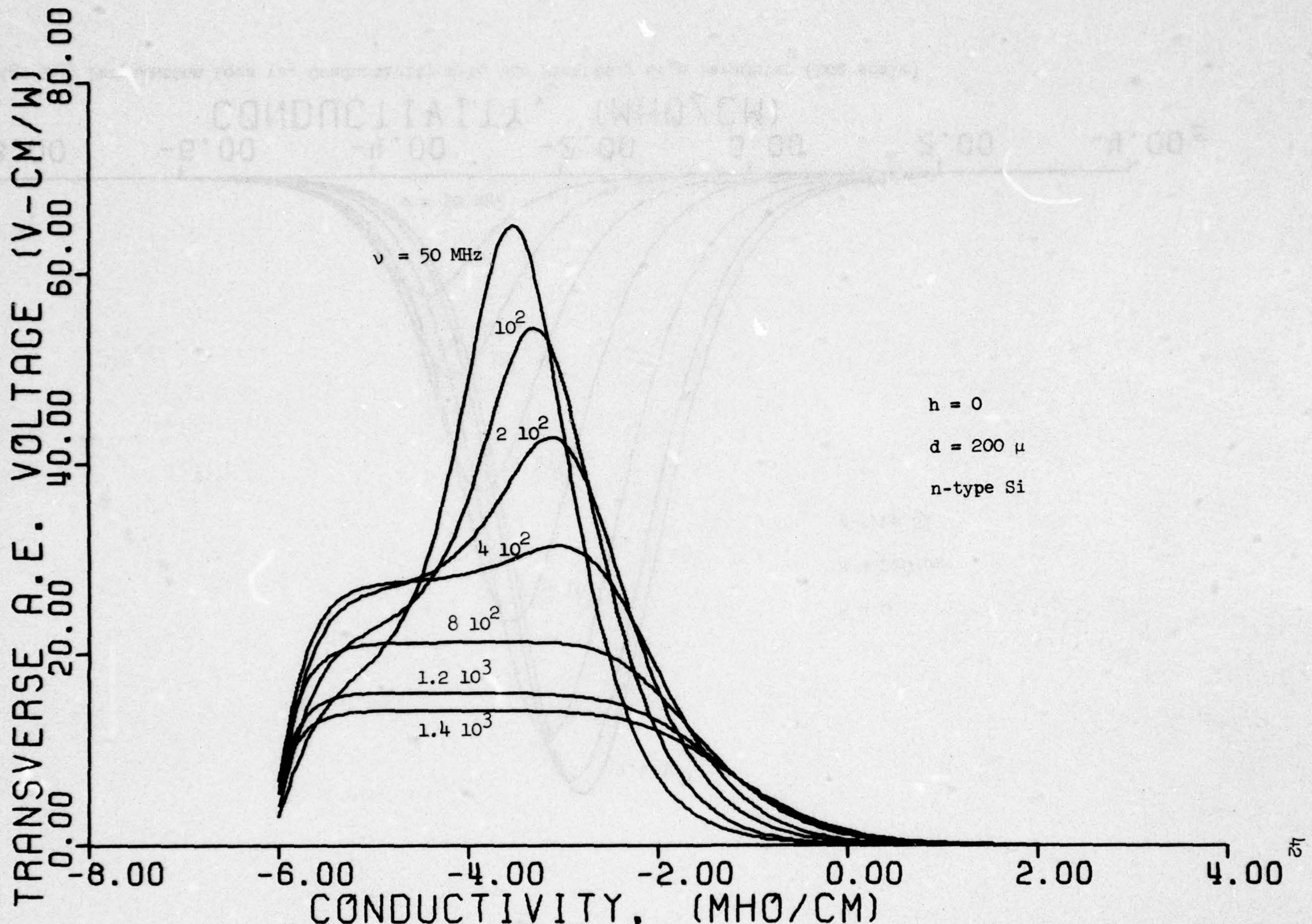

Fig. 2.8 Transverse Acoustoelectric Voltage vs. Conductivity with Frequency as a Parameter (Log scale)

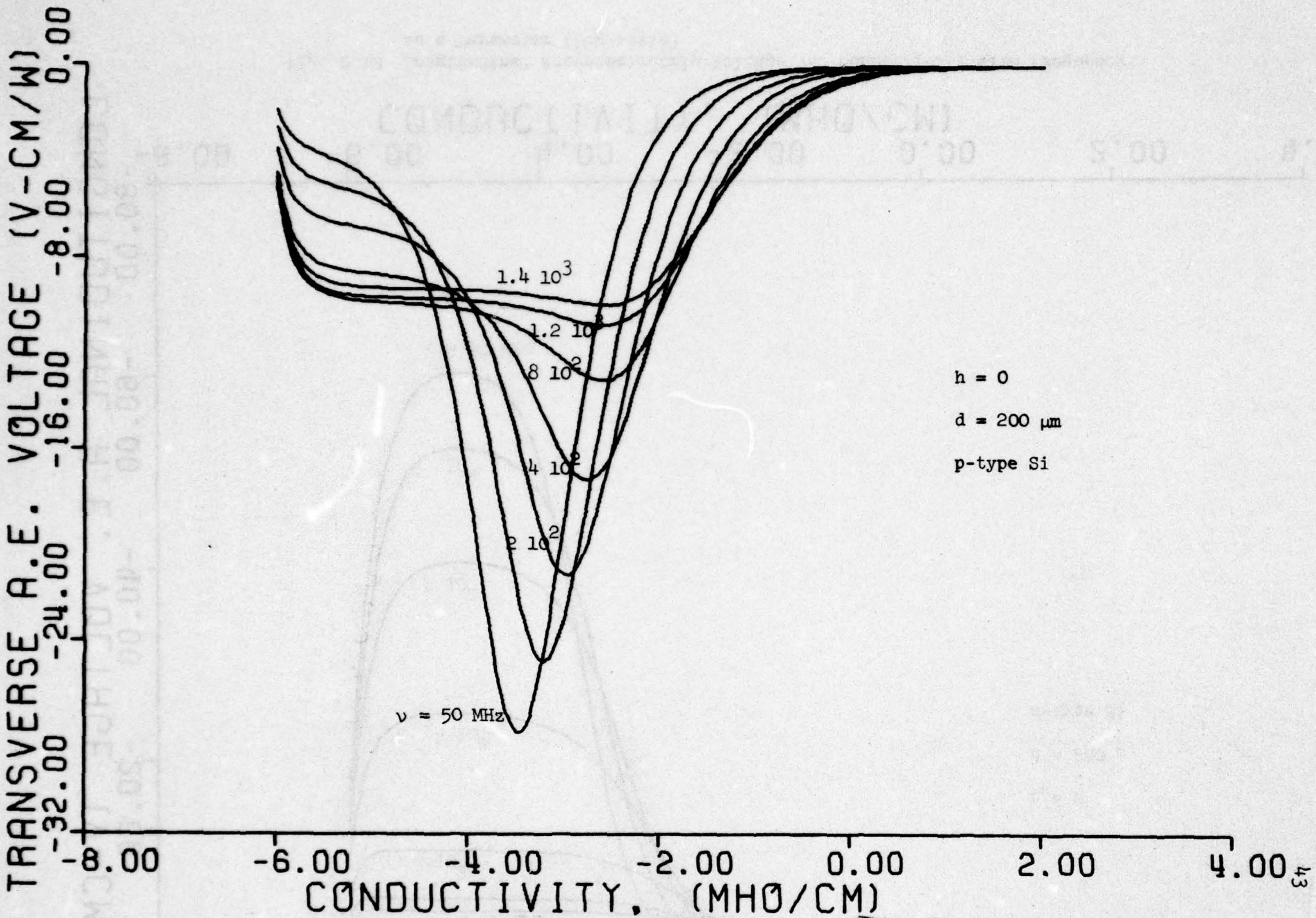

Fig. 2.9 Transverse Acoustoelectric Voltage vs. Conductivity with Frequency as a Parameter (Log scale)

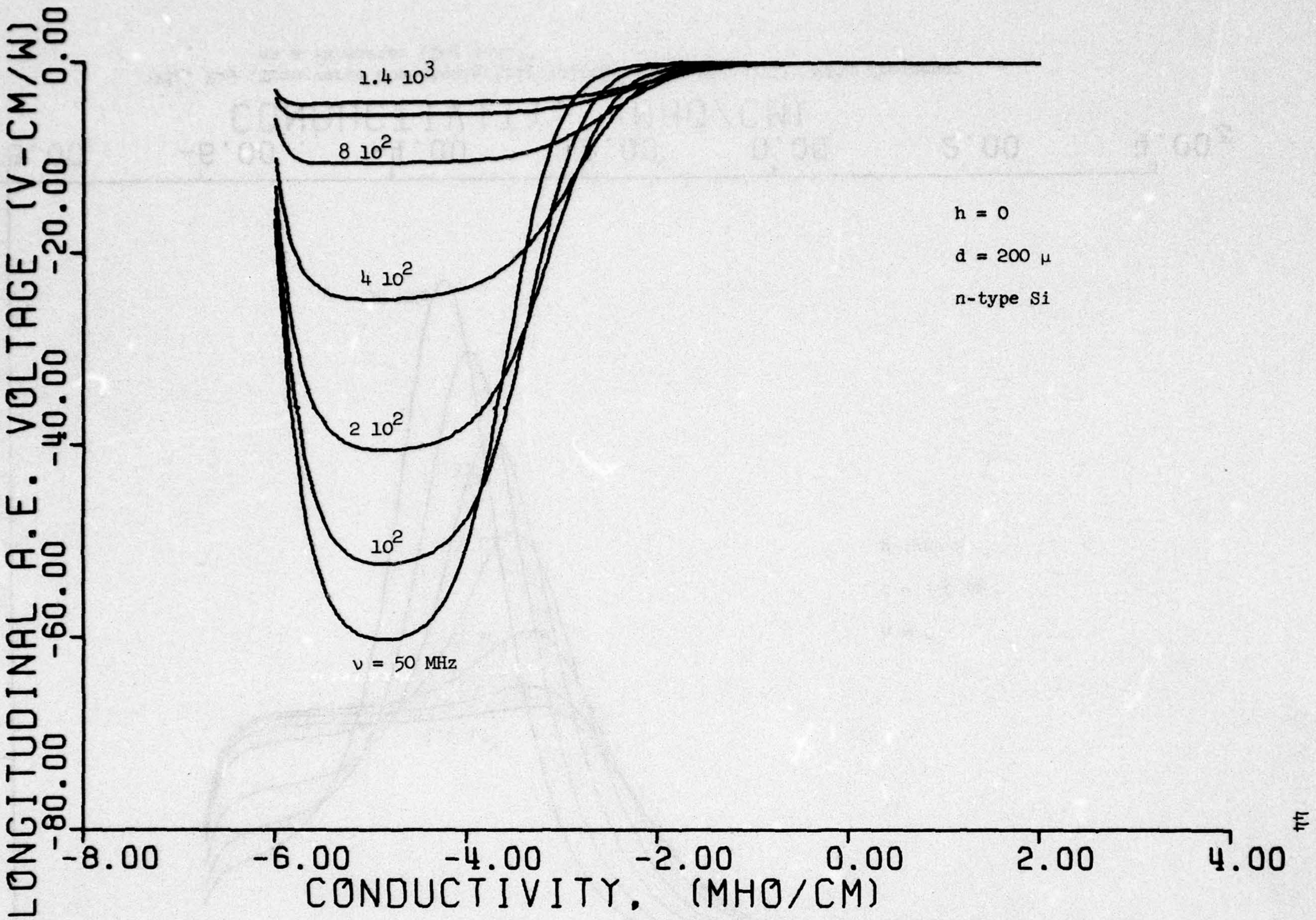

Fig. 2.10 Longitudinal Acoustoelectric Voltage vs. Conductivity with Frequency as a Parameter (Log scale)

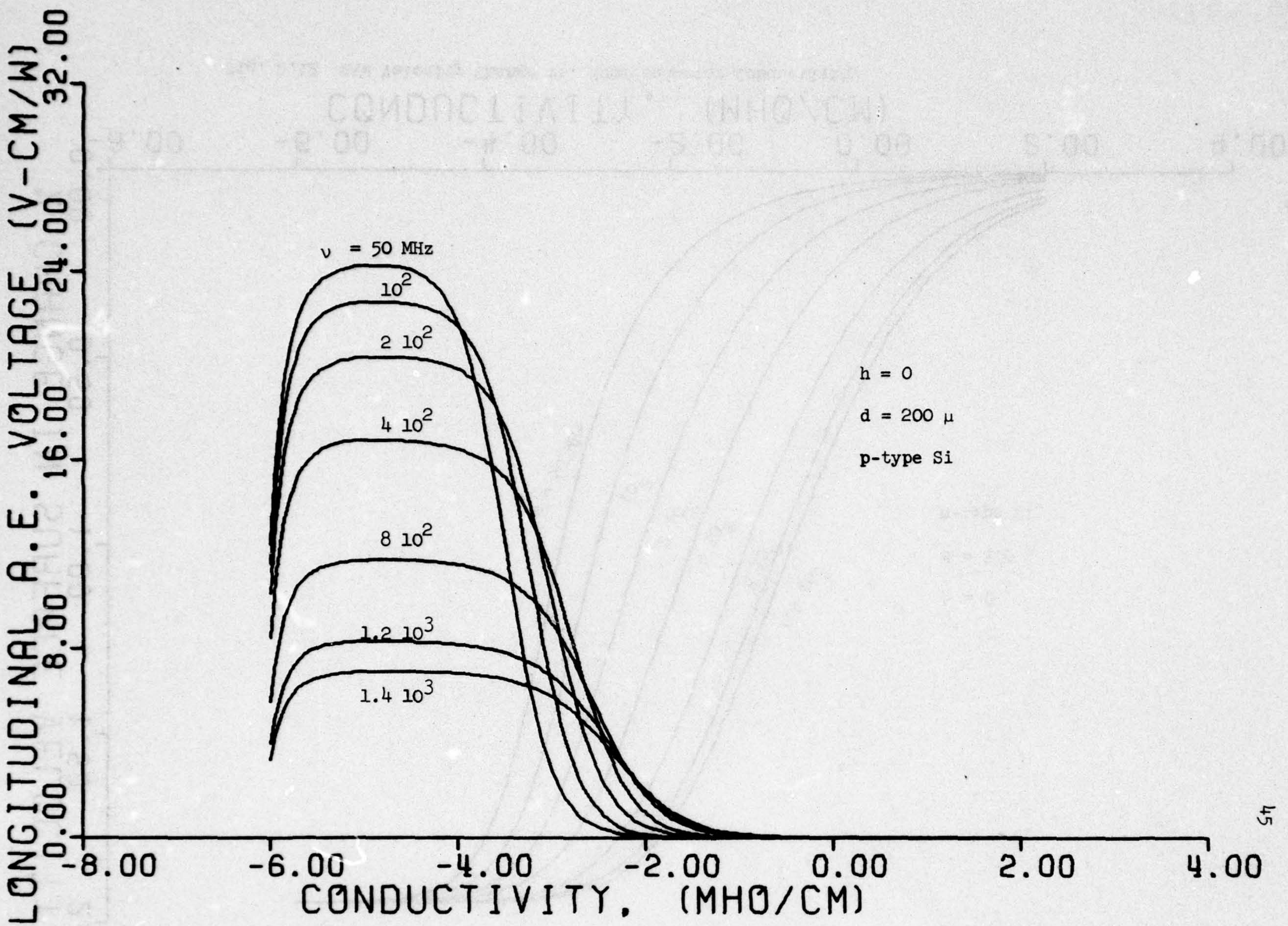

Fig. 2.11 Longitudinal Acoustoelectric Voltage vs. Conductivity with Frequency as a Parameter (Log scale)

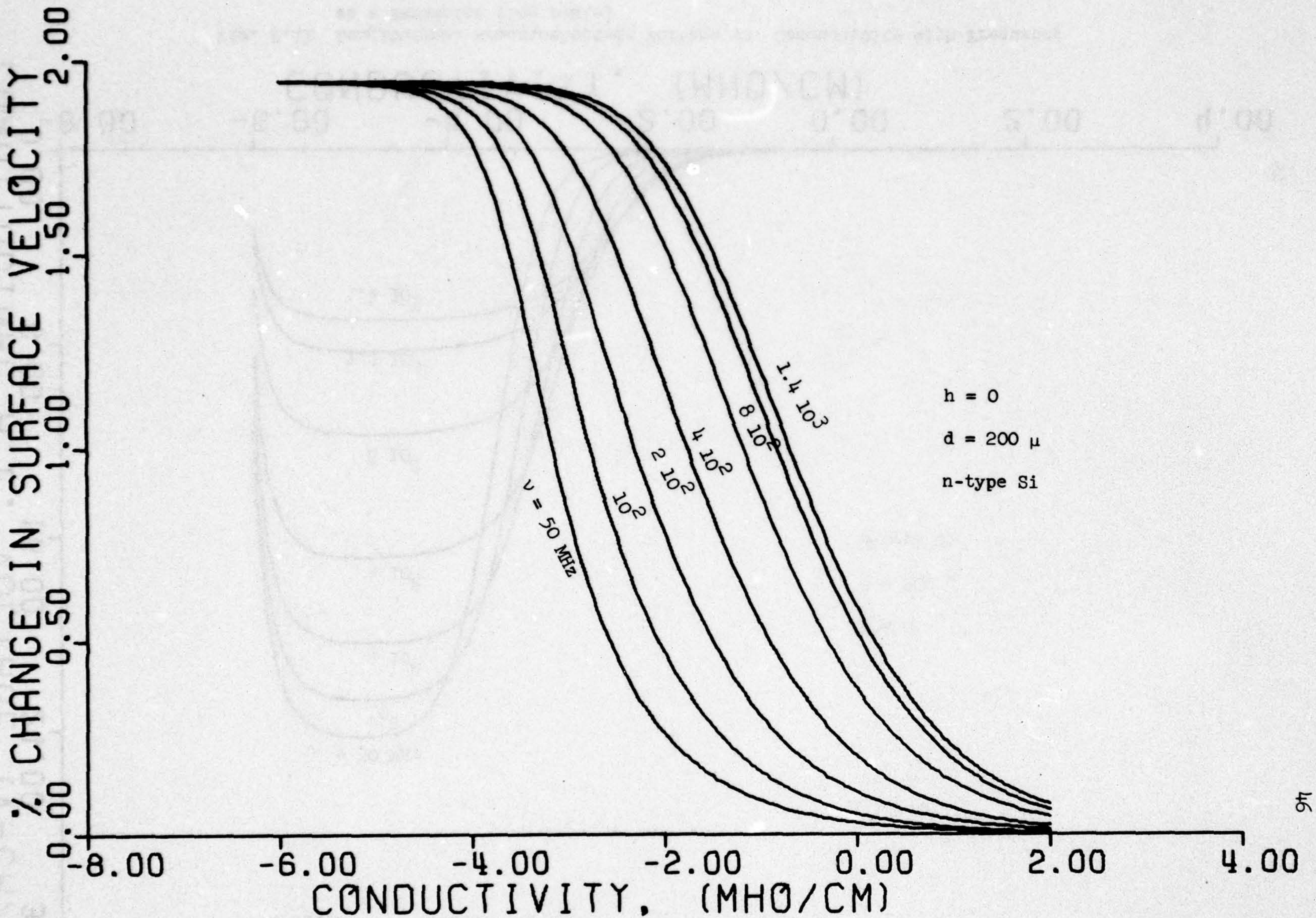

Fig. 2.12 SAW Velocity Change vs. Semiconductor Conductivity

The lifetime of the free carriers will effect the SAW-semiconductor interaction only when it is comparable to the SAW period. In addition to its effect on the surface lifetime, the surface recombination velocity will effect the SAW-semiconductor interaction directly as can be seen in Figs. 2.13 and 2.14. The effective lifetime is used as a parameter ($\tau_n = \tau_p = 1$ μsec), hence the surface recombination reduces the propagation loss and the transverse acoustoelectric voltage only for very high surface recombination velocity (above 10^3 cm/sec). For a real semiconductor, the reduction will start for lower value of surface recombination velocity due to the reduction in the effective lifetime near the surface.

2.3 The Effective Surface Conductivity Approximation for the Off Flat-band Condition

2.3.1 SAW-Semiconductor Interaction in the Off Flat-band Condition

The propagation losses, acoustoelectric voltages, and convolution voltages, all are strongly dependent on the electrical properties of the semiconductor surface such as carrier density, carrier mobility, and density of surface states. As the surface waves propagate under the semiconductor, the longitudinal and transverse electric fields interact with the free carriers causing a current to flow. There will be a power loss per unit volume, absorbed from the SAW which will, therefore, be attenuated. This attenuation is directly related to the semiconductor conductivity as we discussed in the previous sections. For very low conductivity

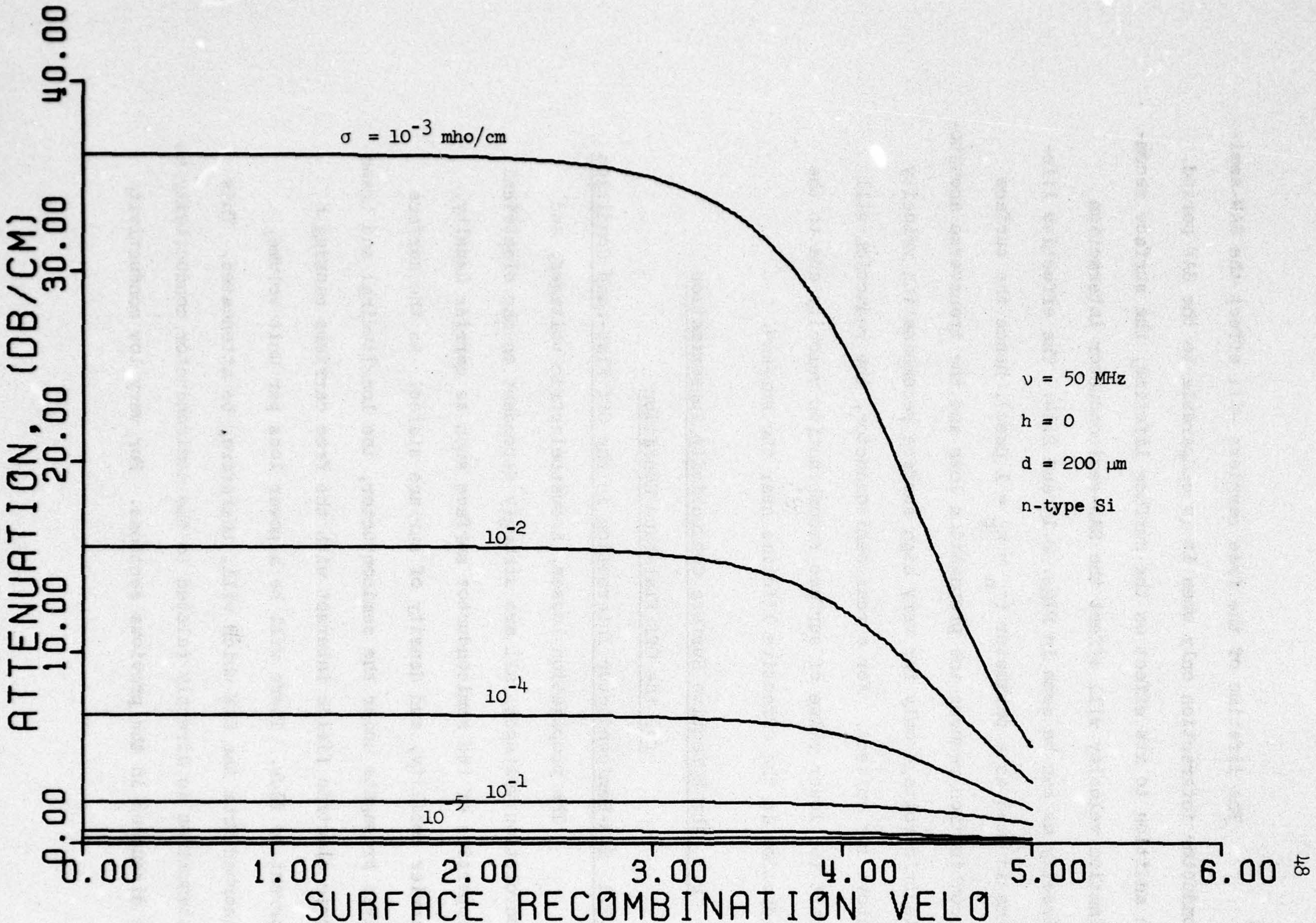

Fig. 2.13 Propagation Loss vs. Surface Recombination Velocity (Log scale cm/sec) with Bulk Conductivity as a Parameter

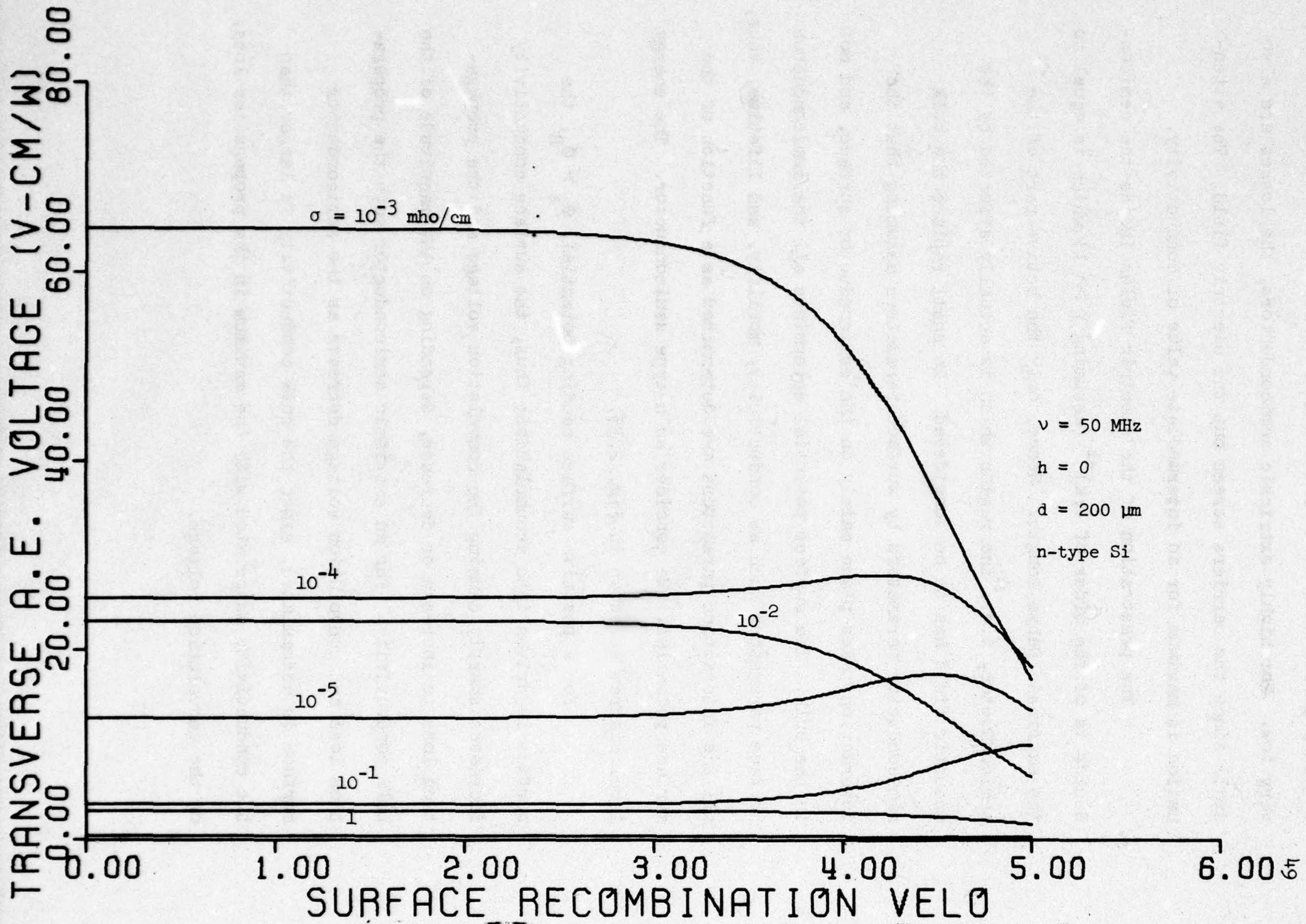

Fig. 2.14 Transverse Acoustoelectric Voltage vs. Surface Recombination Velocity (Log scale, cm/sec) with Bulk Conductivity as a Parameter

the propagation loss is very low since the free carrier density is very low. For highly extrinsic semiconductors, the losses are also small since the carriers screen out the electric field. The attenuation is maximum for an intermediate value of conductivity.

The penetration of the electric fields inside the semiconductor is of the order of $(\gamma k)^{-1}$ (assuming $\gamma \gg 1$) which is equal to the extrinsic Debye length. Hence, only the active part of the semiconductor, i.e., the region which is actually affected by the acoustic field has to be considered. We shall replace the bulk semiconductor parameters by surface parameters assuming that the interaction takes place mainly on the semiconductor surface, and not in the bulk. The surface potential determines all the semiconductor surface parameters such as conductivity, mobility, and lifetime, thus, all the interaction parameters are determined as a function of the surface potential. We consider an n-type semiconductor. The energy level diagram is shown in Fig. 2.15.

For a positive surface bending potential, $\phi_s > \phi_B$, the surface is driven into accumulation; thus, the surface conductivity increases sharply causing the convolution voltage and the propagation loss to increase or decrease, depending on the magnitude of the bulk conductivity. For an extrinsic semiconductor both the propagation loss and convolution voltage decrease as the semiconductor surface is accumulated, since the bulk conductivity is larger than the conductivity associated with the maximum in the propagation loss, or the convolution voltage.

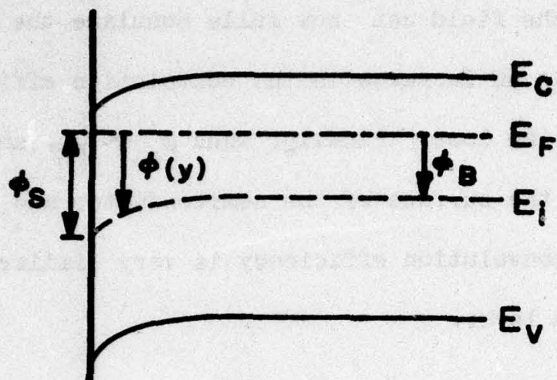

Fig. 2.15a Energy Band Diagram for Accumulation Condition

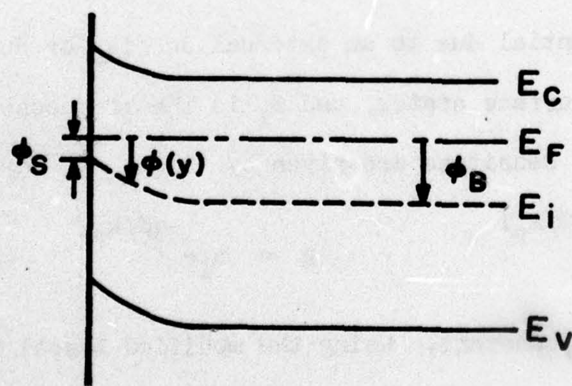

Fig. 2.15b Energy Band Diagram for Depletion Condition

In depletion, $\phi_s < \phi_B$, the nonlinear mechanism becomes more efficient because the field can now fully modulate the carrier density; this shows up as an increase in the convolution efficiency and also in the propagation loss. Finally, when $\phi_s \ll \phi_B$, an inversion layer is formed on the surface of the semiconductor and the effect on the loss and convolution efficiency is very similar to that of the accumulation layer.

2.3.2 The Space Charge Region

Kingston et al.[48] have reported on the relationship between the space charge carrier concentration and the electric field at the semiconductor surface, as a function of the change in the electrostatic potential from bulk to surface. We shall now discuss the effect of the rf acoustic field on the space charge region.

The potential inside the semiconductor is given by

$$\phi = \phi_0(y) + \phi_1(y)\cos(\omega t - kz) \qquad (2.3\text{-}1)$$

where ϕ_0 is the dc potential due to an external dc bias or due to charge trapped in the surface states, and ϕ_1 is the rf acoustic potential. The carrier densities are given by

$$n = n_i e^{q\phi/k_BT} \qquad p = n_i e^{-q\phi/k_BT} \qquad (2.3\text{-}2)$$

where k_B is Boltzmann's constant. Using the modified Bessel function identity,

$$e^{x\cos\Theta} = I_0(x) + 2 \sum_{n=1}^{\infty} I_n(x) \cos n\Theta \qquad (2.3\text{-}3)$$

The small signal carrier density in (2.3-2) is given by

$$n = n_i e^{q\phi_0/k_BT} [1 + 2I_1(x) \cos(\omega t - kz)] \qquad (2.3\text{-}4)$$

where we have used $I_0(x) = 1$ for $x << 1$, where $x = q\phi_1/k_BT$. Due to the linear sum of the dc and ac components in the carrier density for small signal analysis, one can separate Poisson's equation into two independent equations.

$$\nabla^2\phi_0 = \rho/\epsilon_s$$

$$\frac{\partial^2\phi_1}{\partial y^2} - k^2\phi_1 = -q(n_1 - p_1)/\epsilon_s \qquad (2.3\text{-}5)$$

The space charge, ρ is

$$\rho = q(N_D - N_A + p - n)$$

where $N_D - N_A = n_b - p_b$ n_b, p_b are the bulk densities of electrons and holes respectively. The dc Poisson's equation to be solved is, therefore,

$$\frac{\partial^2\phi_0}{\partial y^2} = \frac{2qn_i}{\epsilon_s} (\sinh q\phi_B/k_BT - \sinh q\phi_0/k_BT) \qquad (2.3\text{-}6)$$

where ϕ_B is the bulk potential. If we convert to reduced notation as follows

$$u_O = q\phi_O/k_BT \qquad L_{Di} = (\epsilon_s k_B T/2q^2 n_i)^{1/2}$$

where L_{D_i} in the intrinsic Debye length, Poisson's equation becomes

$$\frac{\partial^2 u_O}{\partial y^2} = \frac{1}{L_{Di}^2}(\sinh u_O - \sinh u_B) \qquad (2.3\text{-}7)$$

Integrating from the bulk toward the surface gives the final result

$$\frac{\partial u_O}{\partial y} = \pm \frac{F(u_O, u_B)}{L_{Di}} \qquad (2.3\text{-}8)$$

where

$$F(u_O, u_B) = [\,2\,(u_B - u_O)\sinh u_B - \cosh u_B + \cosh u_B)]^{1/2}$$

The transverse electric field on the surface is given simply by Equation (2.3-8) where $u_O = u_{sO}$.

The exact solution to the ac Poisson's equation is derived in Section 2.3.4. We first present the effective surface conductivity approximation. In this approximation, the space charge region is removed and replaced by the surface conductivity and the parameter s, the surface recombination velocity, defined through the relationship $U = sn_s = sp_s$, where n_s, p_s are the concentrations of the excess carriers at the surface, and U is the rate of electrons (holes) flowing into a unit surface area.

2.3.3 The Effective Surface Conductivity

The excess concentrations of mobile carriers in the space charge layer expressed as an excess over the value for the flatband condition, per unit surface area is

$$\Delta P = n_i \int_0^{\infty} (e^{-u_O} - e^{-u_B})dx$$

$$\Delta N = n_i \int_0^{\infty} (e^{u_O} - e^{u_B})dx \qquad (2.3\text{-}9)$$

Substituting from Equation (2.3-8) gives

$$\Delta P = n_i L_{Di}\, G(u_s, u_B)$$

$$\Delta N = n_i L_{Di}\, G(-u_s, -u_B) \qquad (2.3\text{-}10)$$

where

$$G(u_s, u_B) = \int_{u_s}^{u_B} \frac{e^{-u_O} - e^{-u_B}}{F(u_O\; u_B)}\, du_O$$

The change in carrier concentration associated with the bending of the energy band results in a change in the surface conductivity. The change in the sheet conductance of the layer is given by

$$\Delta\sigma = q\mu_{ps}\Delta P + q\mu_{ns}\Delta N$$

where μ_{ps} and μ_{ns} are the surface mobilities of holes and electrons respectively. The surface mobilities are different from the bulk mobilities because the surface provides an additional mechanism for

the scattering of free carriers above the bulk-scattering processes. The surface mobilities discussed below assume that the semiconductor surface is a completely diffuse (random) scatterer.[35] The high field effects perpendicular to the semiconductor surface are not considered due to the fact that the propagation loss is mainly due to the longitudinal current, and only the small signal rf current is considered in developing the SAW-semiconductor theory. To obtain higher accuracy in the approximation the mobilities have to be multiplied by a correction factor which will take into account the high field effects, and the scattering mechanism on a real semiconductor

Accumulation Condition

For $u_s > u_B$, the majority carrier concentration near the surface is larger than the bulk value. The carriers are confined to move in a thin region near the surface. The effect of surface scattering may be determined by considering the mobile carriers to be restrained within a potential well, the width of which is equal to twice the center of mass of the excess carrier distribution. This distance, called L_c is found to be

$$L_c = \frac{\int_0^\infty y\,\rho(y)dy}{\int_0^\infty \rho(y)dy} = \frac{U_s}{F(u_B,u_s)} L_{Di} \qquad (2.3\text{-}12)$$

where $U_s = u_s - u_B$ is the surface bending potential, and L_{Di} is the intrinsic Debye length. The surface is considered to act as a diffuse scatter, whereas the edge of the space charge layer is

considered as a specular reflector. The average mobility of this layer is then equal to the surface mobility and is given by[35]

$$\mu_{ns} = \frac{\mu_n}{1 + \lambda_n/L_c(1 + U_s)^{1/2}} \qquad (2.3\text{-}13)$$

for electrons, where $\lambda_n = \mu_n(m^* kT/2\pi q^2)^{1/2}$ is the unilateral mean free path for electrons.

Neglecting the contribution of minority carriers in accumulation layer to the SAW-semiconductor interaction, the effective conductivity under the accumulation condition on the semiconductor surface is

$$\sigma = \sigma_B + q\mu_{ns}\Delta N/2L_c \qquad (2.3\text{-}14)$$

In writing Equation (2.3-14) we assume that most of the interaction between the acoustic field and the free carriers in a semiconductor under the accumulation condition takes place in a distance equal to twice the effective space charge layer width.

Depletion Condition

For $u_s < u_B$, majority carriers are repelled from the surface, whereas the minority carrier concentration near the surface is larger than the bulk value. The depletion layer width is given by

$$w = (2\epsilon_s u_s/qN_D)^{1/2} \qquad (2.3\text{-}15)$$

where N_D is the doping concentration. The surface mobilities are

$$\mu_{ns} = \mu_n \left[1 + \frac{n_b \lambda_n}{\Delta N} (1 - e^{U_s})\right] \qquad (2.3\text{-}16)$$

for electrons,

$$\mu_{ps} = \frac{\mu_p}{1 + \lambda_p / L_c (1 - U_s)^{1/2}} \qquad (2.3\text{-}17)$$

for holes where we used the assumption that the minority carrier (holes) mobility in the depletion layer of an n-type semiconductor is equal to the hole surface mobility in accumulation layer of a p-type semiconductor.

Equation (2.3-16) describes an almost constant surface mobility, less than the bulk mobility, for majority carriers in the depletion layer, whereas Equation (2.3-17) describes a decreasing surface mobility with surface potential for minority carriers in the depletion layer.

The effective conductivity under the depletion condition on the semiconductor surface is

$$\sigma = \sigma_B + (q\mu_{ns}\Delta N + q\mu_{ps}\Delta P)/w \qquad (2.3\text{-}18)$$

It is clear that averaging the excess charge density over the width of the depletion region will introduce an error especially for deep

depletion where the excess minority carrier is very large near the surface of the semiconductor, and it decays exponentially away from the surface. In the next section we shall comment on the validity of this model.

Inversion Condition

When the surface potential is reduced, the depletion width continually increases until an inversion layer sets in. This occurs when u_s is approximately twice the bulk potential. The mobilities are given in the previous section, where we have discussed the depletion condition. Neglecting the contribution of majority carriers in inversion layer, to the SAW-semiconductor interaction, the effective conductivity is

$$\sigma = \sigma_B + q\mu_{ps}\Delta P/2L_c \qquad (2.3\text{-}19)$$

where L_c is defined in Equation (2.3-12).

2.3.4 SAW-Semiconductor Interaction Dependence on the Semiconductor Surface Potential

Using the effective semiconductor surface conductivity, Equations (2.3-14), (2.3-18), and (2.3-19) for accumulation, depletion and inversion respectively, the SAW-semiconductor interaction parameters are calculated numerically for different semiconductor surface potentials. Figures 2.16-2.20 are plots of the propagation loss, transverse acoustoelectric voltage, longitudinal acoustoelectric voltage, convolution voltage, and the change in SAW velocity for n-type silicon where the surface potential is varied from accumulation (u_s positive) to inversion (u_s negative). The frequency

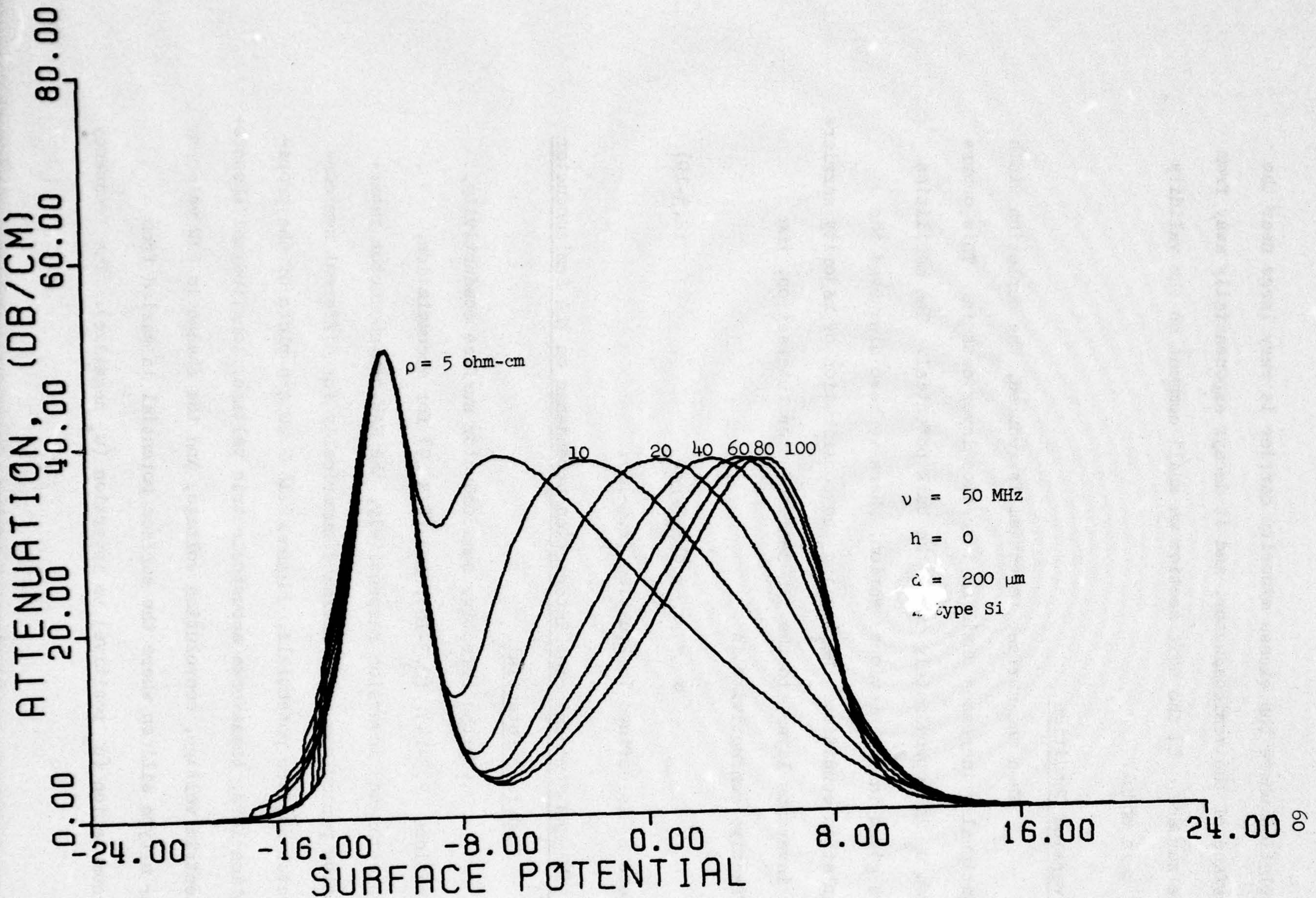

Fig. 2.16 Propagation Loss vs. Semiconductor Surface Potential with Bulk Resistivity as a Parameter

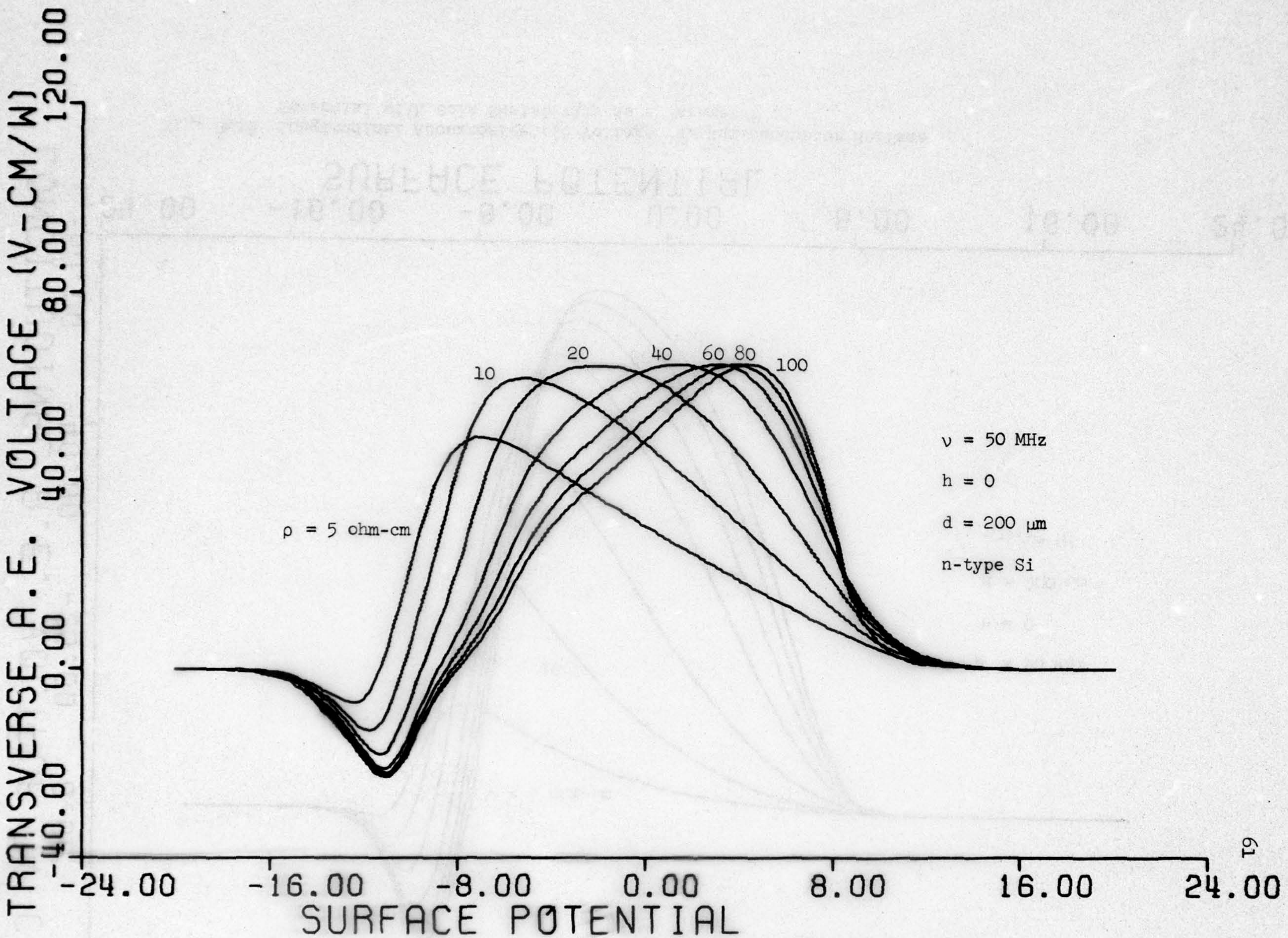

Fig. 2.17 Transverse Acoustoelectric Voltage vs. Semiconductor Surface Potential with Bulk Resistivity as a Parameter

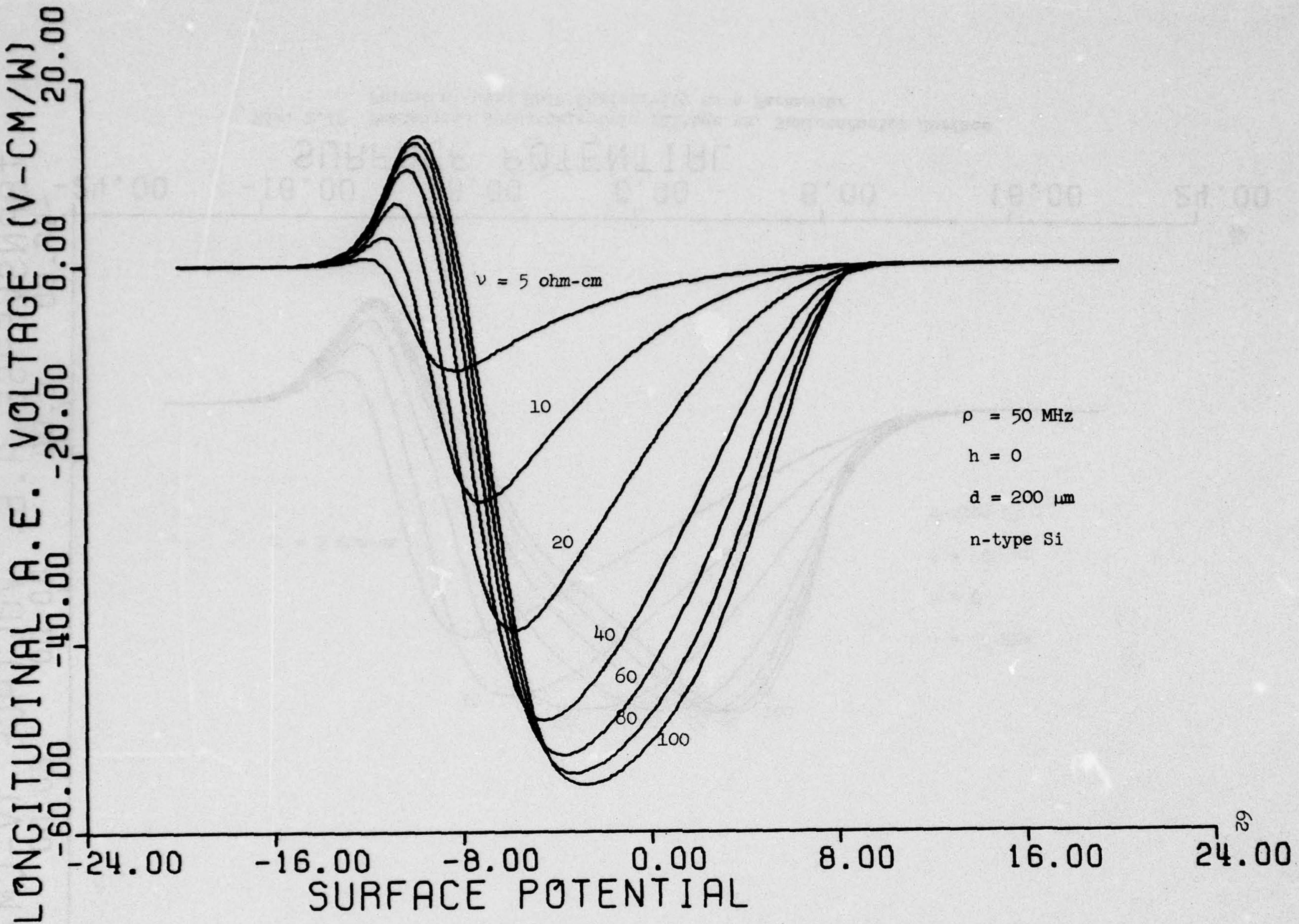

Fig. 2.18 Longitudinal Acoustoelectric Voltage vs. Semiconductor Surface Potential with Bulk Resistivity as a Parameter

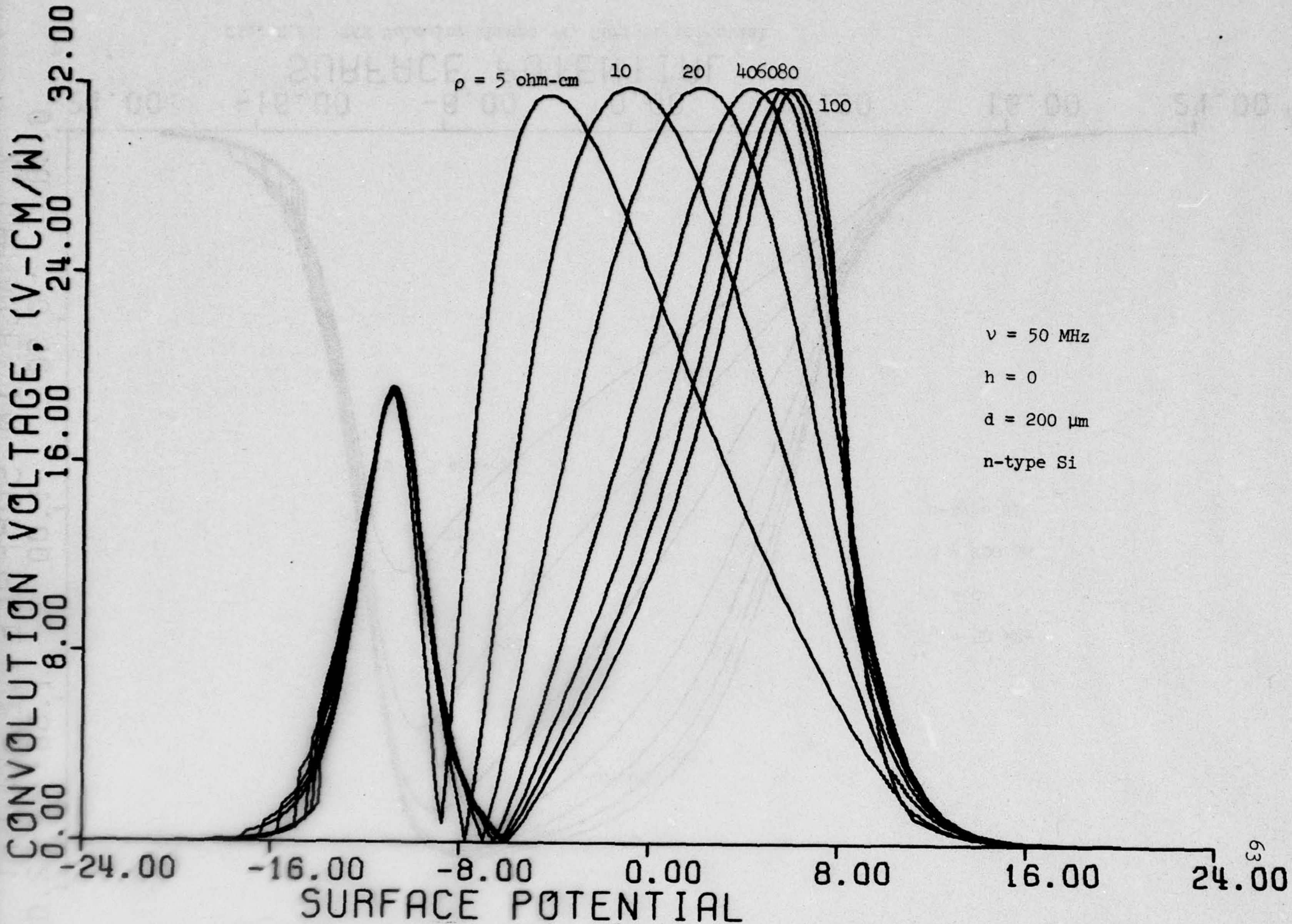

Fig. 2.19 Convolution Voltage vs. Semiconductor Surface Potential with Bulk Resistivity as a Parameter

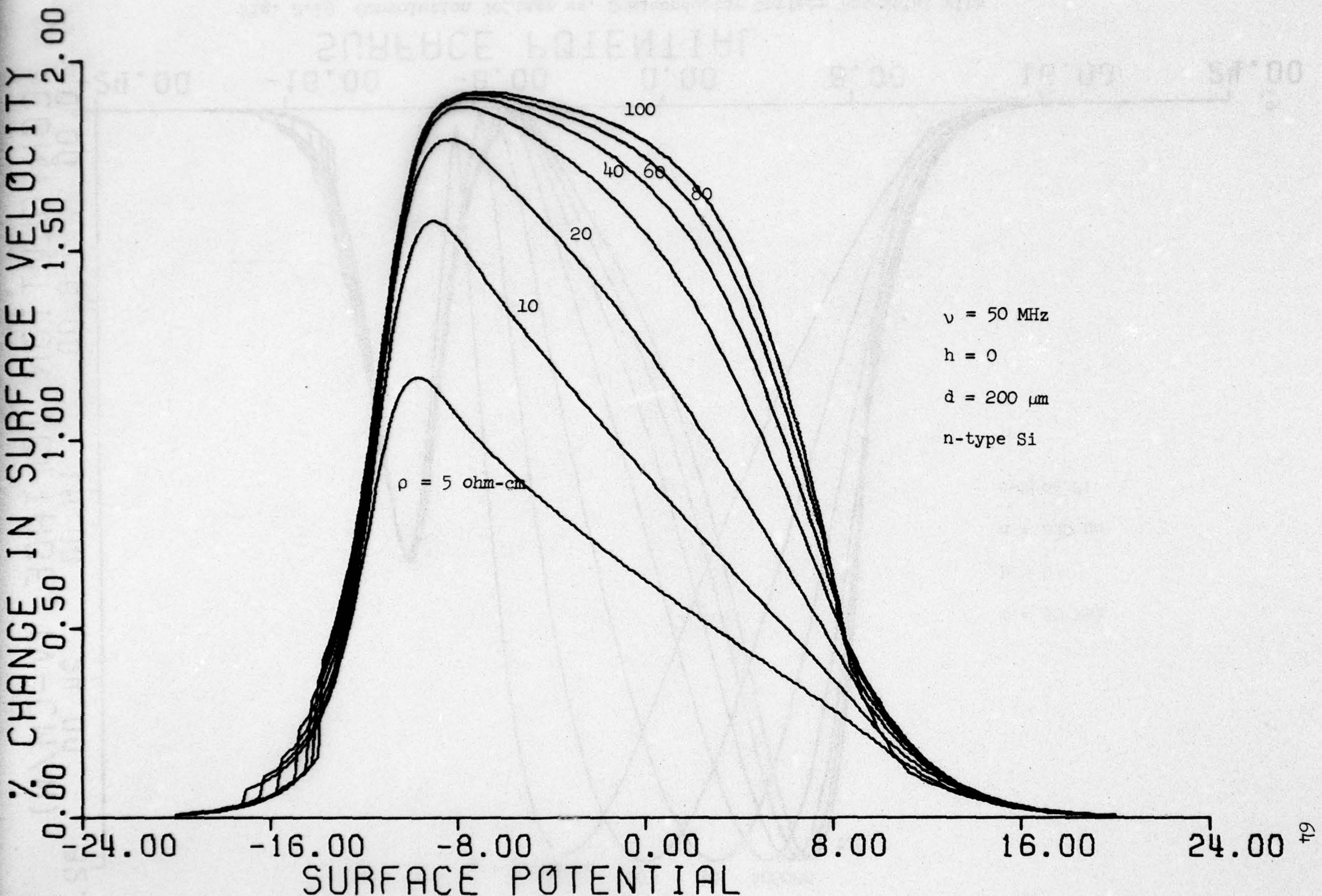

Fig. 2.20 SAW Velocity Change vs. Surface Potential

is 50 MHz and the semiconductor bulk resistivity is the parameter. The double maxima is seen in each of the SAW-semiconductor interaction parameters due to the double maxima in the semiconductor surface conductivity as the surface potential is varied from accumulation (high conductivity) through depletion (low conductivity) to inversion (high conductivity). The dc acoustoelectric voltage also shows inversion in the sign of the dc voltage as the surface majority carriers change from electrons to holes (inversion layer). The plots have s as a fixed parameter. Here $s = 0$, the plots for $s > 0$ have the same shape with lower values for the SAW-semiconductor interaction parameter. In order to include the change in surface recombination velocity, and the effective lifetime in the computations, it is necessary to know the position of the recombination center in the energy gap.

Previous numerical calculations[71] of the delay line attenuation as a function of the semiconductor surface potential show that the two maxima appear only for very high resistivity ($\rho > 400$ ohm-cm), and that the two maxima are equal. The reason for these differences is that in the previous work one carrier interaction and averaging the excess carrier density over the intrinsic Debye length have been used.

2.3.5 The Exact Solution for the Off Flatband Condition

The effective conductivity model for the off flatband condition assumes that we can replace the interaction region of the semiconductor surface by a new layer of constant carrier density

which is given by the average excess carrier density over the space charge region. In this section we present the exact solution for the off flatband condition considering the variation of the carrier density with distance from the surface. Using Fig. 2.14 of the energy band diagram, the carrier density is given by

$$p(y) = \bar{p}(y) + p_1(y)e^{j(\omega t - kz)}$$

$$n(y) = \bar{n}(y) + n_1(y)e^{j(\omega t - kz)} \qquad (2.3\text{-}20)$$

where

$$\bar{p}(y) = n_i e^{-u(y)}$$

$$\bar{n}(y) = n_i e^{u(y)}$$

The electric potential inside the semiconductor is given by the sum of the rf acoustic potential and the dc potential due to an external dc bias

$$\phi = \phi_0(y) + \phi_1(y)e^{j(\omega t - kz)} \qquad (2.3\text{-}21)$$

Using Poisson's equation and the continuity equation (as described in Section 2.2) and separating the continuity equation into its dc and ac terms, the following equation is obtained for the rf acoustic potential.

$$\phi_1'''' - (A_n - A_p)u_0'\phi_1''' - k^2(1 + \gamma^2)\phi_1'' -$$

$$[\frac{q^2}{\epsilon_s kT}(\bar{n} - \bar{p}) - k^2(A_n - A_p)] \quad u_0'\phi_1' + k^4\gamma^2\phi = 0 \qquad (2.3\text{-}22)$$

We use the symbol ' for differentiation with respect to y, and

$$\omega_{Dp} = v_s^2/D_p$$

$$\omega_{Dn} = v_s^2/D_n$$

$$\omega_{Cn}(y) = q\mu_n \bar{n}(y)/\epsilon_s$$

$$\omega_{Cp}(y) = q\mu_p \bar{p}(y)/\epsilon_s$$

$$A_n(y) = \frac{\omega_{Cn}\omega_{Dn}}{\omega_{Cn}\omega_{Dn} + \omega_{Dp}\omega_{Dp}}$$

$$A_p(y) = \frac{\omega_{Cp}\omega_{Dp}}{\omega_{Cn}\omega_{Dn} + \omega_{Cp}\omega_{Dp}}$$

$$\gamma^2(y) = 1 + \frac{u''}{k^2} + \frac{q}{k^2\epsilon_s}\left(\frac{\mu_n\bar{n}}{D_n} + \frac{\mu_p\bar{p}}{D_p}\right) + \frac{j\omega}{k^2}\left(\frac{A_n}{D_n} + \frac{A_p}{D_p}\right)$$

Equation (2.3-22) reduces to the flatband equation for the rf acoustic field, Equation (2.1-9), for $u_0 = u_B$, hence, $u_0' = u_0'' = 0$.

Equation (2.3-22) can be solved only numerically, and four boundary conditions are needed on the semiconductor surface. The solution is very complicated and is very difficult to interpret in a meaningful way. However, it is clear that for near flat-band condition, where u_0' and u_0'' are small, the additional terms in the exact differential equation (Equation 2.3-22), compared to Equation (2.3-18) are very small and can be neglected. "γ" reduces to the definition of γ in Equation (2.3-18), hence, the effective surface conductivity is a good approximation for the SAW-semiconductor interaction for this range.

We can conclude that for semiconductor in flat band condition, two carrier interactions have to be considered for very high resistivity materials, whereas one carrier interaction can be considered for highly extrinsic semiconductors. The lifetime and surface recombination velocity cannot be neglected for materials with very short lifetimes and very high surface recombinations respectively. For semiconductor thickness such that $d \gg \lambda$, simple analytical expression can be used for the SAW-semiconductor interaction parameters, for frequencies less than 200 MHz, and conductivity higher than 10^{-2} mho/cm. For the off flatband condition in shallow depletion or accumulation the interaction can be considered in a similar way to the flatband condition, using the effective surface conductivity approximation.

CHAPTER III

SEMICONDUCTOR SURFACE EVALUATION USING THE SAW CONVOLVER

3.1 Introduction

3.1.1 Experimental Procedure

Determination of electrical properties of semiconductor surfaces is important for solid state device fabrication. It is very much desirable to determine the surface parameters in the neighborhood of the surface without any bulk effect contribution to the measurement procedure, and without any contamination of the semiconductor surface. The separated media space charged coupled convolver satisfies these two conditions for nondestructive evaluation of semiconductor surfaces. The usefulness of the device arises from the fact that electric fields propagating on a piezoelectric substrate penetrate the adjacent semiconductor to a depth of approximately a Debye length. The electric fields interact with the carriers in the semiconductor, which result in attenuation of the acoustic waves,[13,15] change in the acoustic wave velocity,[12] and dc voltages are developed in the semiconductor.[13] When two inputs are applied simultaneously at the two ports of the delay line, a convolution voltage appears across the semiconductor with twice the input frequency.[16]

A proper device for measurement has usually three terminals: terminals "1" and "2" are connected to the transducers of the SAW delay line and terminal "3" is connected to the back side of the semiconductor surface. If both terminals "1" and "2" are fed with

an rf pulse, terminal "3" through a low-pass filter shows the normal component of acoustoelectric voltage, and terminal "2" shows the variation of delay line attenuation, α. Because of this acousto-electric coupling the SAW propagating on the surface of piezoelectric substrate will suffer more attenuation and the delayed rf signal from terminal "2" has an amplitude variation related to the semiconductor surface properties.

Figure 3.1 shows the schematic of the experimental set-up. The delay line is Y-cut, Z-propagating lithium niobate single crystals of 2 mm thickness with an interdigital transducer at each end. The center frequencies of the transducers were either 45, 110, or 230 MHz, each having a bandwidth of approximately 20% of the center frequency. The delay times varied from 6 to 23 μs and the tuned insertion loss of the delay lines ranged from 10 to 23 dB.

In all the experiments reported here, the semiconductor sample was placed directly on the delay line and gentle pressure was applied to achieve uniform interaction. The electric field decay constants at 45, 110 and 230 MHz are 60, 25, and 12 μm respectively. Thus, it is very important, especially at higher frequencies, that no dust particles separate the semiconductor and the delay line surfaces. The top surface of the semiconductor was metalized in general, either by silver paint or evaporation of gold or aluminum, though some experiments were performed using either no top contact at all or an air gap separating the metal contact and the semiconductor top surface. The length of the semiconductor samples varied

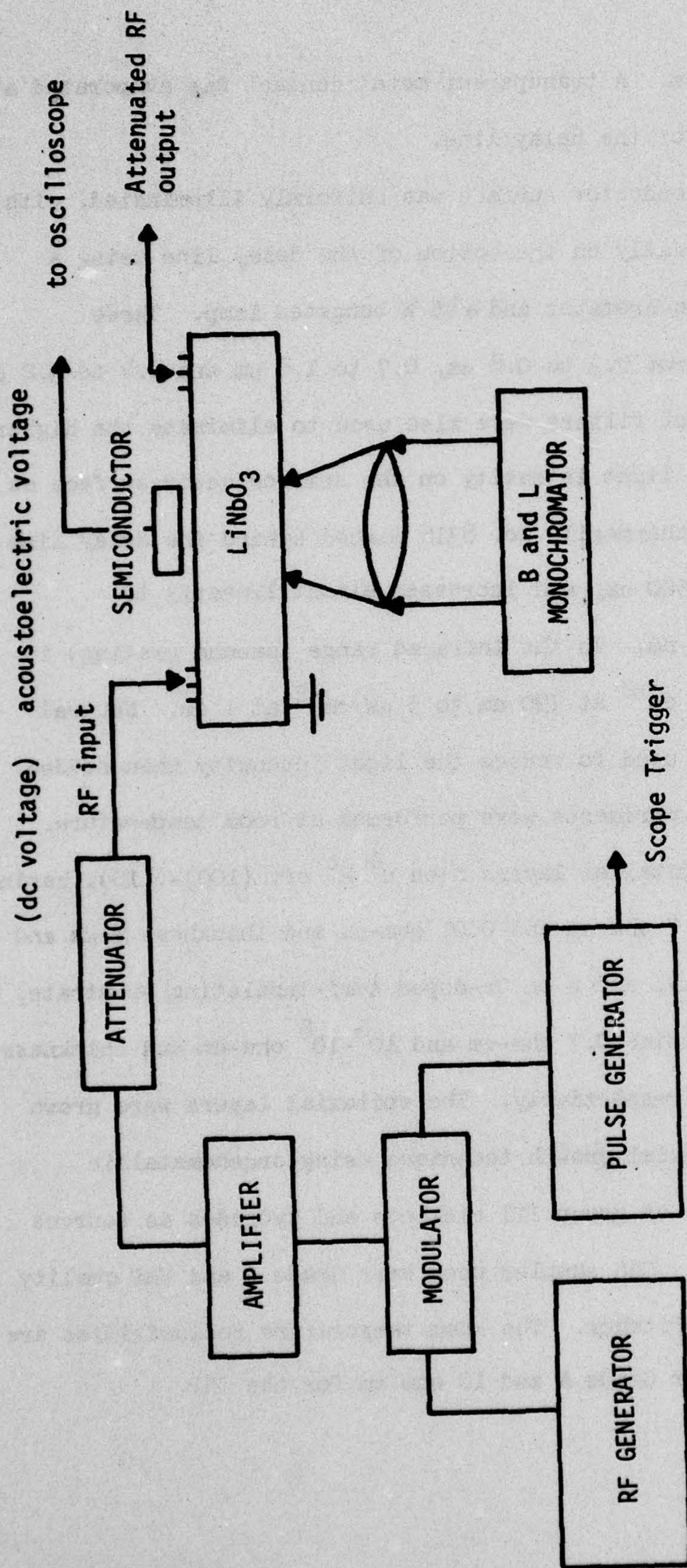

Fig. 3.1 Schematic of the Experimental Set-up

between 0.5 and 4 cm. A transparent metal contact was evaporated at the bottom surface of the delay line.

The semiconductor surface was uniformly illuminated, with light shining vertically on the bottom of the delay line using a Bausch and Lomb monochromator and a 45 W tungsten lamp. Three gratings, ranging from 0.3 to 0.8 μm, 0.7 to 1.6 μm and 1.4 to 3.2 μm, were used. Different filters were also used to eliminate the higher order spectra. The light intensity on the semiconductor surface as measured by Eppley thermopile No. 8316 placed behind the delay line is 0.55 μW cm^{-2} at 500 nm, and increases almost linearly to 1.18 μW cm^{-2} at 700 nm. In the infrared range (second grating) it varies from 2.36 μW cm^{-2} at 790 nm to 5 μW cm^{-2} at 1 μm. Neutral density filters are used to reduce the light intensity when needed.

All the experiments were performed at room temperature. GaAs samples were epitaxial layers n on n^+ 2° off (100)-(110), having the resistivities 0.7 ohm-cm and 0.01 ohm-cm and thickness 2 μm and 15 mils, respectively, and n on Cr-doped semi-insulating substrate, having the resistivities 0.7 ohm-cm and 10^6-10^8 ohm-cm and thickness 2.9 μm and 15 mils, respectively. The epitaxial layers were grown by vapor-phase epitaxial growth technique using organometallic compounds as sources of group III elements and hydrides as sources of group V elements. CdS samples used were Grade A and UHP quality obtained from Eagle Pitcher. The room temperature resistivities are around 10^8 ohm cm for Grade A and 10 ohm cm for the UHP.

The input to the delay line is always in the form of a rectangular rf pulse. The pulse width is varied from a few μs to tens of milliseconds, depending on the requirement. This pulsed method allows one to study the transient response associated with different time constants.

Both acoustoelectric voltage and the attenuation α are used for the study of semiconductor surface. When the attenuation is used, the terminal "3" of the device is free and it can be used to apply a dc electric field normal to the semiconductor surface to change the surface bending potential and bias the initial surface condition to accumulation, depletion or inversion condition.

When V_{ac} is used for surface study the shift in surface potential is done by application of light. Since V_{ac} is a capacitance-coupled potential from the piezoelectric field, it is a transient signal and the steady-state value of the waveform has a zero voltage level.

3.1.2 The Propagation Loss, Transverse Acoustoelectric Voltage, and Convolution Voltage

Due to the nonlinear interaction of the charge carriers near the semiconductor surface with the electric field associated with the SAW, both delay line attenuation and acoustoelectric voltage are a function of the initial condition of semiconductor surface potential u_s prior to the interaction to the SAW. In the absence of surface states the surface potential u_s equals the bulk potential u_B in the semiconductor substrate.

However, the presence of surface states will bend the energy band in the semiconductor, resulting in a non-zero value of the surface bending potential, $U_s = u_s - u_B$, which can be positive or negative dependent on the type of surface traps. When U_s is positive for an n-type sample, the surface charges are accumulated and when U_s is negative, the semiconductor surface is either depleted or inverted. The resulting attenuation α and acoustoelectric V_{ac}, are a function of the amount of bending potential U_s. Light incident on the semiconductor surface can be used to vary U_s, since the incident intensity will change the charge carrier density at the surface (and hence U_s) by band to band carrier generation as well as by filling surface traps.

Each of the four experimentally observable results are dependent on the electrical properties of the semiconductor surface. Therefore, by monitoring the delay line attenuation, the SAW velocity, the acoustoelectric voltage, or the convolution voltage while the semiconductor surface properties are varied, various information on the semiconductor surface can be obtained.

The acoustoelectric voltage and the convolution voltage appear both in the transverse (perpendicular to the direction of the SAW propagation) and longitudinal (along the direction of the SAW propagation) direction. When $\omega_1 = \omega_2$ the longitudinal convolution voltage is zero.[72] In this work we are concerned only with the transverse components of these voltages. Due to the lack of a dc path in

the transverse direction the dc acoustoelectric voltage appears as a transient phenomenon. Figures 3.2 and 3.3 are the observed attenuation, transverse acoustoelectric voltage, and the auto-convolution, for two square pulses.

To explain the shape of the acoustoelectric voltage shown in Fig. 3.2, consider an n-type semiconductor with a moderate density of surface traps and some value of $U_s \neq 0$. When SAW passes under the semiconductor the V_{ac} rises, the surface is depleted resulting in a storage of positive charges at the surface. These surface traps are charged, and screen out a portion of the peak acoustoelectric voltage, until the acoustic pulse exists under the semiconductor. When the acoustic pulse terminates, the resulting output potential reverses and decays to zero. The decay time is the result of discharging the terminal capacitance and relaxation time of surface traps.

The difference in the peak voltages is the portion which is screened out by traps and consequently, is a measure of the density of surface traps. When the surface of semiconductor containing surface traps is illuminated by a moderate light intensity, the surface traps are filled out and no change in the peak voltages can be observed. For semiconductors with low density of surface states, the two peaks are equal.

The change in the semiconductor surface properties can be accomplished by an external dc bias, optical generation of carriers, temperature, and by the rf electric field accompanying the acoustic wave. In this Chapter experimental results of semiconductor surface

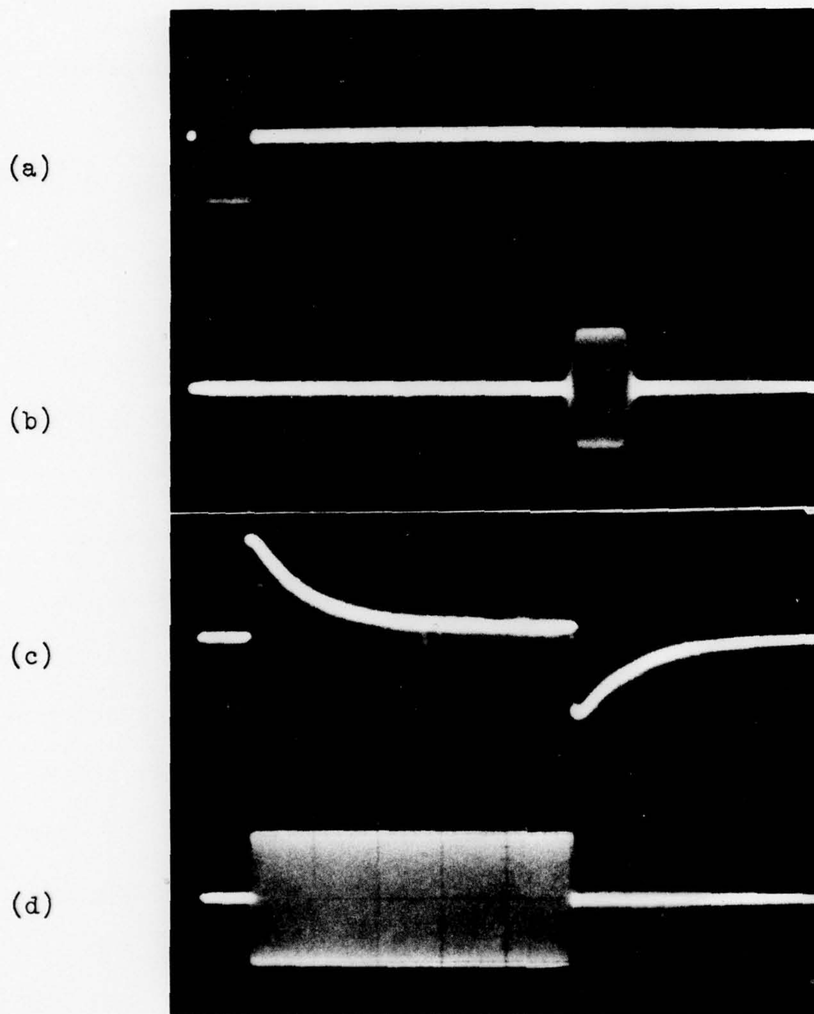

Fig. 3.2: (a) rf Input Pulse to the Delay Line, v = 5 v/div., t = 1 μsec/div.

(b) Attenuated and Delayed Output, v = 1 v/div., t = 1 μsec/div.

(c) Transverse Acoustoelectric Voltage, v = 4 mv/div., t = 0.5 msec/div.

(d) rf Output Pulse from the Delay Line, v = 1 v/div., t = 0.5 msec/div.

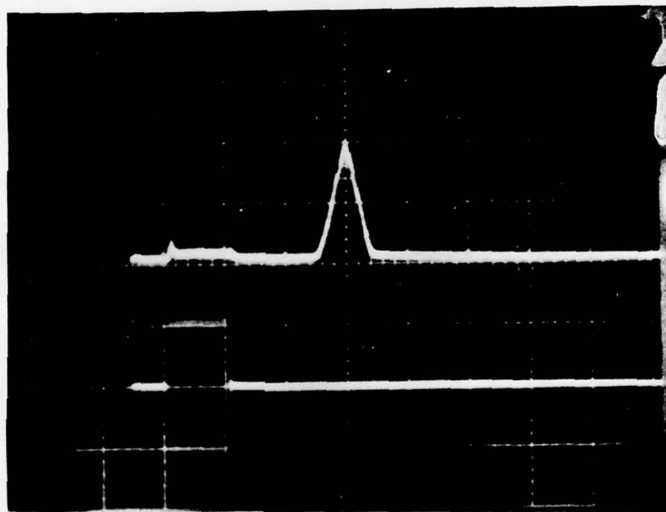

Fig. 3.3 Auto-convolution of Two rf Pulses, t = 1 μsec/div.

evaluation using an external dc bias and optical generation for changing the semiconductor surface properties are presented. We use the space change coupled surface acoustic wave parameters to monitor both the dynamic and static nature of these changes. A comparison is made between the different monitoring techniques in order to determine the sensitivity and accuracy of each one of them.

3.2 Transient Response of the SAW Propagation Loss

3.2.1 Pulsed Field Effect on SAW Attenuation

The primary objective of the pulsed field effect is to study the transient behavior of the induced charge in the semiconductor surface and the interaction processes leading up to the steady state condition. A fast rise time pulse is applied across the semiconductor-delay line structure, and the resulting change in the surface conductance and the density of trapped carriers in the surface states is observed by the propagation loss of the delay line.

Figure 3.4 is the observed output of the delay line when a high voltage dc pulse is applied across the semiconductor-delay line structure. The semiconductor is a 10 ohm-cm, N-type silicon wafer with a (100) surface orientation and high polished surface. Surface damage had been reduced by growing 2000 Å SiO_2 in dry O_2 ambient, which was then removed.

For a positive high voltage dc pulse, Fig. 3.4a, electrons are expelled from the surface and a depletion layer is formed at the surface. The initial rapid decrease in the SAW attenuation

AD-A045 324 RENSSELAER POLYTECHNIC INST TROY NY MICROWAVE ACOUST--ETC F/G 20/12
NONDESTRUCTIVE EVALUATION OF ELECTRICAL PROPERTIES OF SEMICONDU--ETC(U)
JUL 77 H GILBOA, P DAS N00014-75-C-0772
UNCLASSIFIED RPI-MA-ONR-15 NL

2 OF 3
AD
A045 324

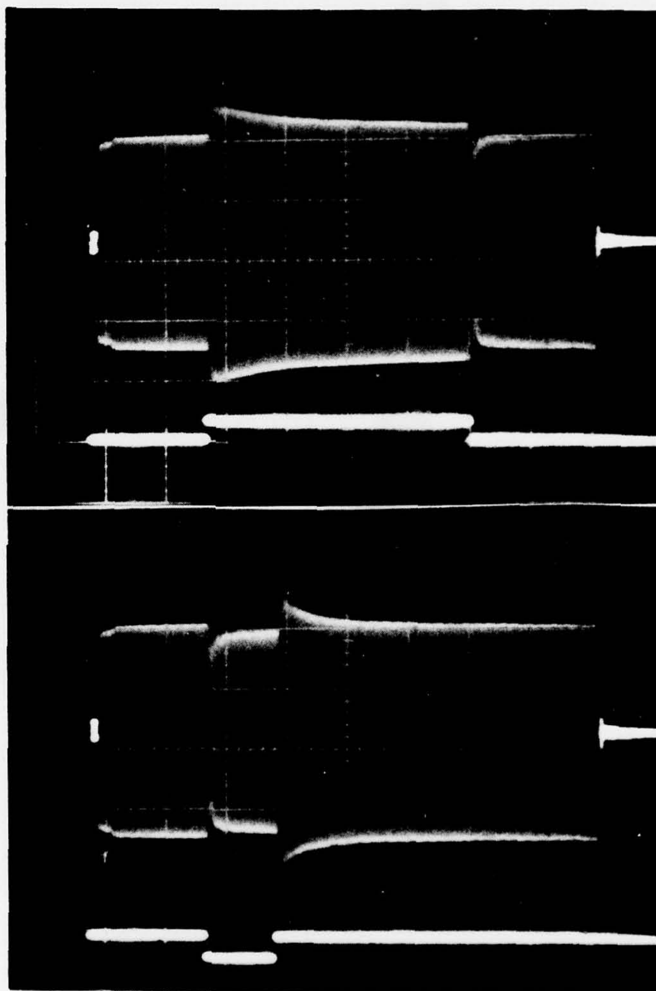

Fig. 3.4 Attenuated rf Plse while an External dc Pulse is Applied Across the Semiconductor Delay Line Structure $v = 0.1$ v/div., $t = 0.1$ msec/div. (a) $V_{dc} = +300$ V; (b) $V_{ac} = -300$ V.

corresponds to the reduction in the surface conductance due to the instantaneous reduction in the density of free carriers near the semiconductor surface. Thereafter, electrons are thermally emitted from the surface states into the conduction band and the surface conductance relaxes toward a new steady state value, which is higher than that at the beginning of the dc pulse. For small variations in the surface conductance, a linear relation between the surface conductance and the SAW propagation loss can be assumed, thus, the relaxation in the delay line attenuation to the steady state condition is with the surface state time constant. This time constant increases exponentially with temperature and, therefore, can be used to determine the energy position of the surface states. At the termination of the pulse, the unbalanced positive charge in the empty states will accumulate the semiconductor surface. An abrupt increase in the propagation loss is observed due to the abrupt increase in the free carrier density. Thereafter, the capture of the free carrier by the empty surface states gives rise to the fast relaxation of the loss back to its value prior to the application of the pulse.

The negative high-voltage dc pulse, Fig. 3.4b, results in an accumulation layer and electrons tend to drop into unoccupied surface states. At the onset of the pulse, the delay line attenuation increases with a very short rise time due to the large increase in the free carrier density near the semiconductor surface. The charging of the surface states is very fast and after approximately 10 μsec, a new steady state is obtained. At the termination of the

pulse, the excess trapped electrons initially act as a source for electric field and a depletion layer is formed. The surface conductance drops abruptly and hence, an abrupt decrease in the propagation loss is observed at the termination of the pulse. The subsequent thermal release of carriers from the surface states gives rise to relaxation of the delay line attenuation back to its value prior to the application of the pulse. The difference in the surface state thermal emission time constant after the termination of the accumulation layer and during the build-up of a depletion layer is that in the first case the relaxation is carried out under an external dc bias such that the surface is in depletion condition. The relaxation time associated with the start of a positive applied pulse is very similar to that associated with the termination of a negative applied pulse. Usually various charge states are involved in the charge capture and emission process. Most likely the fast surface states will be the dominant ones; however, if several sets of fast states are involved in the relaxation process no simple exponential decay is observed. In order that simple relaxation will be observed the steady state occupation of the surface state should be controlled prior to the application of the dc pulse. Alternatively, the relaxation study is done at different temperatures. Each set of surface states will dominate the relaxation process at different temperature ranges and can be singled out accordingly.

In addition to the fast surface states, slow surface states (or the fixed oxide charge) can also participate in the relaxation process. These states are the result of excess silicon species found near the oxide silicon interface, or they are deep level traps due to contamination of the semiconductor surface. The density of slow state is independent of the surface potential; it is located within 100-200 Å of the insulator semiconductor interface, its density is stable under moderate temperature bias tests, and it can be greatly affected by oxidizing conditions. The density of the slow state is on the order of 10^{11}-$10^{12}/cm^2$ for thermally oxided silicon. These states are primarily traps in their behavior, hence the surface states relaxation time constant including charge transfer to slow surface states becomes very long. In most cases, the emission of carriers from slow state is negligible compared to the charge transfer to the fast surface state. However, the charge trapped in the slow states or in the oxide traps may affect the steady state surface potential, which can be different from the surface potential prior to the application of the dc pulse.

The change in steady state surface potential after the application of the dc pulse can be also due to the mobile oxide charges. Alkali ions such as sodium, are highly mobile in silicon dioxide and can cause considerable instabilities. Due to the high voltage dc pulse, these ions may change their position in the oxide and, hence, the steady state surface potential after the pulse is

removed will be changed.

3.2.2 Dynamics of Surface State--The Shockley-Read Model

The process involving carrier exchange between the surface states and the conducting bands can be simplified both theoretically and experimentally if the interaction of the surface states take place with a single band. This requires an extrinsic semiconductor and restricting the surface potential to values corresponding to accumulation and shallow depletion layer only. Under these conditions, minority carriers are effectively absent, and any charge exchange takes place exclusively between the surface states and the majority carrier bands.

Consider an n-type semiconductor. Under no external dc bias, the semiconductor surface will be slightly accumulated due to donor type surface states (this represents the situation in thermally oxided silicon surfaces). Suppose that at $t = 0$, a dc pulse is applied such that the semiconductor surface is accumulated. The charge relaxation time in most cases is very short and immediately after the application of the pulse, the induced charge in the conduction band attains an equilibrium distribution, Fig. 3.5a, the Fermi level being well defined in the space charge region as well as in the bulk. However, the surface states are not yet in equilibrium with the induced charge. Empty states are now under the Fermi level, hence, they will capture free electrons from the conduction band, Fig. 3.5b. When equilibrium conditions are reached, part of the

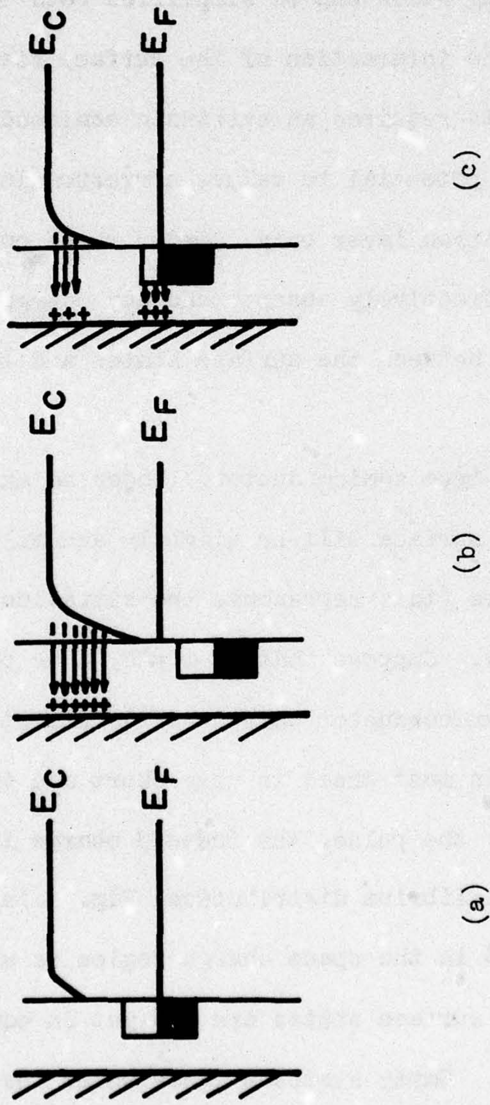

Fig. 3.5 Dynamics of Surface States in Accumulation

(a) Prior to the Pulse

(b) At the Onset of the Pulse

(c) Steady State

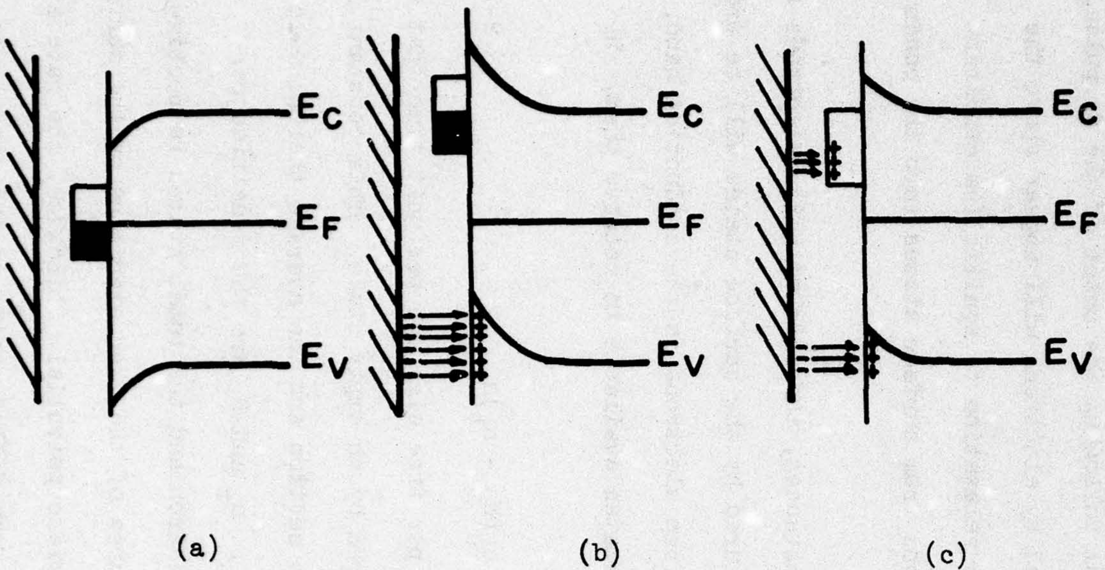

Fig. 3.6 Dynamics of Surface States in Depletion

(a) Prior to the Pulse

(b) At the Onset of the Pulse

(c) Steady State

induced charge resides in the space charge region and the rest in the surface states, Fig. 3.5c.

When the dc pulse is such that the semiconductor surface is depleted, an abrupt reduction of free carriers in the conduction band will appear, Fig. 3.6a. Just following the onset of the dc pulse, surface states fully occupied by electrons will appear above the Fermi level, Fig. 3.6b. The relaxation to equilibrium condition involves emission of electrons from surface states into the conduction band, Fig. 3.6c.

Under these circumstances, the rate at which electrons from the conduction band are captured by the surface states will be proportional to the number of free electrons in the conduction band, and to the number of empty states available to receive them. We may write this as

$$R_{cn} = c_n(N_t - n_t)n_s \qquad (3.2\text{-}1)$$

where c_n is the probability per free electron per unit time that a free electron will be captured by an empty state. This constant is related to the capture cross section and the average thermal velocity by the expression $c_n = v_t\sigma_n$. n_t and N_t are the densities per unit area of the trapped electron and the total states respectively. n_s is the density per unit area of the free electrons on the surface and is determined by the surface potential. Likewise, the rate at which electrons are emitted from filled states to the conduction band will be proportional to the number of filled states and can thus

be expressed as

$$R_{en} = e_n n_t \tag{3.2-2}$$

where e_n is the probability that a full state will emit its electron.

The net rate at which electrons are captured from the conduction band is simply the difference between (3.2-1) and (3.2-2)

$$\frac{dn_t}{dt} = c_n(N_t - n_t)n_s - e_n n_t \tag{3.2-3}$$

separating the free carrier density and the trapped surface density into equilibrium and time-varying parts

$$n_s = n_{s0} + n_s(t)$$

$$n_t = n_{t0} + n_t(t)$$

and substitute these equations into (3.2-3) we obtain

$$0 = c_n n_{s0}(N_t - n_{t0}) - e_n n_{t0} \tag{3.2-4}$$

for the equilibrium carrier density, and

$$\frac{dn_t}{dt} + \left[1 + \frac{n_{t0}}{N_t}\,\frac{n_s(t)}{n_{s0}}\right]\frac{n_t(t)}{\tau_e} = \frac{(N_t - n_{t0})}{\tau_e(N_t/n_{t0})}\,\frac{n_s(t)}{n_{s0}} \tag{3.2-5}$$

for the time varying carrier density, where

$$\tau_e = \frac{1}{c_n n_{s0} + e_n} \tag{3.2-6}$$

τ_e is the surface state emission time constant when the change in the

free carrier density is small. The equilibrium trap density is related to the density of the surface states by the Fermi function F_t

$$n_{t0} = \frac{N_t}{1 + \frac{1}{g}\exp\ (E_t - E_F)/k_B T} = F_t N_t \qquad (3.2\text{-}7)$$

where g is the degeneracy factor.

From the equilibrium equation (3.2-4) we obtain the relation between the emission and capture probability

$$\frac{e_n}{c_n} = n_{s0}\frac{(N_t - n_{t0})}{n_{t0}} = n_1 \qquad (3.2\text{-}8)$$

where $n_1 = N_c e^{-(E_c - E_t)/k_B T}$. The quantity n_1 is the electron concentration which would be present in the conduction band if the Fermi level were to coincide with the trap level E_t.

Consider a dc pulse V = u(t) - u(t-T) applied to a semiconductor such that an abrupt change in the free carrier density occurs. The excess free carrier density at any time is determined by the applied dc pulse and the relaxation of the carriers from the surface states, we can, therefore, write

$$n_s(t) = n_s(0) - n_t(t)$$

Substitute this into Equation (3.2-5) and solving for the excess trapped carrier density results in

$$\frac{n_t(t)}{N_t - n_{t0}} = 2\beta \frac{(1 - e^{t/\tau_f})}{1 + \beta(1+\xi) - \eta - [1 + \beta(1+\xi) + \eta]e^{t/\tau_f}}\, e^{(T-t)/\tau_e}$$

(3.2-9)

where

$$\beta = \frac{n_{t0}}{N_t} \; \frac{n_s(0)}{n_{s0}}$$

$$\xi = \frac{N_t - n_{t0}}{n_s(C)}$$

$$\eta = [1 + 2\beta(1 + \xi) + \beta^2(1 - \xi)^2]^{1/2}$$

$$\tau_f = \tau_e/\eta$$

β is a measure of the nonequilibrium free carrier density at $t = 0$ relative to its equilibrium value. For most cases under consideration ξ is a very small parameter hence, Equation (3.2-9) becomes

$$\frac{n_t(t)}{N_t - n_{t0}} = \frac{2\beta}{1 + \beta(1+\xi) + \eta} \, (1 - e^{-t/\tau_f})e^{(T-t)/\tau_e} \qquad (3.2\text{-}10)$$

Equation (3.2-10) reduces to the equation derived by A. Bers et al.[25], for the special case where the free carrier density near the surface remains constant during the time that the pulse is on. Hence, for $n_s(0) \gg n_t(t)$ or $\xi \ll 1$

$$\frac{n_t(t)}{N_t - n_{t0}} = \frac{\beta}{1 + \beta} \, (1 - e^{t/\tau_f})e^{(T-t)/\tau_e} \qquad (3.2\text{-}11)$$

where

$$\tau_f = \tau_e/1 + \beta$$

The time constant τ_e describes the discharging of the surface state after the dc pulse is removed, whereas τ_f is the time constant for

filling the surface states during the pulse. For large change in the free carrier density by the dc pulse $\beta >> 1$ and hence, $\tau_f << \tau_e$, whereas for small signal $\beta \cong 1$ and $\tau_f \cong \tau_e$.

The dynamics of continum surface state is very similar to the single state dynamics presented above, and for most cases the single state is found to be a very good approximation for the continuum surface states.

3.2.3 Free Carrier Density at the Semiconductor Surface

In Chapter II we derived the relation between space charge, carrier concentration and electric field at a semiconductor surface as a function of the surface potential. For an extrinsic semiconductor, the solution can be very much simplified. Neglecting the contribution of minority carriers to the space charge, Equation (2.3-7) becomes

$$\frac{\partial^2 u}{\partial y^2} = \frac{q^2 n_b}{k_B T \epsilon_s} (e^{u-u_B} - 1) \qquad (3.2\text{-}12)$$

Integrating from bulk toward the surface gives

$$\left(\frac{D_s}{D_0}\right)^2 = \frac{n_s}{n_b} - \left(1 + \ln \frac{n_s}{n_b}\right) \qquad (3.2\text{-}13)$$

where

$$D_s = -\epsilon_s \frac{\partial \phi}{\partial y}\bigg|_{y'=0}$$

is the electric displacement perpendicular to the surface, and

$$D_0 = e n_b \lambda_D \sqrt{2}$$

is a constant, which can be regarded as the electric displacement due to a surface charge $en_b \lambda_D \sqrt{2}$. We can distinguish two main regimes:

a. Depletion

When $n_s < n_b$

$$\left(\frac{D_s}{D_0}\right)^2 = -1 - \ln \frac{n_s}{n_b}$$

or

$$\frac{n_s}{n_b} = \exp\left[-\left(\frac{D_s}{D_0}\right)^2 - 1\right] \qquad (3.2\text{-}14)$$

b. Accumulation

$n_s > n_b$

$$\left(\frac{D_s}{D_0}\right)^2 = \frac{n_s}{n_b} - 1$$

$$\frac{n_s}{n_b} = 1 + \left(\frac{D_s}{D_0}\right)^2 \qquad (3.2\text{-}15)$$

Equations (3.2-14) and (3.2-15) describe the relation between the free carrier density on an extrinsic semiconductor surface, and the displacement field perpendicular to the surface.

3.2.4 Energy and Capture Cross Section Distribution of Fast Surface State

The steady state propagation loss of the delay line as a function of the applied dc bias across the semiconductor-delay line structure is shown in Fig. 3.7. The input voltage to the inter-

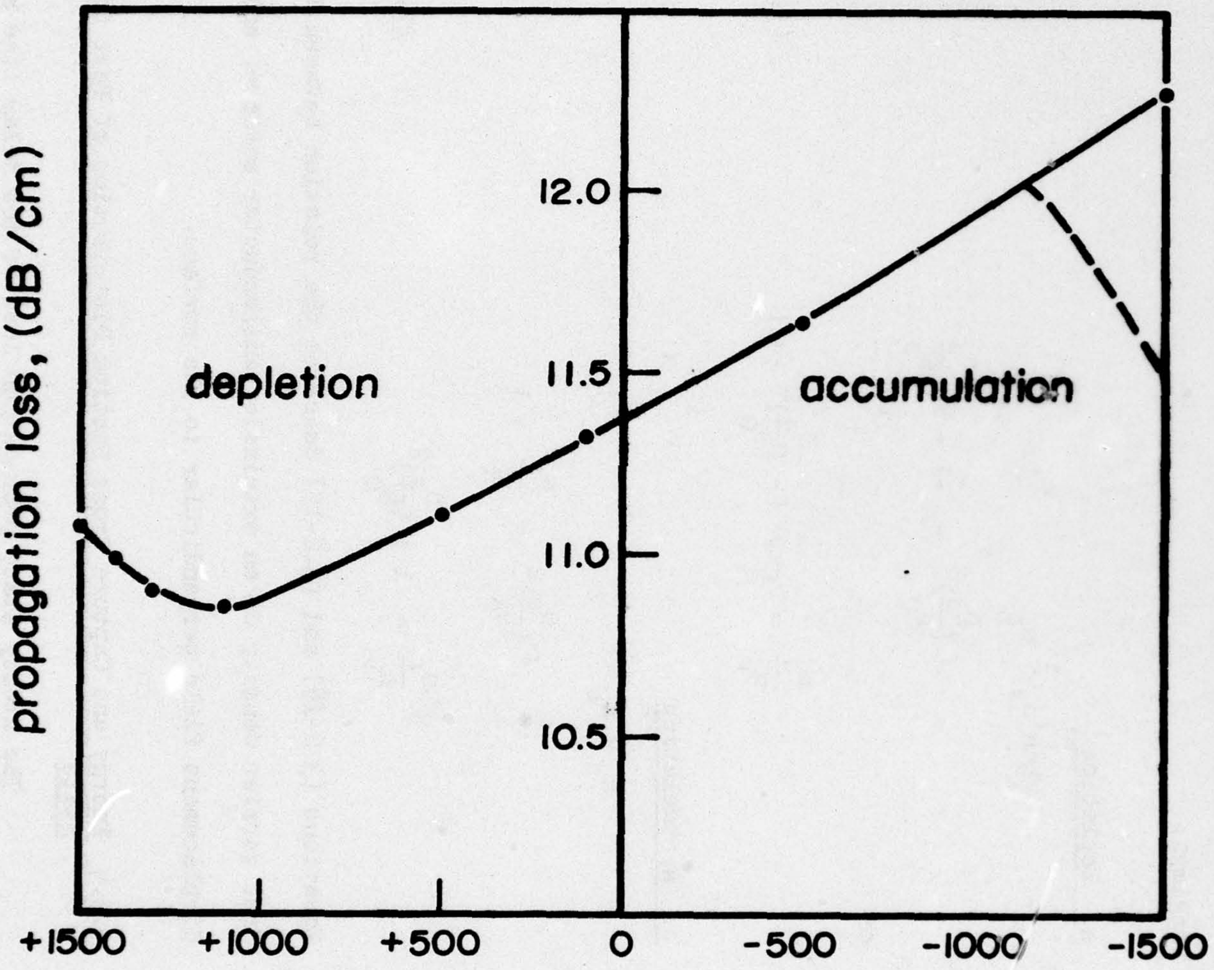

Fig. 3.7 Steady State Propagation Loss vs. External dc Bias

digital transducer is 10 V peak to peak. As the surface potential is changed from accumulation to depletion the propagation loss decreases. In deep depletion the propagation loss starts to increase due to the contribution of minority carriers. In order to observe the maximum in the delay line attenuation in the accumulation region, higher voltages are needed. However, the maximum can be observed at lower voltages if the input SAW power is reduced (dashed line), because the acoustoelectric interaction by itself biases the semiconductor such that a depletion layer is obtained if the SAW power input is reduced, the external applied dc voltage needed to accumulate the semiconductor surface is also reduced.

The relation between the electric field perpendicular to the semiconductor surface and the surface potential is given by Equation (2.3-8). Due to the low capacitance of the piezoelectric substrate ($d_p = 2$ mm, $\epsilon_p = 50\,\epsilon_0$) compared to the airgap capacitance ($h < 1\ \mu$m, $\epsilon = \epsilon_0$), all the voltage is dropped across the piezoelectric substrate. Using the continuity of the transverse displacement field, the displacement field on the semiconductor surface is given by

$$D_s(-h) = \epsilon_p V_G / d_p \qquad (3.2\text{-}16)$$

Equations (2.3-8) and (3.2-16) enable us to calculate the surface potential for a given dc bias. However, only the relative position of the surface potential can be obtained, due to the band bending prior to the application of the external dc pulse, resulting from the surface state and the semiconductor-SAW interaction. Only

for low level SAW input power and low density of surface states, flat band condition can be assumed prior to the application of the dc pulse.

The relaxation of the propagation loss during an external applied dc pulse such that the semiconductor surface is depleted is given by Equation (3.2-10). Assuming that the relaxation of the delay line attenuation follows linearly the relaxation of the free carriers, we can write,

$$\alpha(t) - \alpha(0) = a(1 - e^{-t/\tau_f}) \qquad (3.2\text{-}17)$$

where

$$\tau_f = \tau_e/\eta = \tau_e/(1 + \beta)$$

β is a negative quantity smaller than unity, hence the time constant for the relaxation of the carriers from surface states under depletion condition become larger than the free field relaxation time constant ($\tau_f > \tau_e$). This time constant becomes larger as the semiconductor surface is biased into deep depletion, as can be observed experimentally.

Figure 3.8 is a plot of the propagation loss relaxation during depletion condition on the semiconductor surface. The change in the trapped carriers in surface states is related to the change in the perpendicular displacement field by

$$D_{ss} = D_a - e(n_t - n_{t0}) \qquad (3.2\text{-}18)$$

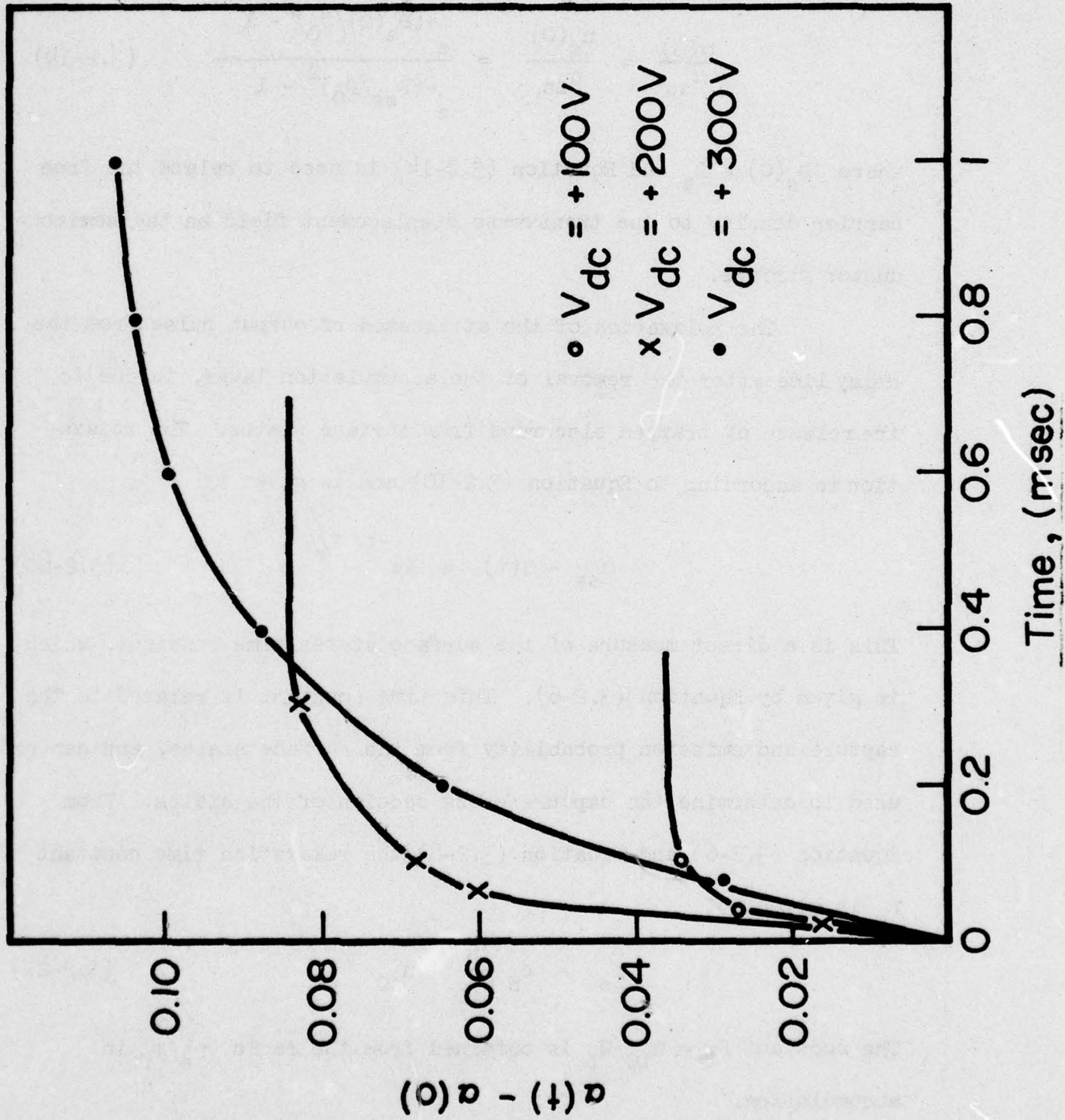

Fig. 3.8 Propagation Loss Relaxation During Depletion Bias

where D_{ss} is the steady state displacement field and D_a is the applied displacement field on the semiconductor surface. The change in the displacement field is given by

$$\frac{\alpha(0)}{\alpha_{ss}} = \frac{n_s(0)}{n_{ss}} = \frac{e^{-(D_s(0)/D_0)^2} - 1}{e^{-(D_{ss}/D_0)^2} - 1} \qquad (3.2\text{-}19)$$

where $D_s(0) = D_a$ and Equation (3.2-14) is used to relate the free carrier density to the transverse displacement field on the semiconductor surface.

The relaxation of the attenuated rf output pulse from the delay line after the removal of the accumulation layer, is due to the release of trapped electrons from surface states. The relaxation is according to Equation (3.2-10) and is given by

$$\alpha_{ss} - \alpha(t) = Ae^{-t/\tau_e} \qquad (3.2\text{-}20)$$

This is a direct measure of the surface states time constant, which is given by Equation (3.2-6). This time constant is related to the capture and emission probability from the surface states, and can be used to determine the capture cross section of the states. From Equation (3.2-6) and Equation (3.2-8) the relaxation time constant τ_e is given by

$$\tau_e = c_n \frac{N_t}{n_{t0}} n_{s0} \qquad (3.2\text{-}21)$$

The constant $F_t = n_{t0}/N_t$ is obtained from the ratio τ_e/τ_f in accumulation.

$$F_t = \frac{n_{t0}}{N_t} = (\frac{\tau_e}{\tau_f} - 1)\frac{n_{s0}}{n_s(0)} \tag{3.2-22}$$

The ratio n_{t0}/N_t is found to be in our case 0.41. Hence using Equation (3.2-21) the capture probability can be found for each external dc bias.

Figure 3.9 is the experimental observation of the relaxation time constant after the negative dc bias is removed (accumulation). As the semiconductor surface is accumulated more, the surface state time constant increases due to the decrease in the capture cross section of surface states that are closer to the conduction band.

Equation (3.2-18) gives the density of trapped carriers in the surface states due to an external applied field such that the semiconductor surface is accumulated. Here the displacement field is given by

$$\frac{\alpha(0)}{\alpha_{ss}} = \frac{n_s(0)}{n_{ss}} = \frac{(D_s(0)/D_0)^2 + 1}{(D_{ss}/D_0)^2 + 1} \tag{3.2-23}$$

where $D_s(0) = D_a$ and D_{ss} is the steady state displacement field under accumulation condition.

Table 2.1 summarizes the experimental results obtained from the dynamics of the propagation loss.

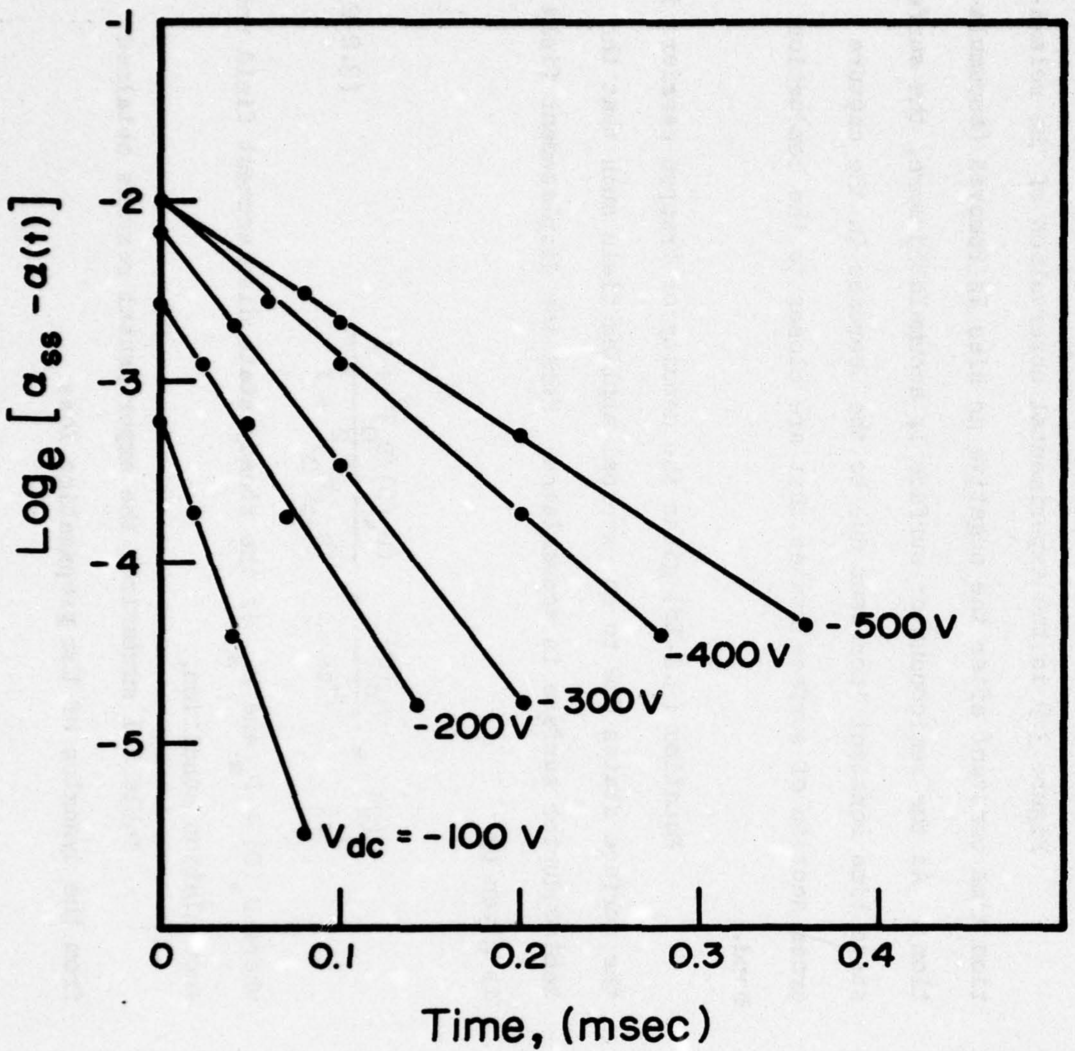

Fig. 3.9 Propagation Loss Time Constant After the Negative (Accumulation) dc Bias is Removed

Δu_s	n_t, cm^{-2}	τ_f, μsec	τ_e, μsec
4	1.17×10^9	10.36	151.4
3	8.49×10^8	18.31	110
2.5	5.12×10^8	19.34	78.1
2	2.26×10^8	22.31	63.4
1	0.84×10^7	19.67	33
-3	0.86×10^8	---	26.16
-8	0.85×10^8	---	55.16

Table 3.1: Excess trapped carriers in surface states, filling time constant and emission time constant for various changes in surface potential

Figure 3.10 is a plot of the electron capture cross section as a function of the change in the surface potential. It is observed that the capture cross section is constant in the depletion region and decreases in the accumulation region. The reason for the decrease in majority carriers (electrons) capture cross section, towards the conduction band is possibly due to the screening effect of free carriers at the interface as proposed by Nathanson.[49] Since the Debye length at the surface changes with $n_s^{-1/2}$ an exponential decrease of A_n is observed.

Figure 3.11 shows the density of surface states ($cm^{-2}eV^{-1}$) as a function of the change in surface potential. It is observed that the surface state density is lowest around the middle of the

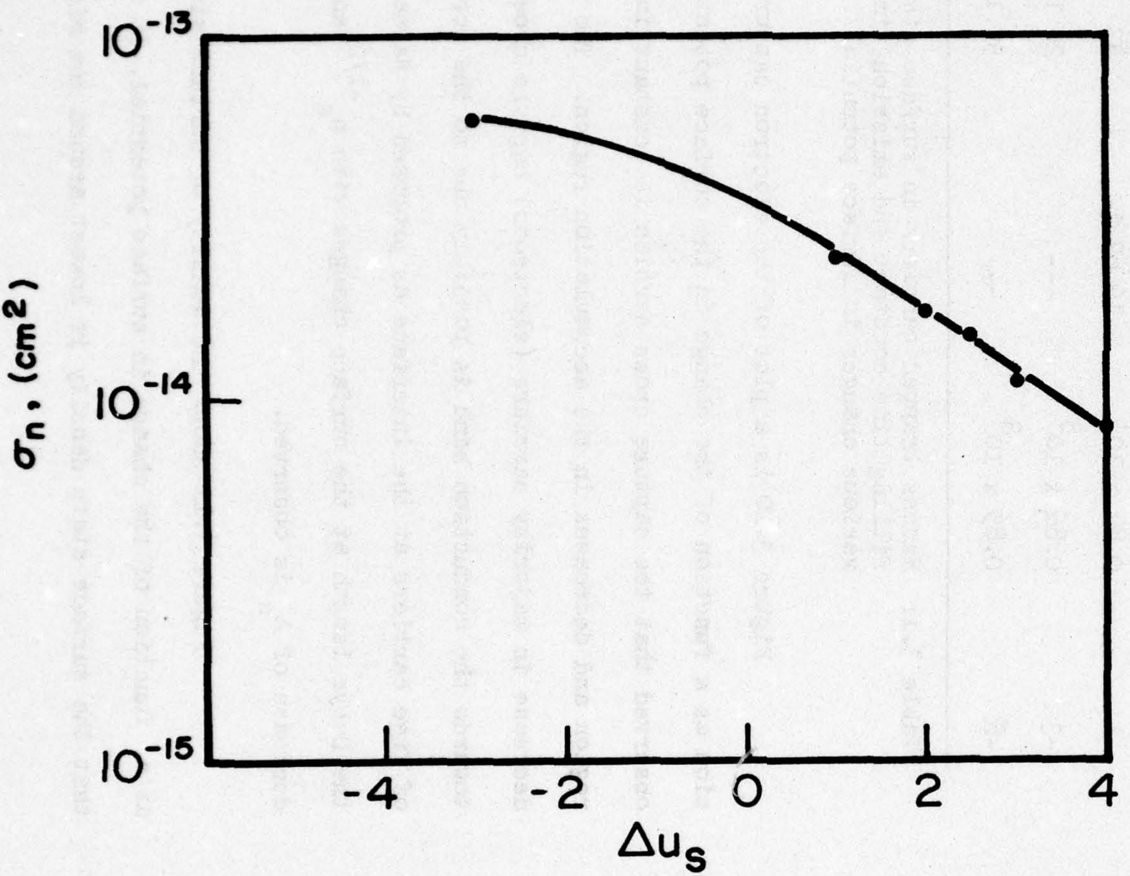

Fig. 3.10 Capture Cross Section vs. the Change in Semiconductor Surface Potential for n-type Si 10 ohm-cm

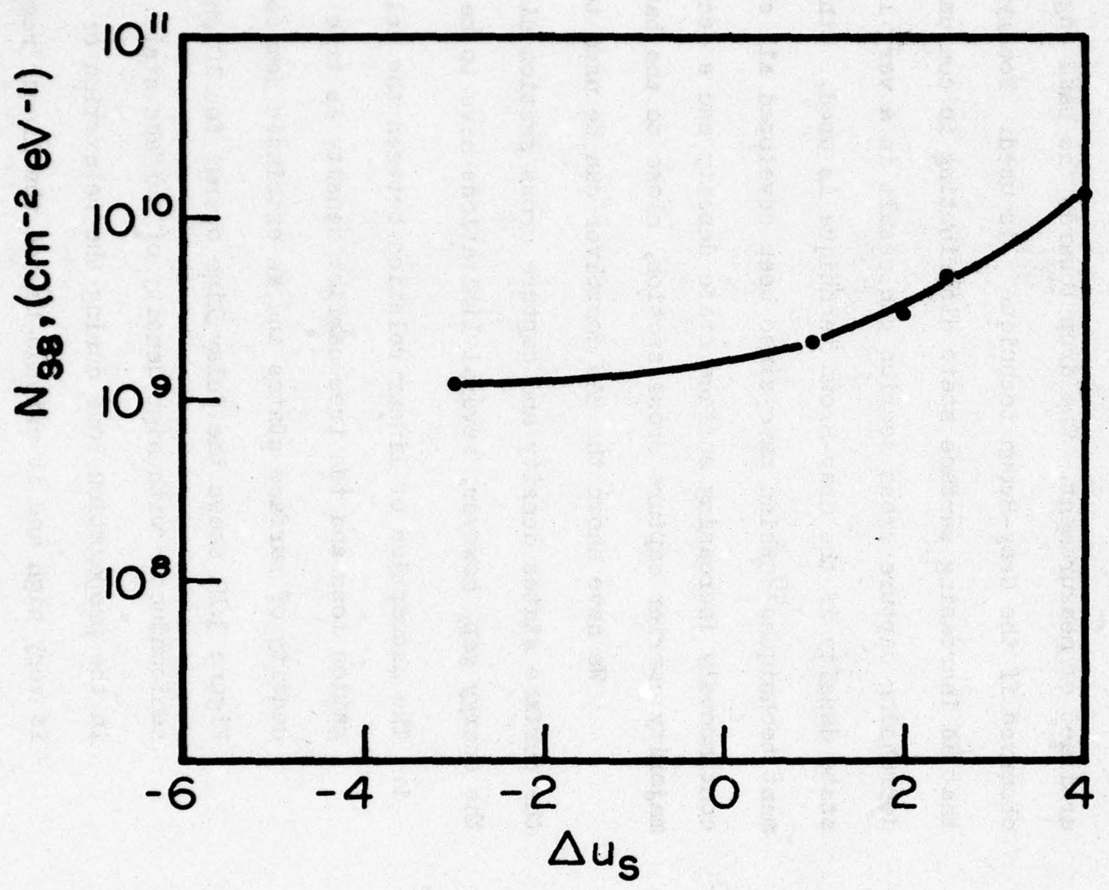

Fig. 3.11 Density of Surface States vs. the Change in Semiconductor Surface Potential for n-type Si 10 ohm-cm

gap and increases towards the conduction band. For a long time it was believed that surface state density goes down toward the band edges. It has now become apparent that this drop may have been an artifact of measurement. The drop towards the band edges is only observed if the Gray-Brown technique[39] is used. Boudry[50] has shown that an increasing surface state distributing in conjunction with a decreasing capture cross section can result in a very low surface state density if the Gray-Brown technique is used. Other measurement techniques[40] which have since been developed all show a continuously increasing surface state density and a decrease in the majority carrier capture cross section, close to the band edges.

We have shown the SAW convolver can be used to determine the surface states density and capture cross section distribution in the energy gap, however, several limitations have to be considered.

i. The assumption of linear relation between the delay line propagation loss and the free carrier density is true only for low density of surface states and an extrinsic semiconductor. Figure 3.12 shows the delay line output for 10 ohm-cm N-type semiconductor with high density of surface state. The change in the propagation loss during the relaxation of surface states is very high and it extends beyond the linear region of the attenuation-surface potential. Due to the large number of free carriers released from the surface state, the change in the surface potential is no longer small and a maximum in the propagation loss is observed.

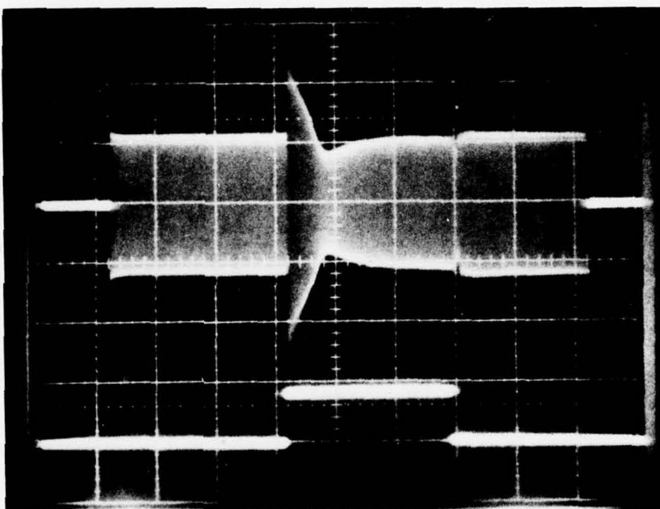

Fig. 3.12 Transient Response of the SAW Propagation Loss for 10 ohm-cm n-type Si with High Density of Surface States. t = 0.5 msec/div., v = 100 mv/div.

ii. In order to get absolute values of surface potential very low SAW input power is needed, such that no change in the semiconductor surface potential occurs prior to the application of the external dc bias. This requires a special care in the device fabrication such as uniformity of the air gap, thin substrate in order to reduce the external dc bias, and very low propagation loss in the device.

iii. Only the shallow depletion region can be studied by this technique due to the fact that the effective conductivity model is not valid for deep depletion. An accurate theory has to be used for the deep depletion region.

iv. There are no restrictions for the deep accumulation region, hence, it is possible to study surface state properties very close to the conduction band. However, the signal to noise ratio increases when very high voltages are applied to our devices. This can be eliminated by special care in the device fabrication.

3.2.5 Slow Surface States

Surface states relaxation can be dominated by slow surface states. In this case, the relaxation of the attenuated rf pulse is very long, of the order of msec or more. Figure 3.13a shows the output of the delay line for a negative dc bias (accumulation) applied

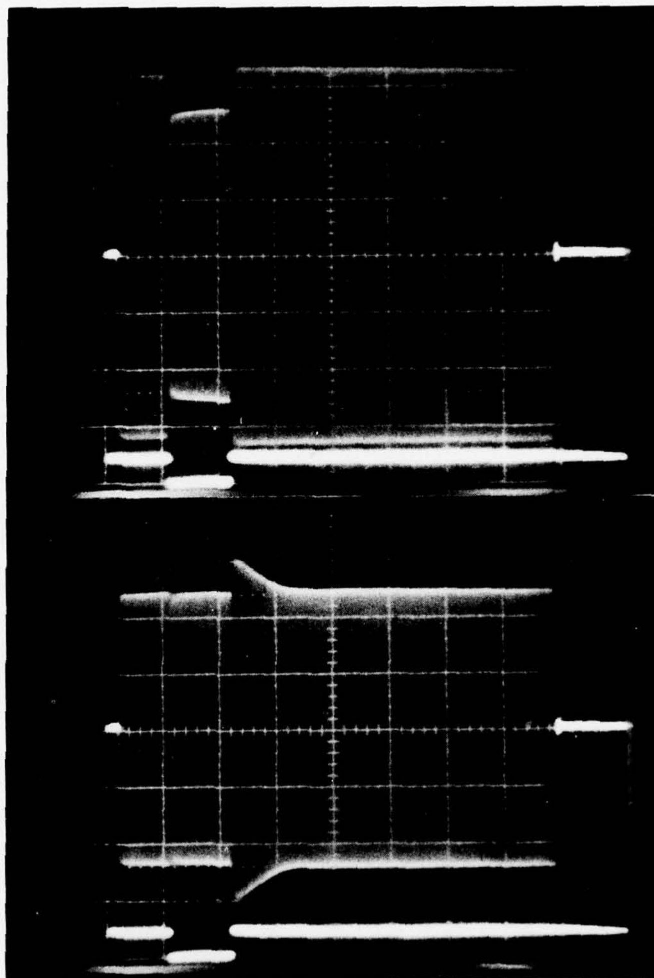

Fig. 3.13a Transient Response of the Delay Line Attenuation Dominated by Slow Surface States (a) dark (b) with light; 1 mw cm^{-2} v = 50 mv/div., t = 1 msec/div., V_{dc} = -400 V

across the semiconductor and delay line structure. The semiconductor is n-type 10 ohm-cm silicon, no special treatments have been done to reduce the density of the interface states. For real surfaces, slow surface states are trapping center, whereas the fast surface states are recombination centers. For very high density of slow states the surface states relaxation can completely dominate the relaxation process. Typically, the slow-state density is at least 10^{11} cm^{-2}. The effect of the slow states on the transient response of the delay line attenuation is to make the relaxation time longer. Hence, the first part of the decay is due to the fast states whereas the long tail in the relaxation is due to the slow states. It is possible to eliminate slow states from participating in the charge exchange with the conduction band by filling them by means of an additional dc pulse prior to the transient study, or eliminate the long tail by light as seen in Fig. 3.13b. This technique is very hard to implement in our case and thus it is recommended that for fast states study, a special surface treatment will be done in order to reduce the slow states density. Optical absorption by the slow states is used in Chapter IV to study the location of slow states. Figures 3.13b and 3.14 show the sensitivity of these states to optical excitation.

Fig. 3.13b Time Constant of the Delay Line Attenuation vs. Light Intensity

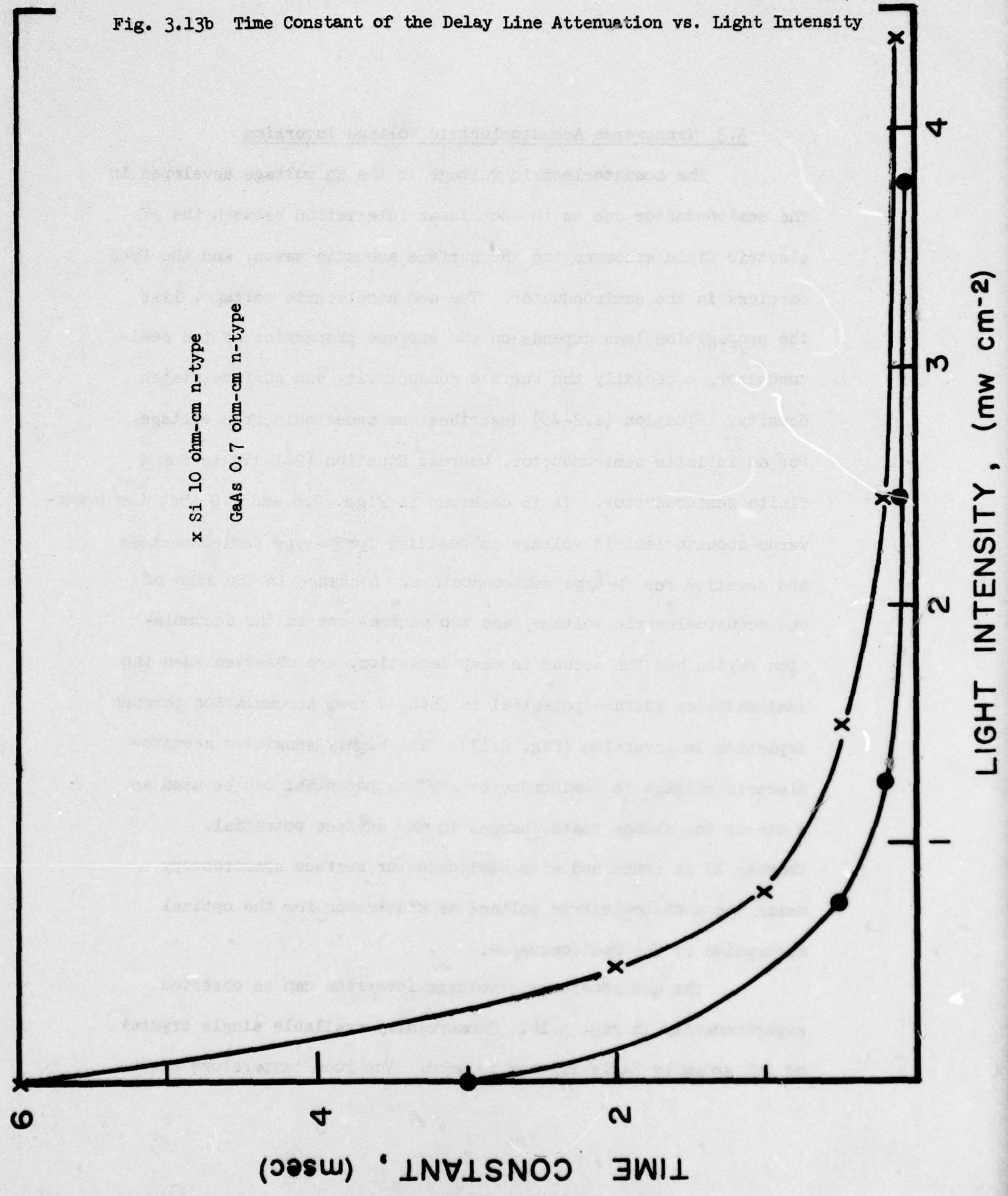

3.3 Transverse Acoustoelectric Voltage Inversion

The acoustoelectric voltage is the dc voltage developed in the semiconductor due to the nonlinear interaction between the rf electric field accompanying the surface acoustic waves, and the free carriers in the semiconductor. The acoustoelectric voltage, like the propagation loss depends on the surface properties of the semiconductor, especially the surface conductivity and surface states density. Equation (2.2-15) describes the acoustoelectric voltage for an infinite semiconductor, whereas Equation (2.1-17) is for a finite semiconductor. It is observed in Figs. 2.8 and 2.9 that the transverse acoustoelectric voltage is positive for n-type semiconductors and negative for p-type semiconductors. A change in the sign of the acoustoelectric voltage, and two maxima--one in the accumulation region and the second in deep depletion, are observed when the semiconductor surface potential is changed from accumulation through depletion to inversion (Fig. 2.17). The highly sensitive acoustoelectric voltage to semiconductor surface potential can be used as a sensor for steady state changes in the surface potential. Chapter IV is concerned with semiconductor surface spectroscopy using the acoustoelectric voltage as a detector for the optical absorption by the semiconductor.

The acoustoelectric voltage inversion can be observed experimentally in Fig. 3.14. Commercially available single crystal of CdS grown by Eagle-Pitcher is used. The room temperature resis-

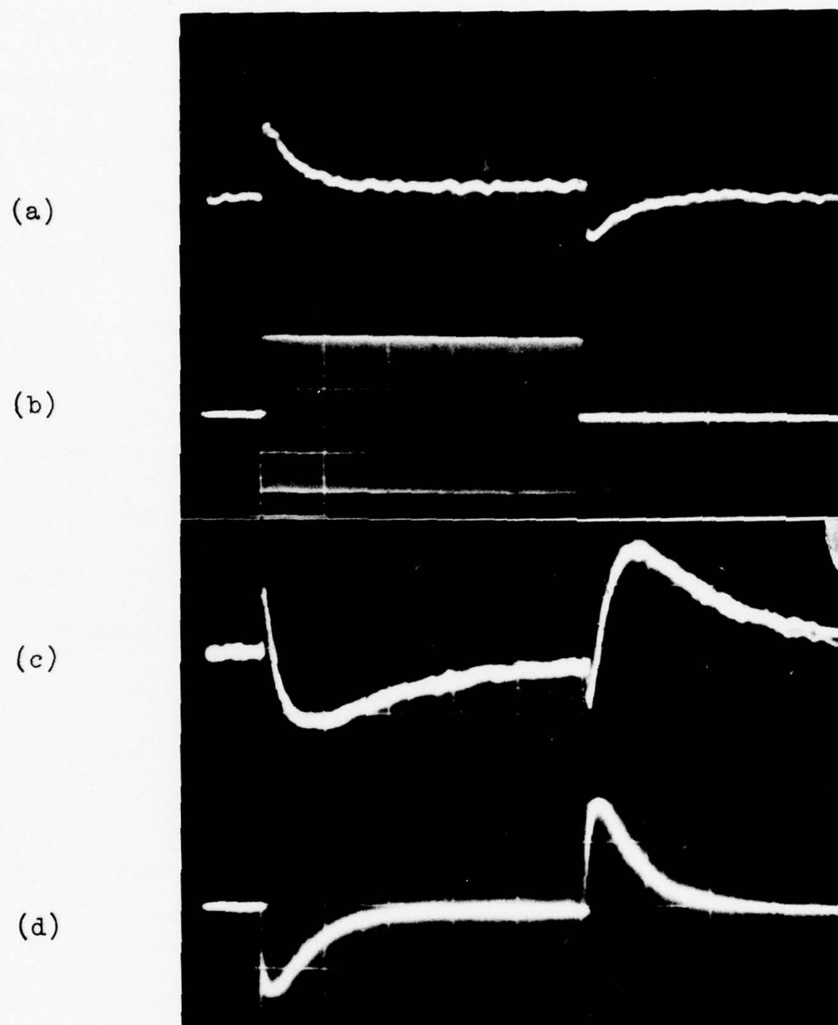

Fig. 3.14 Transverse Acoustoelectric Voltage Inversion

(a) Dark Condition, (b) Attenuated rf Output Pulse, (c) Light Intensity 2.88 mw cm^{-2}, (d) Light Intensity 5.55 mw cm^{-2}. t = 5 msec/div., V_a = 0.4 mv/div., V_c = 8 mv/div., V_d = 9 mv/div.

tivity is around 10^8 ohm-cm (Grade A crystal). The dark acousto-electric voltage for 10 V peak-to-peak input voltage and 25 msec duration pulse is shown in Fig. 3.14a. The acoustoelectric voltage is very low due to the high resistivity of the crystal. When light of intensity 2.88 mw cm^{-2} is applied on the semiconductor surface from the bottom of the delay line, a transient phenomenon is observed, and the transverse acoustoelectric voltage reverses polarity before decaying to zero, as seen in Fig. 3.14c.

Fig. 3.14b. A steady state condition in which a transition from positive to negative peak acoustoelectric voltage is obtained at the beginning of the rf pulse. Both the positive and the negative peak voltages remain constant as long as the light intensity is constant. At the end of the rf pulse, a similar transition can be observed with different time constants and peak voltages. When the light intensity increased to 5.55 mw cm^{-2}, a complete acoustoelectric voltage inversion occurs, a negative peak acoustoelectric voltage appears at the beginning of the rf pulse compared to the positive peak voltage in dark condition. During the acoustoelectric voltage inversion, the difference between the peak voltages at the beginning and at the end of the rf pulse, also changes sign, Fig. 3.15. In dark condition, the first peak is larger than the second peak, whereas after inversion, the second peak is larger than the first one.

A possible mechanism for the acoustoelectric voltage inversion is that under low level generation of hole-electron pairs, the photoconductive Grade A CdS surface potential will be in near

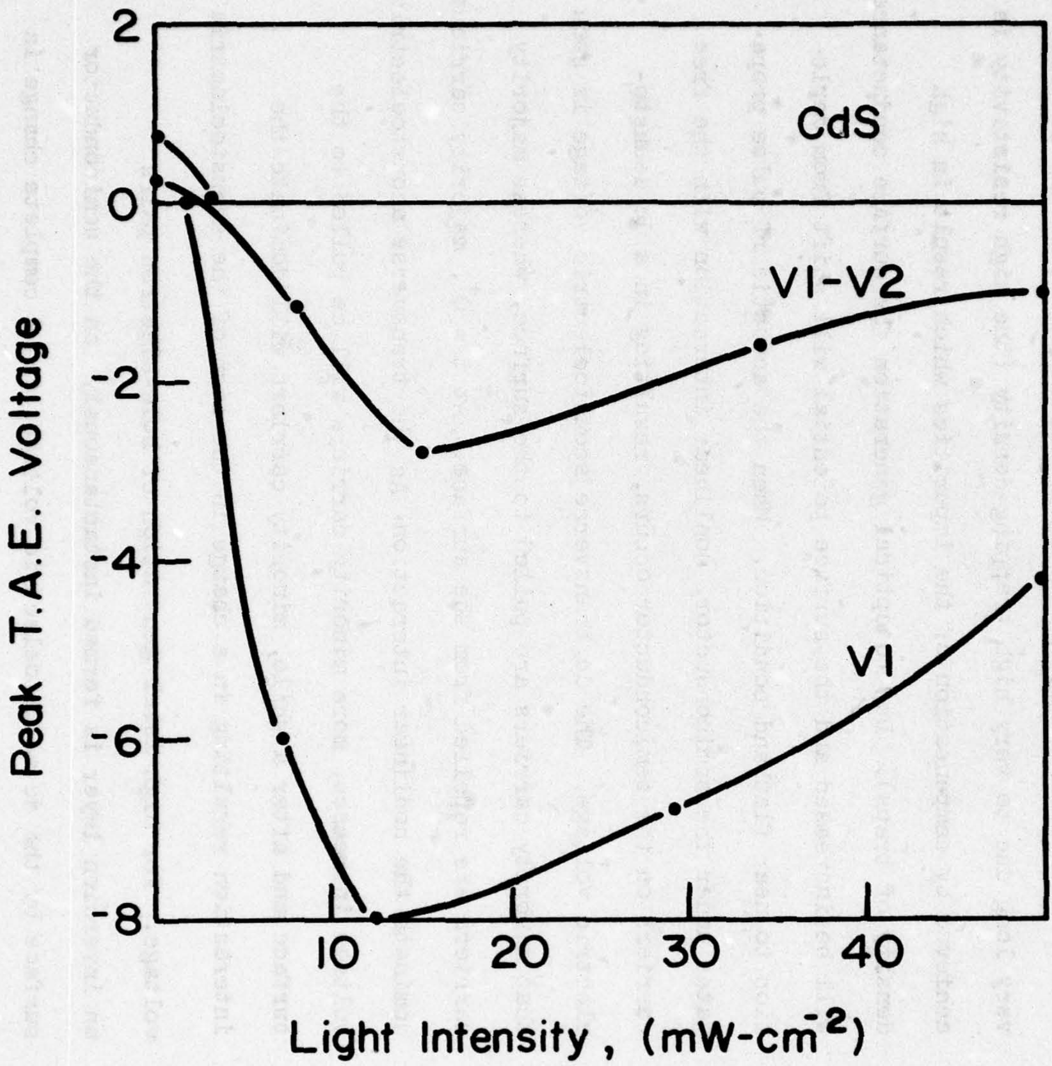

Fig. 3.15 Peak Transverse Acoustoelectric Voltage, at the Beginning of the rf Pulse, and the Difference Between the Two Peaks vs. Light Intensity

flat-band condition. The reason for that is that minority carrier lifetime in CdS is very short, whereas majority carrier lifetime is very long due to very high trapping density (the high resistivity is achieved by compensation of the impurities which result in high density of traps). Due to optical generation the surface conductance will be increased and the surface potential will shift from depletion to near flatband condition. When the acoustic rf pulse propagates under the semiconductor, nonlinear interaction with the free carriers on the semiconductor occurs, resulting in a dc acoustoelectric voltage. The dc transverse acoustoelectric voltage is such that minority carriers are pulled to the surface, whereas majority carriers are repelled from the surface. At $t = 0^+$, majority carriers dominate the nonlinear interaction. As the transverse acoustoelectric voltage increases, more minority carriers will be pulled to the surface and after a while, minority carriers will dominate the interaction resulting in a change in the sign of the acoustoelectric voltage. For high level generation of hole-electron pairs an inversion layer is formed instantaneously on the semiconductor surface by the dc acoustoelectric voltage, and a complete change in the voltage sign is observed.

To eliminate the inversion layer due to the dc transverse acoustoelectric voltage, a small signal rf pulse is needed as can be observed in Fig. 3.16. When the input voltage to the interdigital

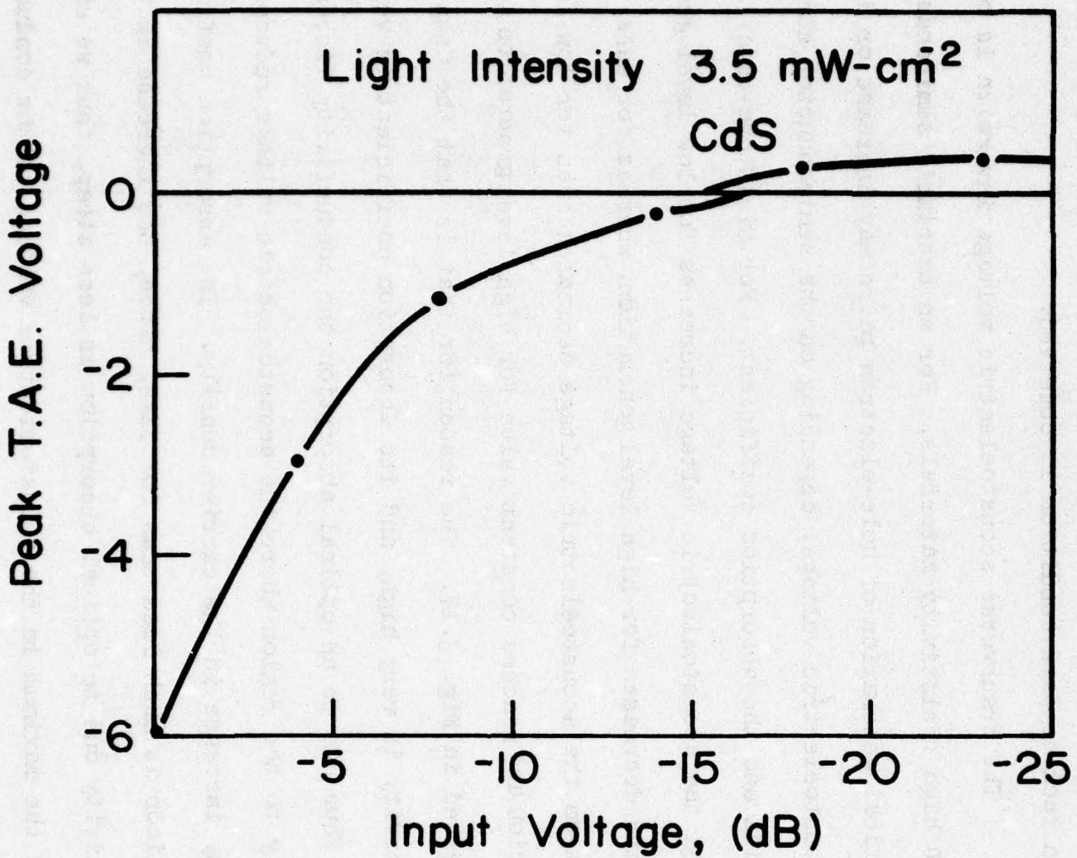

Fig. 3.16 Peak Transverse Acoustoelectric Voltage vs. Input Voltage to the Interdigital Transducer. The Transition Region shown by Double Value of Peak Voltages Associated with the Negative and Positive Peak Voltages appear at the Beginning of the rf Pulse.

transducer is reduced, the inversion layer disappears, and a change in sign back to dark condition is observed.

The transverse acoustoelectric voltage inversion is observed only in high resistivity materials. For an extrinsic semiconductor the optical generation of hole-electron pairs may increase or decrease the acoustoelectric voltage, depending on the semiconductor surface potential and the absorption coefficient. For Si 10 ohm-cm n-type material the acoustoelectric voltage increases for low level generation, and decreases for high level generation, whereas for GaAs 0.7 ohm-cm the acoustoelectric voltage decreases even for low level generation and reaches constant value for high level generation as can be observed in Fig. 3.17. The reason for that is that the GaAs conductivity is very high, and its absorption coefficient is very high. Thus due to an optical absorption the conductivity increases abruptly to the region where the acoustoelectric voltage reduces with any increase in the carrier density. The absorption coefficient for silicon is much less than for GaAs, hence, the increase in the conductivity due to optical absorption is less steep, thus we can observe the maximum in the acoustoelectric voltage as the conductivity increases.

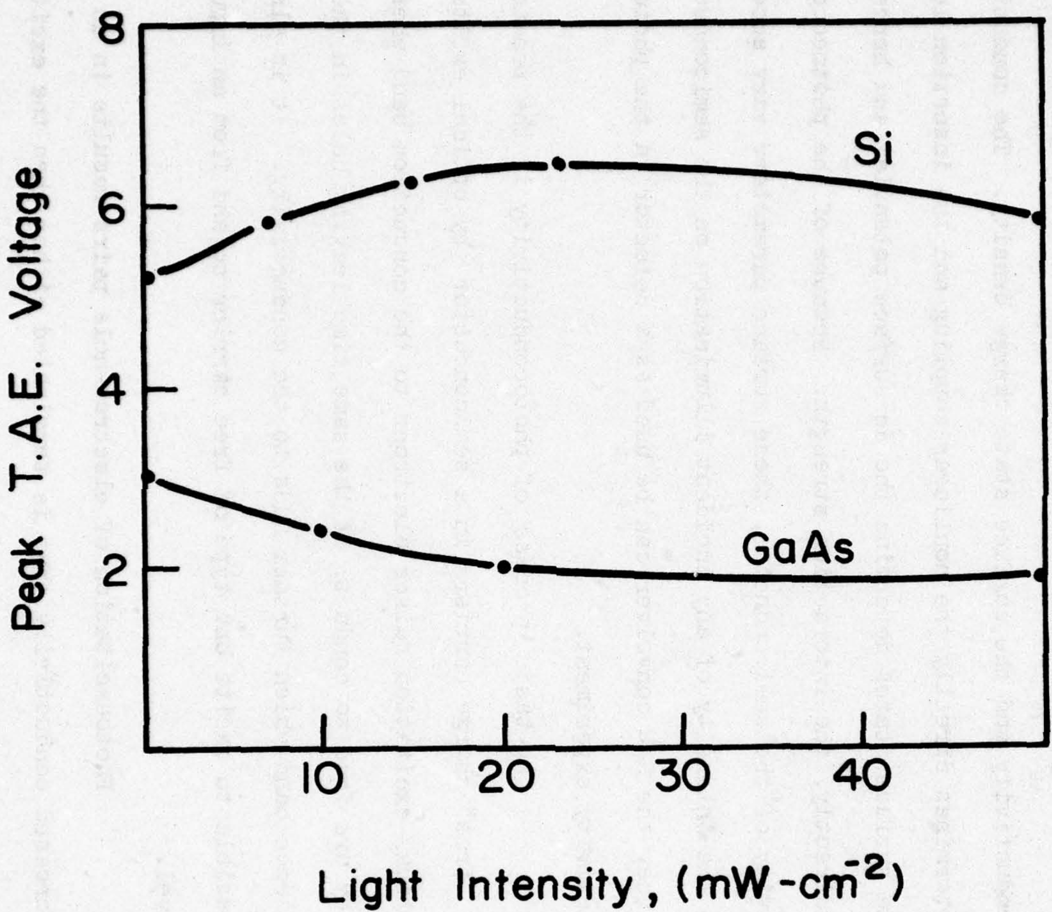

Fig. 3.17 Peak Transverse Acoustoelectric Voltage vs. Light Intensity for Silicon, 10 ohm-cm n-type, and GaAs 0.7 ohm-cm n-type

3.4 Photoconductivity Study using SAW Convolver

The coupling between acoustic surface wave and the semiconductor in the separated medium configuration depends on the electronic properties of the semiconductor surface, specifically the conductivity and the surface state charge density. The conductivity determines directly the nonlinear coupling and the insertion loss, the surface states determine the dc surface potential and hence, indirectly, the interaction strength. Because of the photoconductivity of the semiconductor, these surface parameters vary according to the intensity of any incident illumination on the semiconductor, hence, the SAW convolver can be used as a detector in the photoconductivity experiment.

The basic process of photoconductivity is the production of "free" charge carriers in a semiconductor by optical excitation. Optical excitation raises electrons to the conduction band where they are free to conduct, at the same time leaving holes in the valence band which further adds to the conductivity. It is also possible to excite one type of free carrier to and from an impurity level.

Photoexcitation of electron-hole pairs results in an increased conductivity that is terminated either when the excited carriers recombine, or when carriers are drawn out by the electrodes affixed to the crystal, without being replenished from the opposite electrode. The lifetime of a free carrier is the length of time that it is available to contribute to the conductivity. We may associate

a lifetime with each of the carriers, so that it is possible to relate the carrier density to the generation rate, g sec^{-1} cm^{-3}

$$n = g\ \tau_n$$
$$p = g\ \tau_p \qquad (3.4\text{-}1)$$

where p and n are the density of the photoexcited free carriers, τ_p and τ_n are the hole and electron lifetimes respectively. The photoconductivity decay after the light source is removed is given by

$$\sigma(t) = \sigma_0 + qg(\mu_n \tau_n + \mu_p \tau_p)e^{-t/\tau_0}$$

where τ_0 is the photoconductivity response time.

The response time is equal to the minority carriers lifetimes only when direct recombination dominates the recombination process, and $\tau_n = \tau_p$. When the recombination process occurs via various recombination centers in the energy gap, the response time is larger than the lifetime. The reason for that is that we must wait not only for the free electrons to be captured into the recombination states, but also for the trapped electrons to be emptied into the recombination states via thermal excitation into the conduction band and subsequent capture. Hence, the decay time of the photocurrent will be increased by

$$\tau_{on} = (1 + \frac{n_t}{n})\ \tau_n$$
$$\tau_{op} = (1 + \frac{p_t}{p})\ \tau_p \qquad (3.4\text{-}2)$$

where n_t and p_t are the density of trapped carriers after illumination.

For low level generation of hole-electron pairs, the change in surface conductivity is small, and a linear relation between the propagation loss and the surface conductivity can be assumed. We can write

$$\alpha(t) = a\ \sigma(t) \tag{3.4-3}$$

where $\alpha(t)$ is defined by the relation

$$\frac{V_{out}}{V_{in}} = e^{-\alpha l} \tag{3.4-4}$$

where l is the semiconductor length, and V_{in}, V_{out} are the input and output voltages to the delay line, respectively.

The measurement system is shown in Fig. 3.18. A xenon flash tube is used as a source of the visible light to illuminate the sample. The measurement begins with a trigger pulse starting the oscilloscope sweep and the multiple generator. One pulse is used to modulate the cw input to the delay line, the other is used to trigger the pulse generator which is turning on the flash tube. The flash tube produces an intense light pulse for about 4 μsec. At the peak of the light pulse, which occurs about 2 μsec from the time the

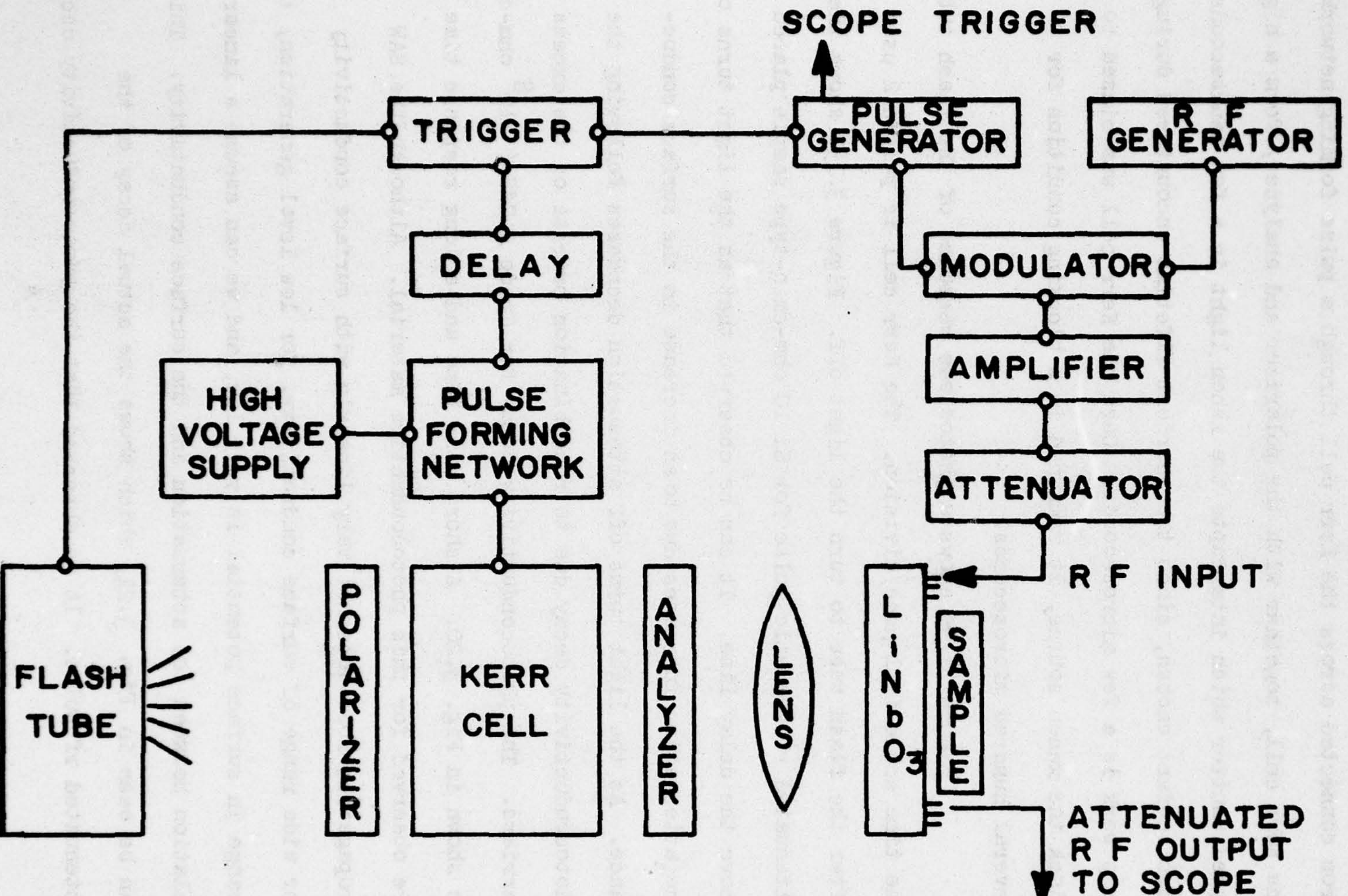

Fig. 3.18 Block Diagram for the Photoconductivity Study using the SAW Convolver

flash tube is turned on, a pulse is used to fire the hydrogen thyratron connected across the Kerr cell through a pulse forming network. The Kerr cell, together with the polarizer and analyzer, form a high speed shutter which interrupts the xenon light in a few nanoseconds. This is fast enough, since the shortest lifetime encountered during this work is a few microseconds. Once the Kerr cell was biased to block the xenon source, it remained in a blocking condition for several hundred microseconds.

Figure 3.19a shows a photodiode response of the flash tube. The time scale is 1 μsec/division. The Kerr cell is pulsed 2 μsec after the flash tube to turn the light off. Figure 3.19b shows the attenuated rf acoustic pulse for Si 10 ohm-cm n-type sample placed above the delay line. It can be observed that as the light turns on the attenuation increases due to an increase in the surface conductance. As the light turns off attenuation decreases following the photoconductivity decay due to recombination process of the excess carriers. The photoconductivity decay for Grade A CdS (10^8 ohm-cm) is shown in Fig. 3.20. A short rise time and a long response time are observed for this photoconductive material. Although the SAW propagation loss does not vary linearly with surface conductivity for wide range of surface conductivity, for low level generation, the change in surface potential is very low, and we can assume a linear relation between the attenuation and the surface conductivity. This can be seen in Fig. 3.21, which shows the actual decay of the attenuated rf pulse. It is observed that the photoconductivity decay

(a)

(b)

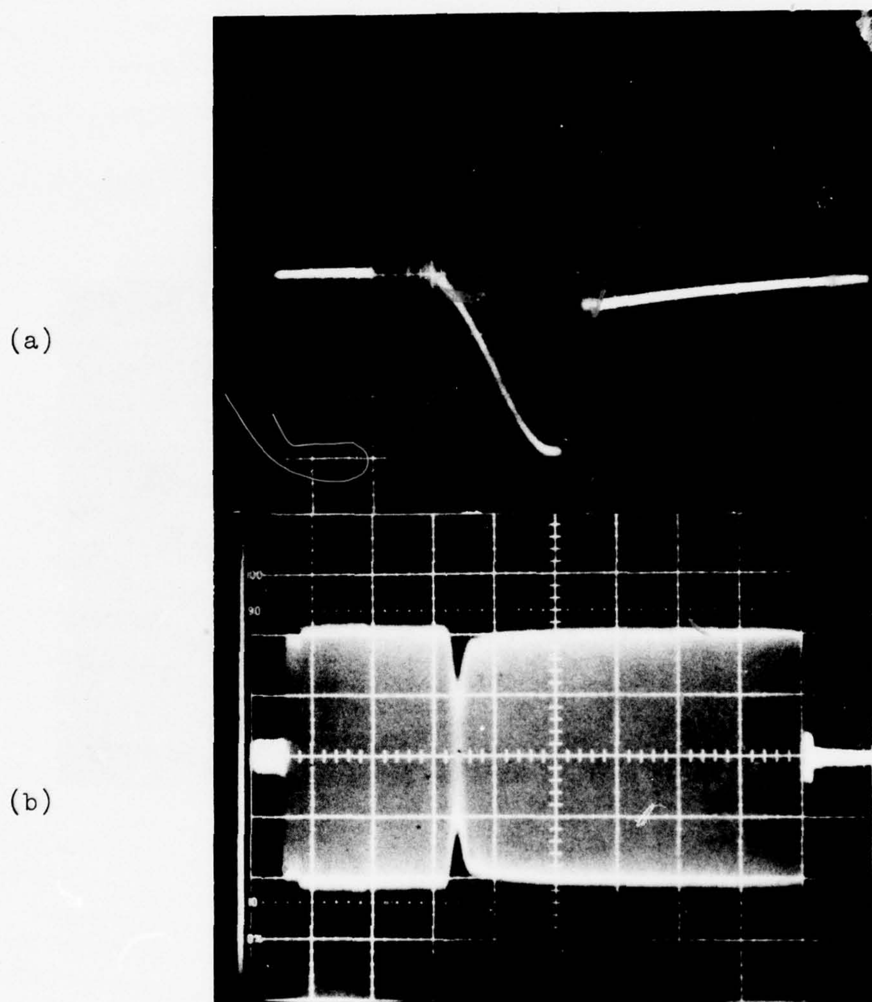

Fig. 3.19 (a) Photodiode Response to the Pulse of Light
$t = 1\ \mu sec/div.$

(b) Photoconductivity Decay as Observed by the Delay Line Output, for n-type 10 ohm-cm Si. $V = 100\ mv/div.$
$t = 20\ \mu sec/div.$

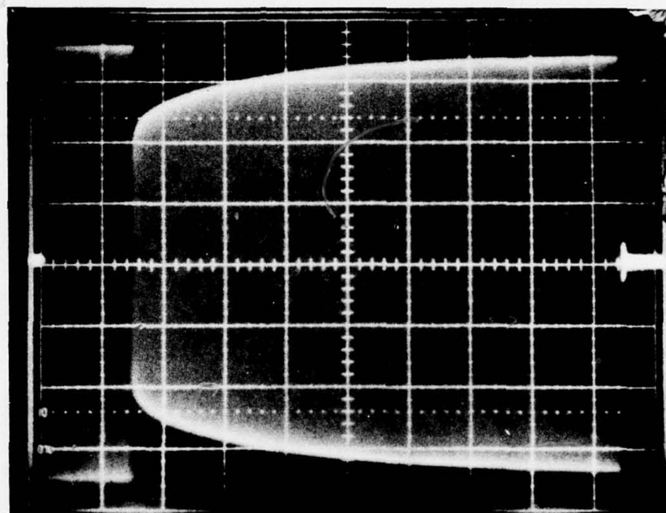

Fig. 3.20 Photoconductivity Decay as Observed by the Delay Line Output of Grade A CdS. V = 0.2 V/div., t = 0.5 msec/div.

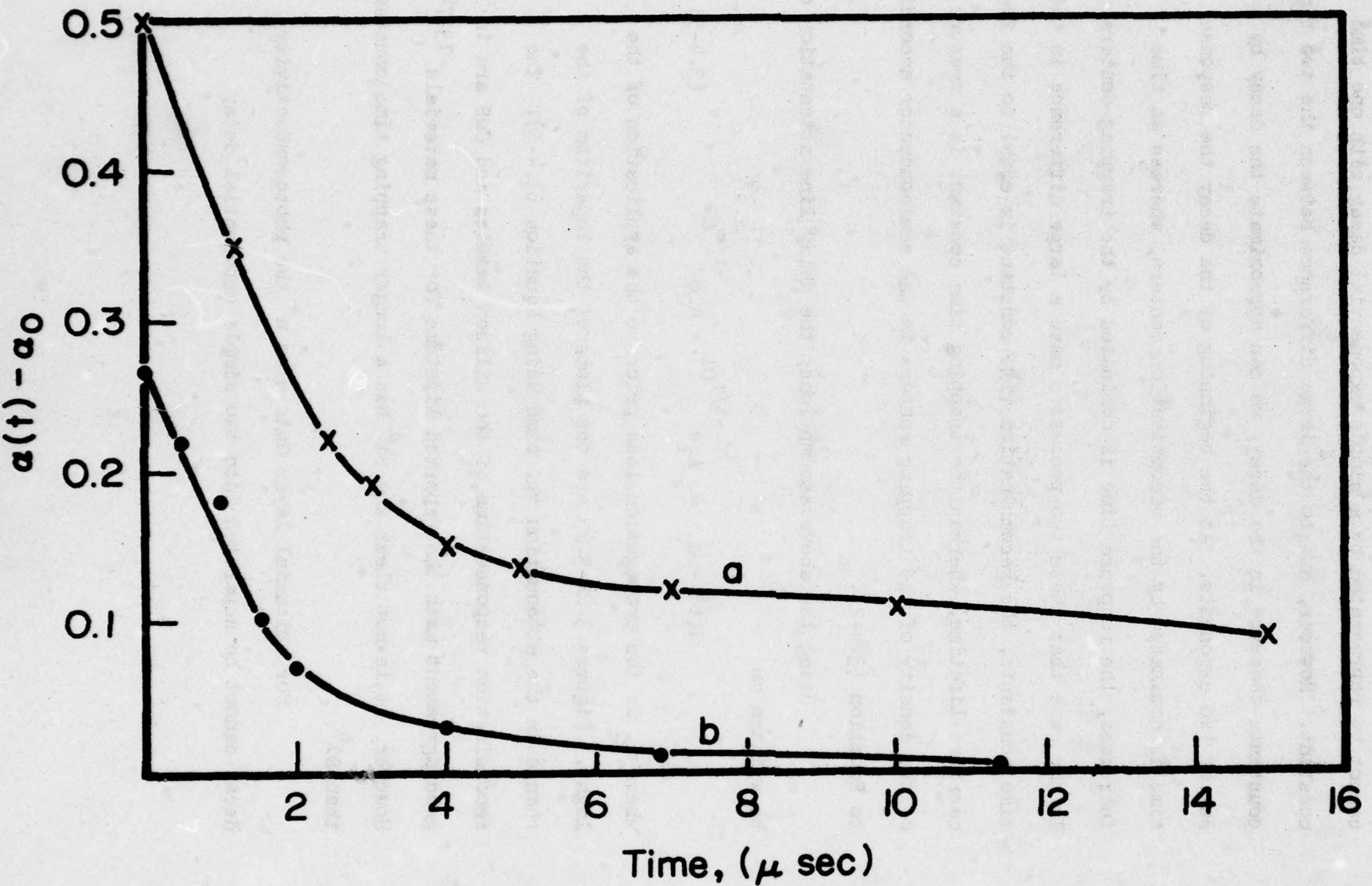

Fig. 3.21 Photoconductivity Decay vs. Time for Si 10 ohm-cm n-type

cannot be represented by a simple exponential decay with one time constant. However, due to the large difference between the two time constants observed in the decay, we can approximate the decay by a sum of two exponents. At the beginning of the decay the response time is dominated by the recombination centers, whereas as time increases, the response time is dominated by the trapping centers. In the case that these two processes have a large difference in their time constants, the recombination time constant is equal to the free carriers lifetime, whereas the trapping time constant is a measure of the density of the trapping centers in the semiconductor according to Equation (3.4-2).

Using the above assumptions, the delay line attenuation can be written as

$$\alpha(t) - \alpha_0 = A_1 e^{-t/\tau_{01}} + A_2 e^{-t/\tau_{02}} \qquad (3.4\text{-}5)$$

where α_0 is the propagation loss prior to the application of the light. Figures 3.22-3.23 are the plots of the logarithm of the change in the attenuation vs. time using Equation (3.4-5). The recombination response time of the silicon samples and CdS are in good agreement with the reported lifetime for these materials.[73-74] However, it is not clear why Si^a has a longer trapping time constant than Si^b.

For epitaxial layer GaAs n on n^+ the photoconductivity decay cannot be separated into two simple exponential decay

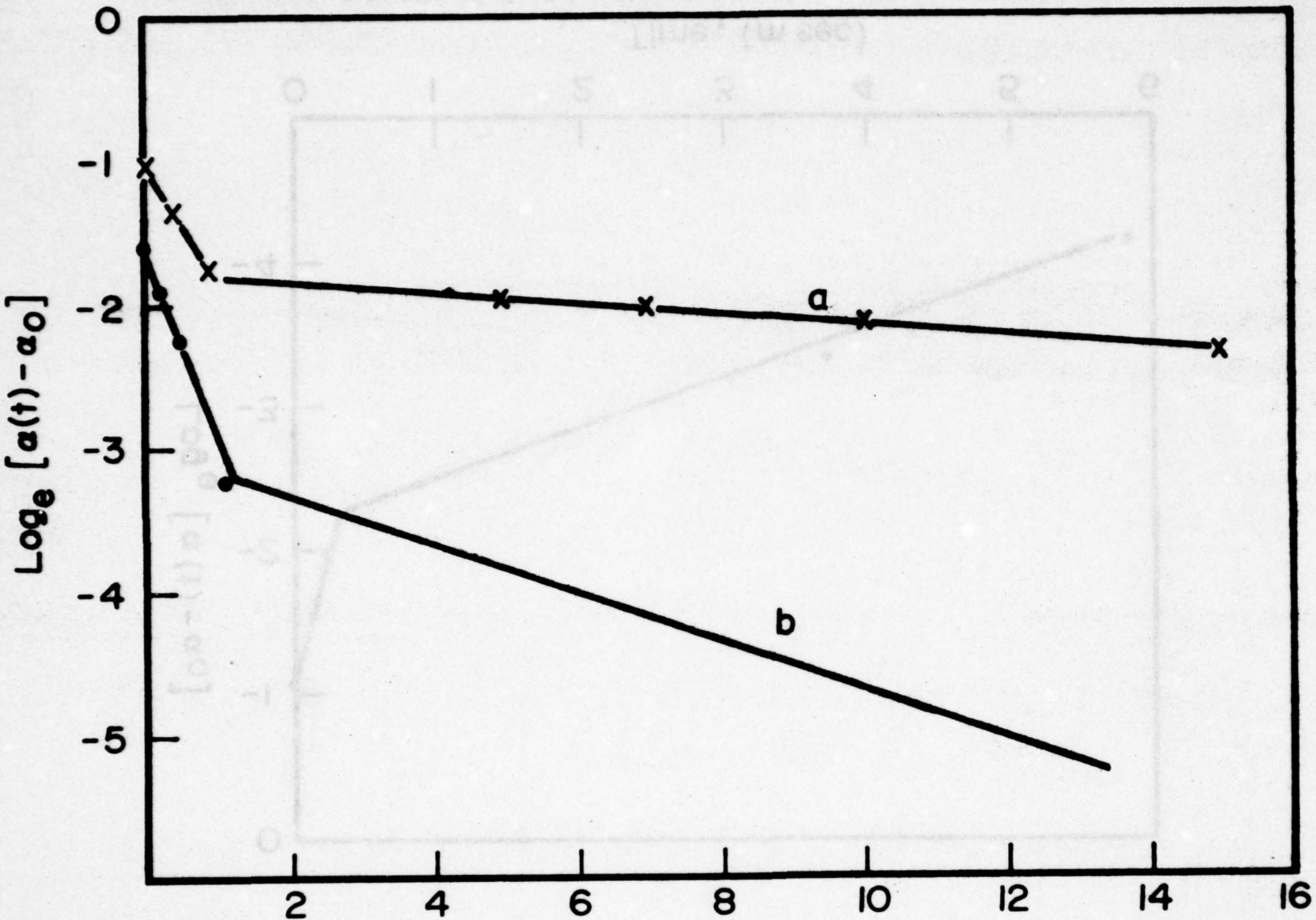

Fig. 3.22 Logarithm of the Delay Line Attenuation vs. Time for Si 10 ohm-cm n-type

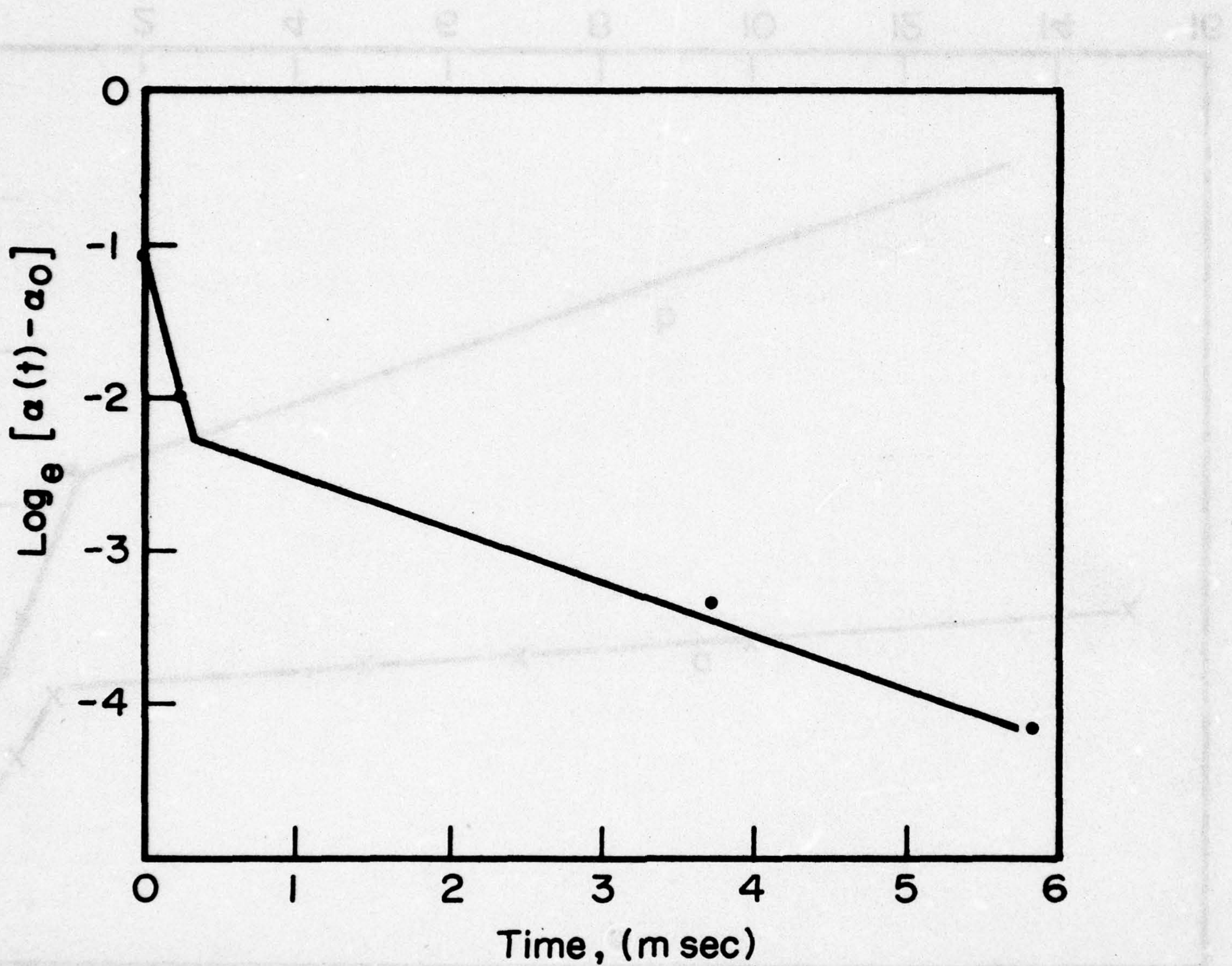

Fig. 3.23 Logarithm of the Delay Line Attenuation vs. Time for CdS Grade A 10^8 ohm-cm n-type

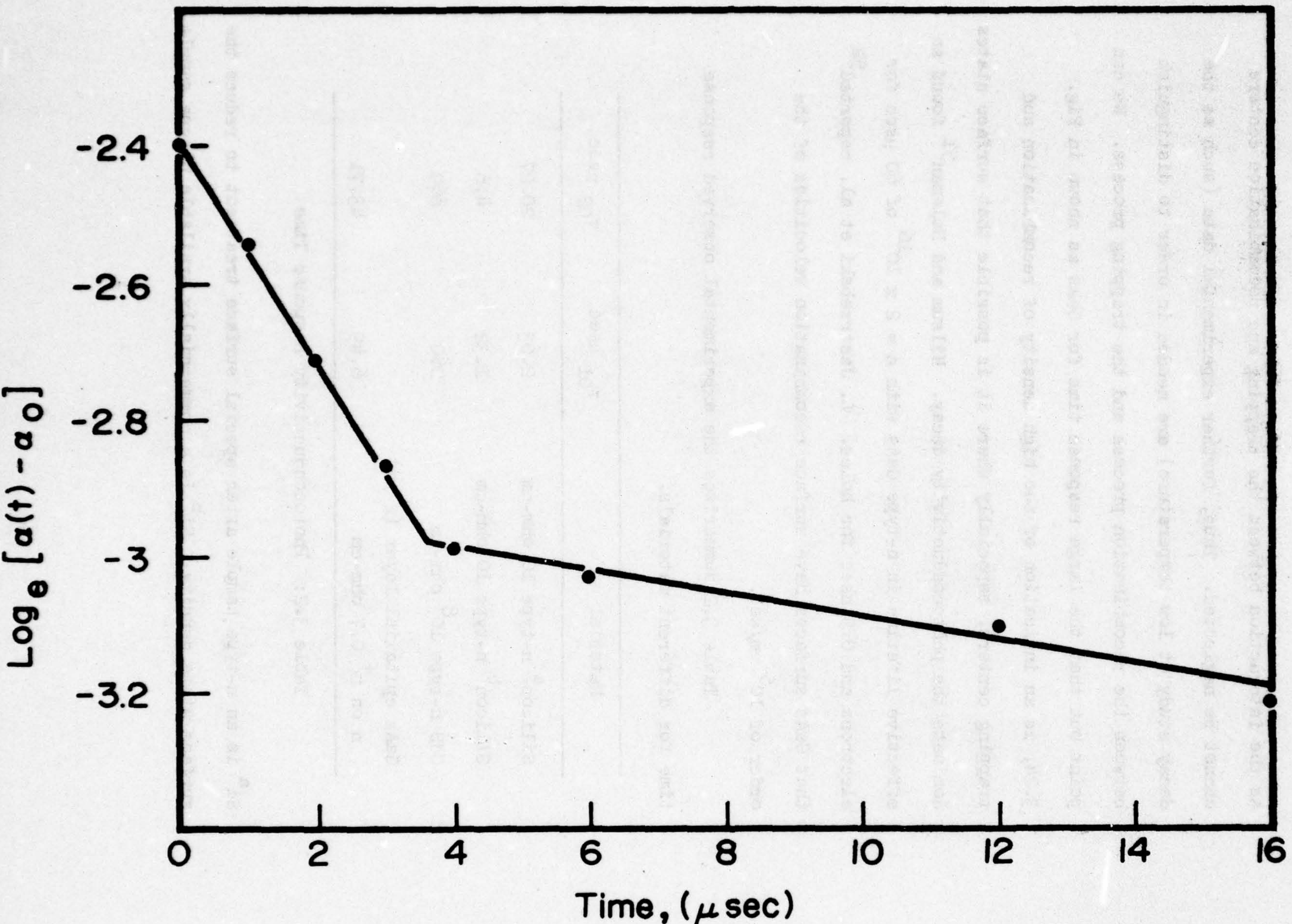

Fig. 3.24 Logarithm of the Delay Line Attenuation vs. Time for GaAs 0.7 ohm-cm n-type

as the interaction between the trapping and recombination centers cannot be neglected. Thus, further experimental data (such as the decay study at low temperature) are needed in order to distinguish between the recombination process and the trapping process. We can point out that the large response time for GaAs as shown in Fig. 3.24, is an indication of the high density of recombination and trapping centers, especially where it is possible that surface states dominate the photoconductivity decay. Hilsum and Holeman[51] found an effective lifetime in n-type GaAs with $n = 2 \times 10^{16}$ of 60 μsec for electrons and 0.5 nsec for holes. L. Jastrzebski et al. reported[52] that GaAs surfaces have surface recombination velocities of the order of 10^5 cm/sec.

Table 3.2 summarizes the experimental observed response time for different materials.

Material	τ_{01} μsec	τ_{02} μsec
Silicon[a] n-type 10 ohm-cm	2.03	20.27
Silicon[b] n-type 10 ohm-cm	1.32	4.6
CdS n-type 10^8 ohm-cm	260	869
GaAs epitaxial layer (2 μm) n on n^+ 0.7 ohm-cm	6.49	43.71

Table 3.2: Photoconductivity Response Time

Si[a] is an n-type sample after special surface treatment to reduce the surface state density. Si[b] is a commercially available n-type sample.

The main advantage of the photoconductivity study using the SAW convolver is the absence of any contact to the semiconductor, however, several limitations should be considered:

i. The semiconductor-SAW interaction is a surface phenomena, hence the recombination process of free carriers as observed by the delay line output is due to bulk recombination and surface recombination. The response time is a function of an effective lifetime τ_{eff}, which takes into account the cross section diffusion current, and is related to the bulk lifetime, surface recombination velocity, and cross section dimensions. The separate surface and bulk parameters can be obtained from a measurement of effective lifetime provided the dimensions of the sample are properly controlled. In filaments of small cross section or small bulk lifetime $\tau_{eff} = \tau_b$, where τ_b is the bulk lifetime. For thin samples, on the other hand, surface recombination may become dominant and can be determined directly. For intermediate conditions, additional data have to be used.

ii. In the absence of any biasing voltage, the n-type Si semiconductor is assumed to be in flat band condition or slightly in accumulation. When a surface acoustic wave propagates under the semiconductor an rf electric field and a dc acoustoelectric voltage

are generated on the semiconductor surface. The overall effect of the acoustic field will be to deplete the surface. The dc acoustoelectric field is also in the direction to reject majority carriers from the surface. We can conclude that the additional electric fields near the semiconductor surface will cause a difference in the optical generation density of carriers. Low level SAW input power is needed in order to keep the condition $n = p$ near the semiconductor surface.

The recombination process during the photoconductivity decay involves both bulk and surface recombination. It is possible to separate these two recombination mechanisms by applying an external dc bias across the semiconductor-delay line structure. When a depletion layer is generated at the surface of the semiconductor a decrease in the propagation loss is observed. Under illumination, minority carriers generated in the depletion layer are pulled almost instantaneously towards the surface, due to the influence of the large electric field in the depletion layer. At the same time, electrons move towards the bulk of the semiconductor. Due to the presence of the surface states the holes will either be trapped or will be accumulated near the semiconductor surface as free carriers (the surface will be in inversion of deep depletion condition).

Hence, after the optical excitation the steady state propagation loss will be higher than the loss prior to the excitation due to the high density of free carriers near the surface and due to the screening of the external dc bias by the additional trapped carriers in the surface states.

Figure 3.25 shows a plot of the envelope of the attenuated rf pulse recorded by an x-y plotter for three different biases (for Si^b). The effect of minority carriers accumulating near the semiconductor surface is observed by the new steady state formed after the photoconductivity decay is terminated. For negative bias such that the semiconductor surface is accumulated, the steady state after the optical generation, is changed only by a small amount due to the majority carriers trapped in the surface states.

The response time for all three different biases is very similar. This is an indication that bulk recombination dominates the photoconductivity decay, as indeed one would expect for silicon where lifetime is large and surface recombination is very low. It is possible, however, to observe the surface recombination contribution to the photoconductivity decay in GaAs. For large negative voltages (-900 V and above) the response time becomes larger due to the reduction in the surface recombination velocity. The reason for the high voltages needed to accumulate the surface such that the reduction in surface recombination can be observed is due to internal depletion caused by the acoustoelectric interaction. The signal to noise ratio

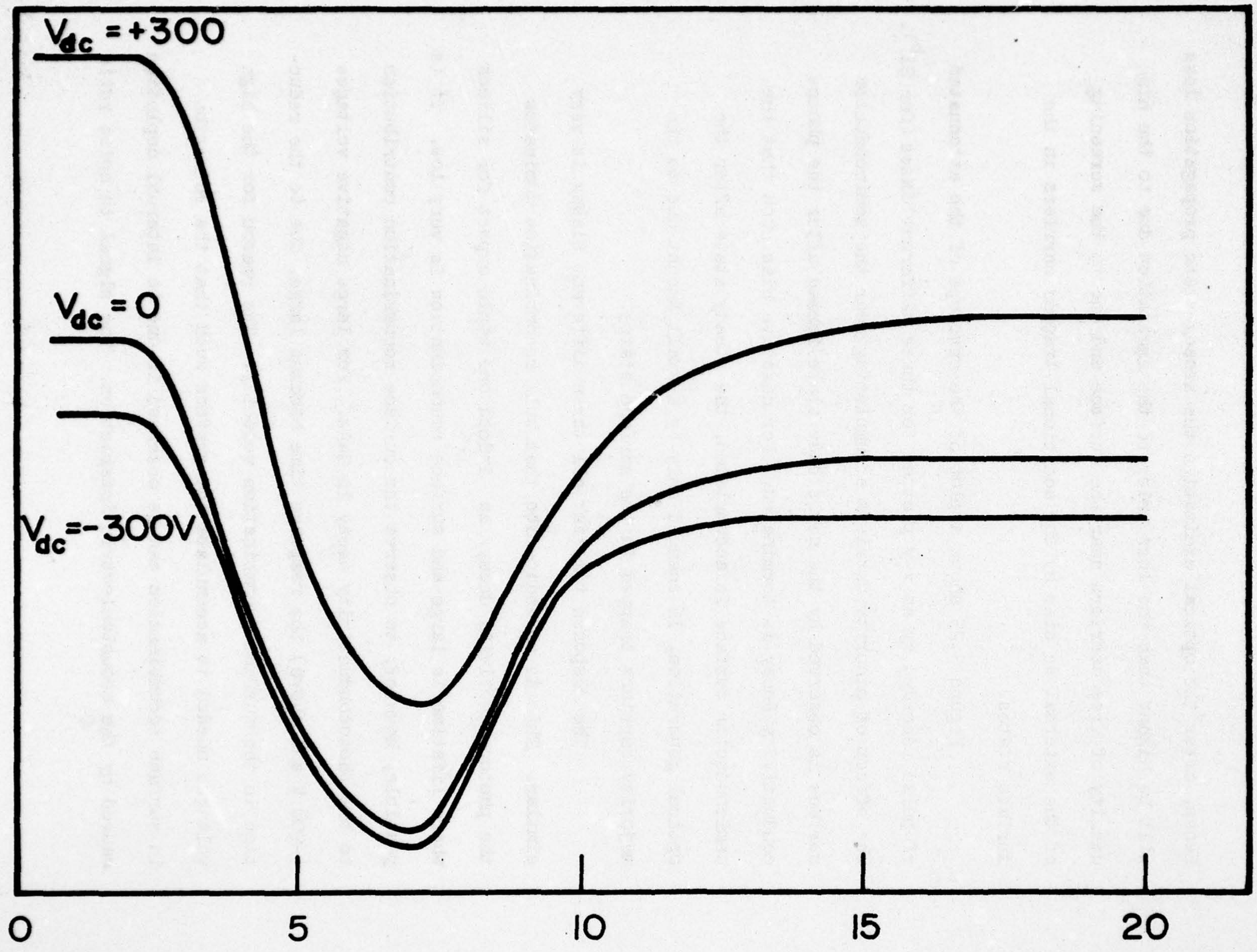

Fig. 3.25 Photoconductivity Decay for n-type Si (Si^b) while an External dc Bias

for this range of voltages is too high for valuable measurement by the x-y plotter. Thus, low level SAW input power is required for observing the contribution of surface recombination to the response time. In addition, the external dc bias can be reduced by using very thin piezoelectric substrates.

3.5 Semiconductor Surface Study using SAW Velocity Change

The space charge coupled interaction of SAW propagating on a piezoelectric substrate with a semiconductor placed in proximity gives rise to a change in the SAW velocity. The change in SAW velocity (like the attenuation, dc acoustoelectric voltage, and convolution voltage), depends strongly on the semiconductor surface conductivity and the density of active surface states. The first one determines directly the change in SAW velocity to an electrical load to the surface; the surface states determine the change in SAW velocity indirectly by affecting the semiconductor surface potential.

By mixing the delay line output with a suitable reference while the surface potential is externally disturbed, the change in SAW velocity can be accurately measured. This method is very sensitive and a change in SAW velocity on the order of 10^{-3} precent is measurable with a simple experimental set-up. This velocity change corresponds to a disturbance in surface potential less than 2 mV.

The experimental arrangement is shown in Fig. 3.26. An rf is fed to a power splitter and one of the outputs is passed through the delay line. The delayed output is amplitude limited by a two-

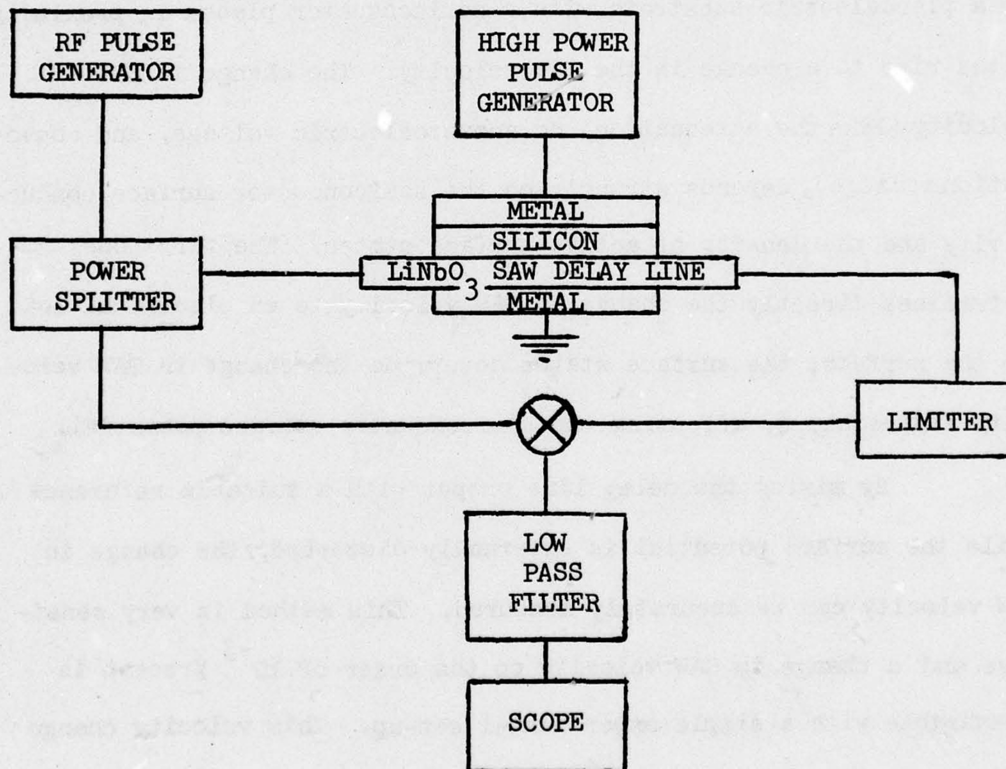

Fig. 3.26 Experimental Arrangement for Observing SAW Velocity Change

sided limiter such as saturated amplifier, and then attenuated and applied to the mixer. The reference signal to this mixer is the second output of the splitter and its output is filtered to obtain the dc component. The result, observed on the oscilloscope, is a voltage which is a function of phase difference between the two signals. Figure 3.27 is a multiple exposure photograph of the mixer output when the surface is undisturbed. The mixer output varies with the input frequency completing one cycle every 90 KHz, corresponding to a 4 cm interaction range and a SAW velocity $v_{so} = 3.6 \times 10^5$ cm after silicon is placed on $LiNbO_3$.

The frequency is adjusted for mixer output at zero level and the silicon surface is disturbed by the application of a plate voltage pulse, V_{dc}, across the silicon $LiNbO_3$ structure. The effects of this voltage on the delay line output are shown in Fig. 3.28a. The amplitude variations are undesirable since they will contribute to the dc component of the mixer output and distort the phase information. Figure 3.28b shows the rf output after the limiter and Fig. 3.28d is the voltage associated with the phase difference between the two signals. Since the frequency is now constant, the change in the phase is caused by a change in the velocity of the acoustic wave.

Consider the case of an undisturbed silicon surface where the reference signal is cos ωt and the output of the delay line is cos $(\omega t + \phi)$. The phase difference is

$$\phi = \omega L/V_S \qquad (3.5\text{-}1)$$

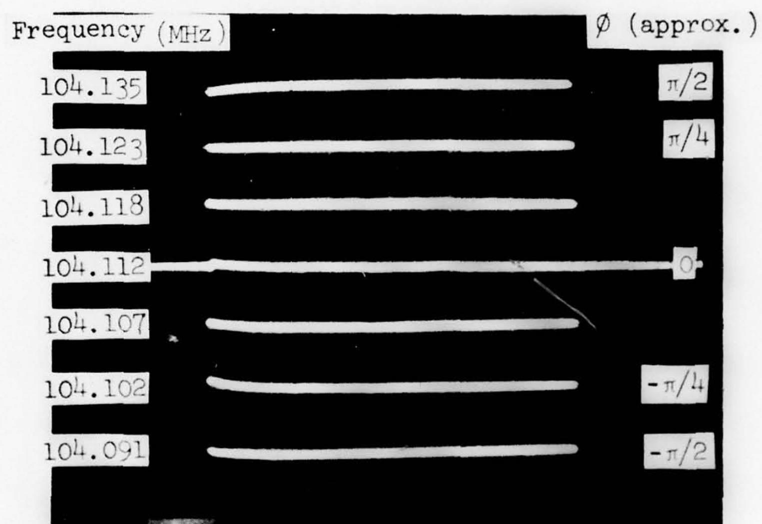

Fig. 3.27 Multiexposure Photograph Showing the Variation of Mixer Output as a Function of Frequency. t = 0.1 msec/div., V = 0.2 v/div.

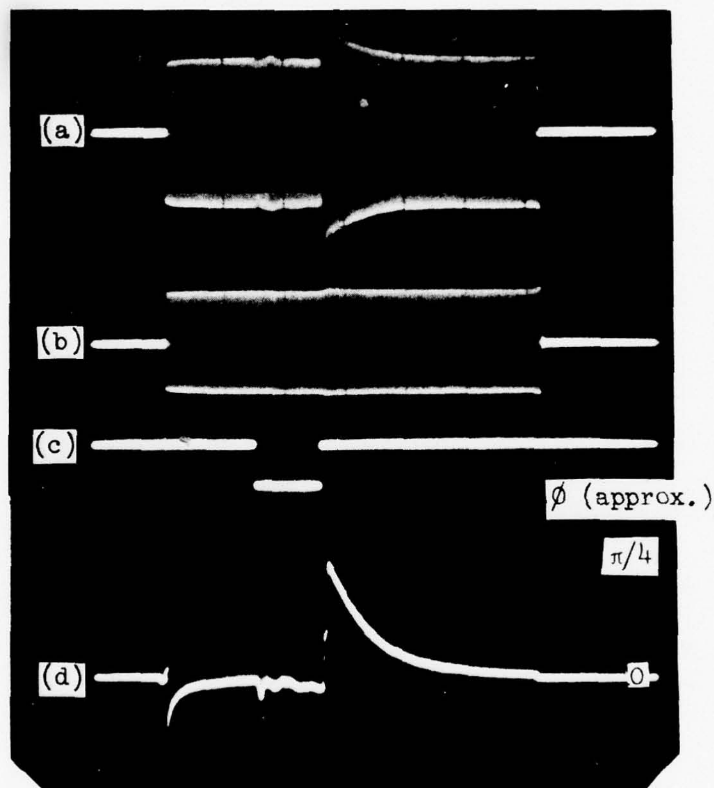

Fig. 3.28 SAW Velocity Disturbed by an Externally Applied dc Bias

(a) Delay Line Output

(b) Input to the Mixer

(c) Applied dc Voltage

(d) Mixer Output After Filtering

where L is the length of the interaction region and v_s is the velocity of the acoustic wave which is a function of surface potential.

Assuming V_O is the dc component of the mixer output, which is a sinusoidal function of phase, and V_{Omax} is its peak value then,

$$V_O = V_{Omax} \sin \phi \qquad (3.5\text{-}2)$$

or

$$V_O = V_{Omax} \sin \omega L/v_s \qquad (3.5\text{-}3)$$

from (3.5-3) we get,

$$V_S = \frac{\omega L}{\sin^{-1}(V_O/_{Omax})} \qquad (3.5\text{-}4)$$

Using Equation (3.5-4) one can determine experimentally the surface wave velocity as a function of the external dc bias or the semiconductor surface potential. These curves can be compared to the theoretical curves obtained from Equation (2.1-3).

The theoretical curves are shown in Figs. 2.15 and 2.20. The change in SAW velocity from metalized surface is plotted as a function of the semiconductor conductivity and the surface potential. If one operates the SAW convolver at low level signal, the absolute value of the semiconductor surface potential can be obtained experimentally. The experimental curve will be shifted to the right or to the left, according to the type of surface state, by the amount,

$$V_{ss} = \frac{Q_{ss}}{C_{ox}} \qquad (3.5\text{-}5)$$

Thus, similar to the shift in the C-V curves of an MOS structure the density of surface charge Q_{ss}, can be determined by the shift in the SAW velocity vs. dc bias curves. Not only the SAW velocity can be used to determine the surface charge, but in principle all other SAW-semiconductor interaction parameters can be used in the same way. Although the measurements of the change in SAW velocity are very sensitive, and very low external dc bias is needed compared to the dc bias needed in the study of the transient response of the attenuated rf pulse, the interpretation of the experimental results is harder and it is beyond the scope of this work.

CHAPTER IV

SEMICONDUCTOR SURFACE SPECTROSCOPY USING THE SAW CONVOLVER

4.1 Absorption Process in Semiconductors

The most direct method for probing the band structure of semiconductors is to measure the absorption spectrum. In the absorption process, a photon of a known energy excites an electron from a lower to higher state. The absorption is expressed in terms of a coefficient which is defined as the relative rate of decrease in the light intensity along its propagation path. Several possible transitions exist in a semiconductor, among them are: band-to-band, between impurities and bands, transition by free carriers within a band, between sub-bands, excitons, and the resonance due to lattice and impurities vibration. Each of the above possible transitions dominate the absorption process at different photon energies. Our study is concerned mainly with band-to-band transition, and transition between impurities and bands. A review on the optical process in semiconductors can be found in the books by J. I. Pankov[53] and T. S. Moss.[54]

The band-to-band transition refers to the excitation of electrons from the valence band to the conduction band. Because the momentum of a photon (h/λ, where λ is the wavelength of light) is very small compared to the crystal momentum (h/a, where a is the lattice constant) the photon absorption process should conserve the momentum of the electron. In some semiconductors (GaAs, CdS) the minimum of the conduction band and the maximum of the valence band

both occur at $k = 0$, hence the onset of absorption will occur at $h\nu = E_g$ as a result of direct transition. The absorption coefficient rises rapidly to about 10^4 cm^{-1} (GaAs) due to the high probability for this transition. The reason for the high probability is that no change in momentum occurs during this transition. In some semiconductors (Si, Ge) the minimum of the conduction band occurs in a different region in the k space from the maximum of the valence band. Optical transition requires the participation of photons in order to conserve momentum, due to the change in the electron wave vector. The phonons may be absorbed or emitted during this transition. These indirect transitions occur with lower probability, and give rise to absorption edge which is less steep than for direct transition.

Optical transition between states in the energy gap and the bands occurs for photon energy less than the gap energy. Absorption peaks are obtained for different states as the photon energy is changed. Although the density of final states (in the band) increases with energy, the absorption coefficient due to the transition from impurity state to conduction band, decreases with energy. This decrease of the absorption coefficient with energy beyond the broad peak is due to a rapid decrease of the transition probability away from the bottom of the conduction band. The reason for this decrease is that the impurity states have limited extent in the k space, the probability of finding electrons in the impurity state is higher for k_0, where k_0 is the wave vector at the bottom of the conduction band.

Indirect transition from impurity state to the conduction band has also less probability due to requirements of momentum conservation.

Optical excitation of carriers will both change the semiconductor conductivity and the charge trapped in the surface state. These changes will affect the semiconductor-SAW interaction, hence, it is possible to monitor the absorption process in semiconductors by measuring the SAW convolver attenuation, acoustoelectric voltage and convolution voltage for various wavelengths of light. In this Chapter semiconductor spectroscopy using the SAW convolver is presented. The semiconductors used in this study are CdS and 2 μm epitaxial layer GaAs n on n^+.

4.2 Transverse Acoustoelectric Voltage Inversion and its Application to Semiconductor Surface Study: CdS

Optical generation of free carriers changes the electrical properties of the semiconductor space charge region. The dc acoustoelectric voltage developed during the nonlinear space charge coupled SAW semiconductor interaction is strongly dependent on the electrical properties of the semiconductor space charge region, hence, it can serve as a detector for optical generation of free carriers. Figure 4.1 shows a very simple equivalent circuit for the transverse acoustoelectric voltage. The circuit includes constant capacitance C_T, such as the substrate and air gap capacitances, and light dependent capacitances such as the surface state and space charge capacitances. The semiconductor is considered to be under weak depletion condition. Under heavy inversion condition the surface state capacitance C_S

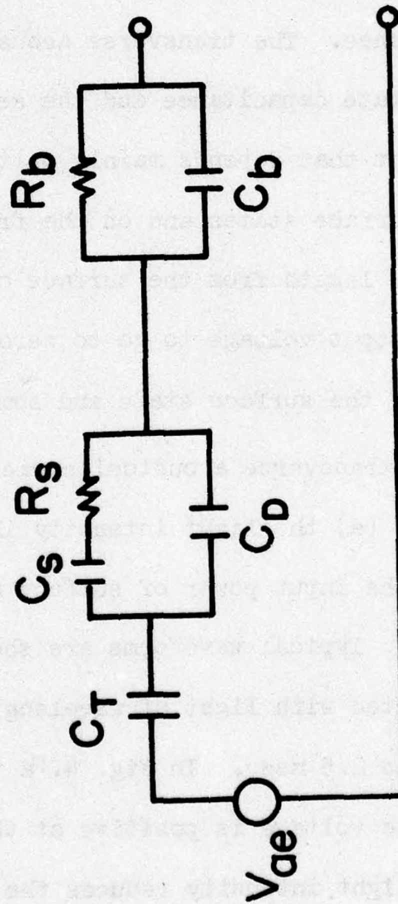

Fig. 4.1 Equivalent Circuit for the Transverse Acoustoelectric Voltage

can be assumed to be essentially zero ($C_S \ll C_B$). The high input impedance to the oscilloscope has a 1 M Ω resistance and 20 pf capacitance which, under most of the conditions of the experiment, has very low effect on the magnitude and the decay constant of the acoustoelectric voltage. It is observed that the transverse acousto-electric voltage is a transient phenomena. The decay constants depend mostly on the surface state capacitance and the depletion layer capacitance. The transverse acoustoelectric voltage charges the surface state capacitance and the semiconductor capacitance with a time constant that depends mainly on the population and depopulation of the surface states and on the free carrier concentration within a Debye length from the surface of the semiconductor, thus causing the output voltage to go to zero owing mainly to the discharging of the surface state and semiconductor capacitance.

The transverse acoustoelectric voltage inversion is strongly dependent on: (a) the light intensity illuminating the semiconductor surface; (b) the input power of surface acoustic wave; (c) incident photon energy. Typical waveforms are shown in Fig. 4.2 for CdS when it is illuminated with light of wavelength 499 nm. The length of the rf pulse is 2.5 msec. In Fig. 4.2a it is observed that the peak acoustoelectric voltage is positive at the beginning of the rf pulse. Reducing the light intensity reduces the peak voltage and it becomes negative on further reduction. Figure 4.2b shows the peak voltage inversion immediately after the light source is removed. The peak voltage switches from positive to negative in a very short time and then it starts to decay very slowly as discussed later on.

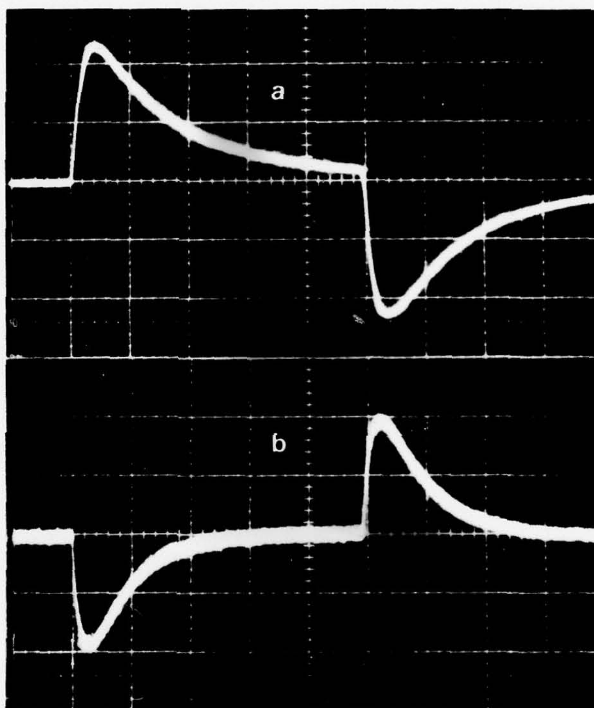

Fig. 4.2 Transverse Acoustoelectric Voltage. Horizontal scale: 0.5 msec/div. (a) With Light of Wavelength 499 nm Illuminating the Semiconductor Surface. Vertical scale: 18.75 mV/div. (b) Immediately After the Light Source is Removed. Vertical scale: 7.5 mV/div.

The dependence of the transverse acoustoelectric voltage inversion on the input power of the SAW is shown in Fig. 4.3. The plot of the peak acoustoelectric voltage as a function of the rf voltage applied to the input transducer shows that for dark condition the peak voltage is positive for 10 V peak to peak rf voltage and becomes negative for lower input voltages. The switching occurs at an input level of O1.4 dB and a maximum is observed at -4 dB attenuation of the input voltage. Beyond that, the peak transverse voltage reduces as the input voltage is reduced. The acoustoelectric voltage inversion due to change in input power of SAW was also observed when light illuminated the semiconductor surface at certain wavelengths of light. This will be discussed later. The transverse acoustoelectric voltage inversion phenomena is discussed in detail in Section 3.3.

The dependence of the transverse acoustoelectric voltage inversion on the incident photon energy is shown in Fig. 4.4. The change of the wavelength of light between 470 nm and 550 nm results in two inversions in the peak voltage, one around 494 nm and the second aroung 530 nm. It is important to notice that at wavelengths of light around the inversion of the peak voltage quasi-steady state condition occurs. Both negative and positive voltages appear; each having different amplitudes and different time constants associated with the decay of the voltages to zero.

The spectral response of the transverse peak acoustoelectric voltage measured at the beginning of the rf pulse is shown in Fig. 4.5 for Grade A CdS. The peak voltage is normalized to the radiant

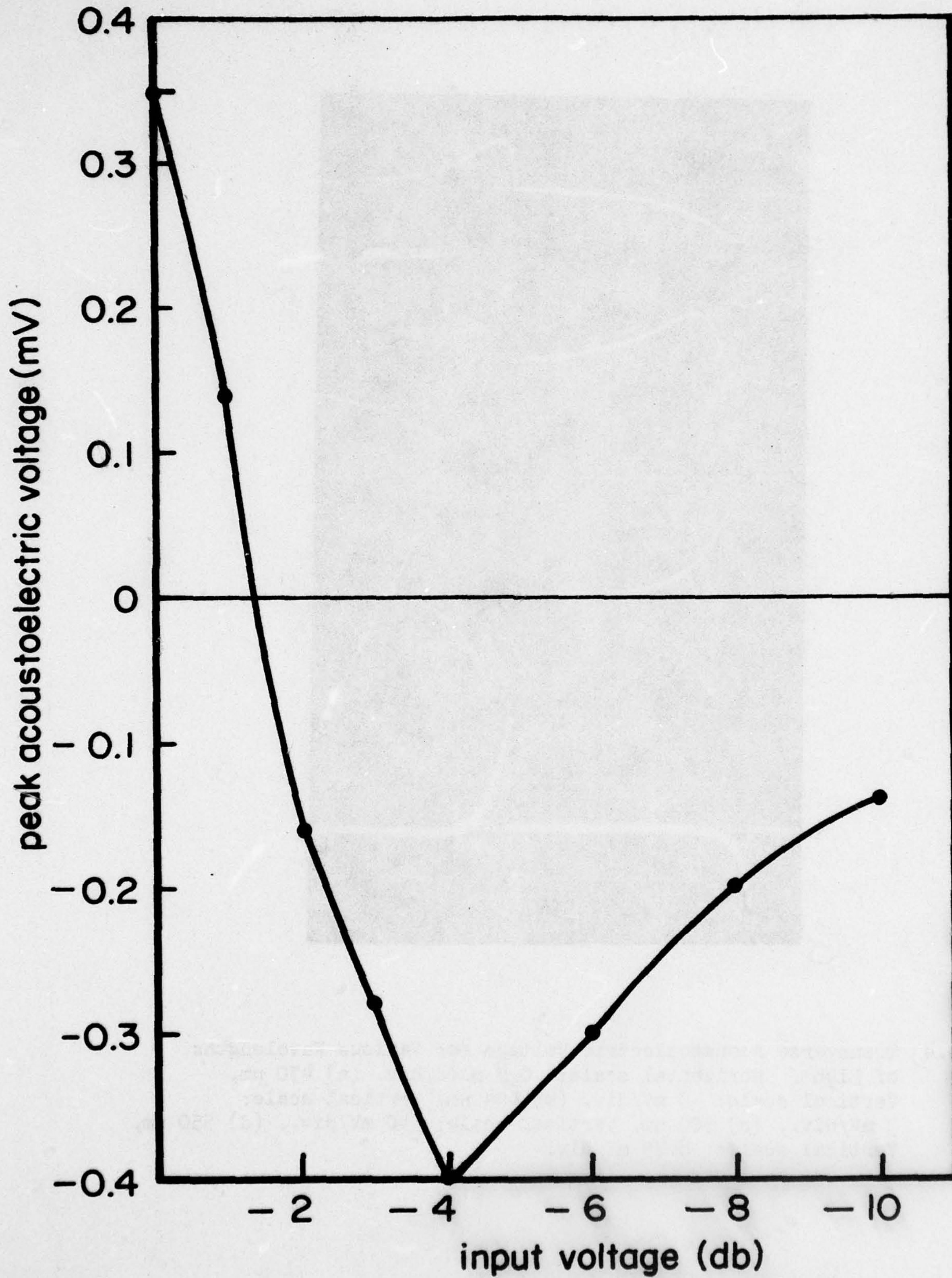

Fig. 4.3 Plot of Peak Transverse Acoustoelectric Voltage as a Function of the Input rf Voltage. At Zero dB the Input rf Voltage to the Delay Line is 10 V p-p.

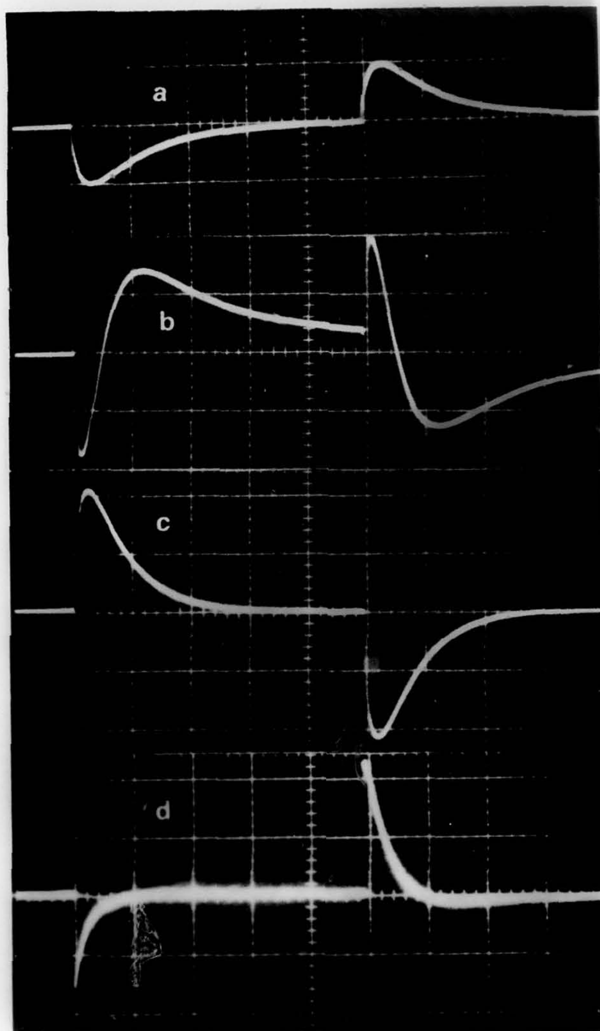

Fig. 4.4 Transverse Acoustoelectric Voltage for Various Wavelengths of Light. Horizontal scale: 0.5 msec/div. (a) 470 nm, Vertical scale: 8 mV/div. (b) 494 nm, Vertical scale: 3 mV/div., (c) 500 nm, Vertical scale: 40 mV/div., (d) 550 nm, Vertical scale: 8.75 mV/div.

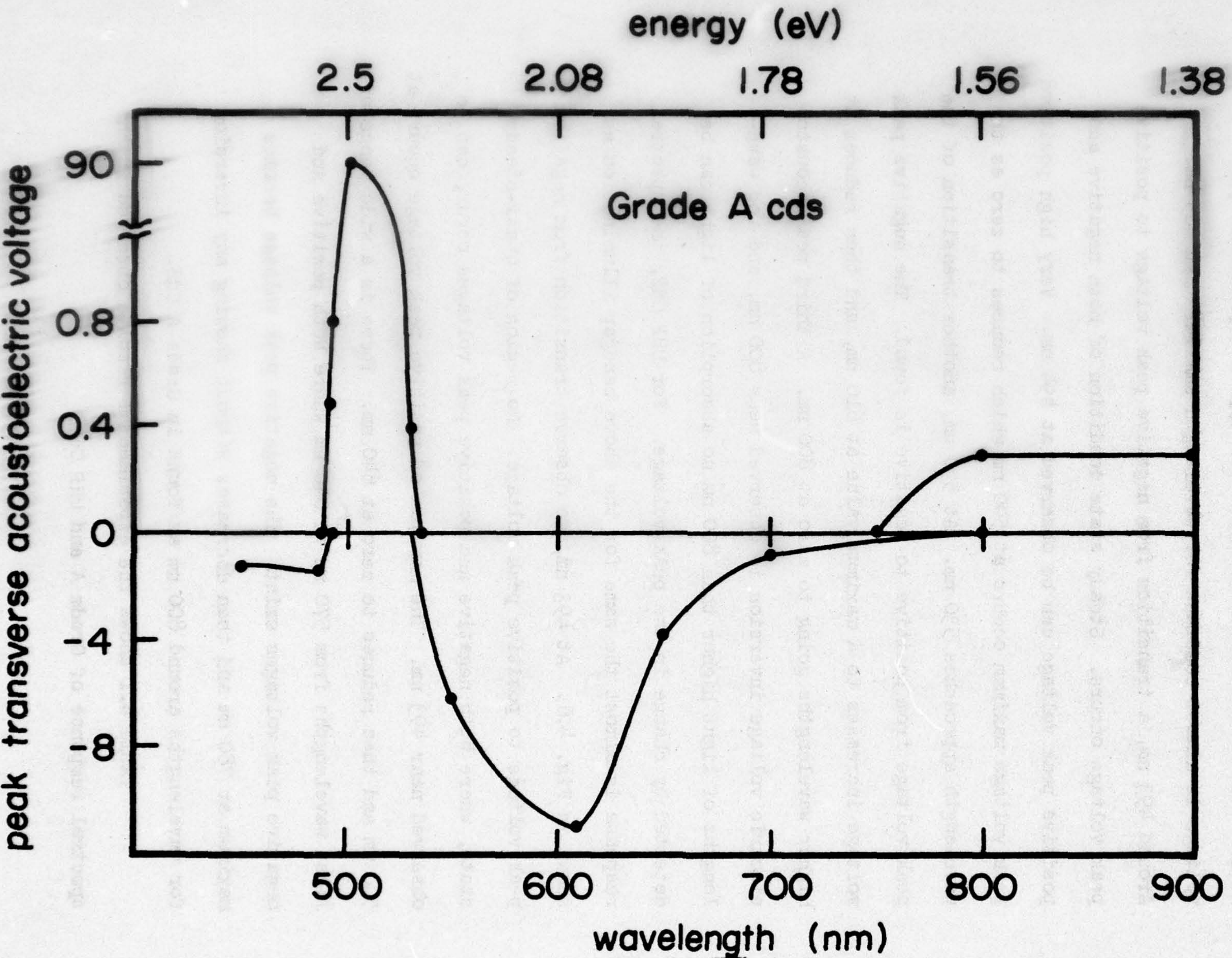

Fig. 4.5 The Spectral Response of the Peak Transverse Acoustoelectric Voltage, Measured at the Beginning of the rf Pulse in Grade A CdS. The Transition Region is Shown by Double Value of Peak Voltages Associated with the Negative and Positive Peak Voltages Appear at the Beginning of the rf Pulse. The Vertical Scale is Normalized to the Radiant Flux Output of the Monochromator.

output flux of the monochromator. For type A crystal the peak voltage is almost constant for wavelength smaller than 485 nm. Around 493 nm, a transition from negative peak voltage to positive peak voltage occurs. Steady state condition of both negative and positive peak voltage can be observed at 494 nm. Very high positive peak voltage maximum occurs at 500 nm which reduces to zero as the wavelength approaches 530 nm. At 530 nm, another transition of the peak voltage from positive to negative is found. The negative peak voltage increases to a maximum value at 610 nm, and then reduces at higher wavelengths going to zero at 800 nm. A third peak acousto-electric voltage inversion is observed near 800 nm, and for wavelengths of light higher than 800 nm no absorption of light can be detected by change in the peak voltage. For UHP CdS, the spectral response is almost the same for the above bandgap illumination as shown in Fig. 4.6. At 493 nm, we observe transition from negative peak voltage to positive peak voltage. No region of quasi-steady state, where both negative and positive peak voltages occur, can be observed near 493 nm. The maximum of positive peak voltage occurs at 530 nm and then reduces to zero at 640 nm. There is a wide range of light wavelengths from 570 nm to 640 nm where both positive and negative peak voltages exist. The negative peak voltage becomes maximum at 780 nm and then decreases without showing any inversion for wavelengths around 800 nm as found in Grade A CdS.

Table 4.1 shows the experimental results observed in the spectral response of Grade A and UHP CdS.

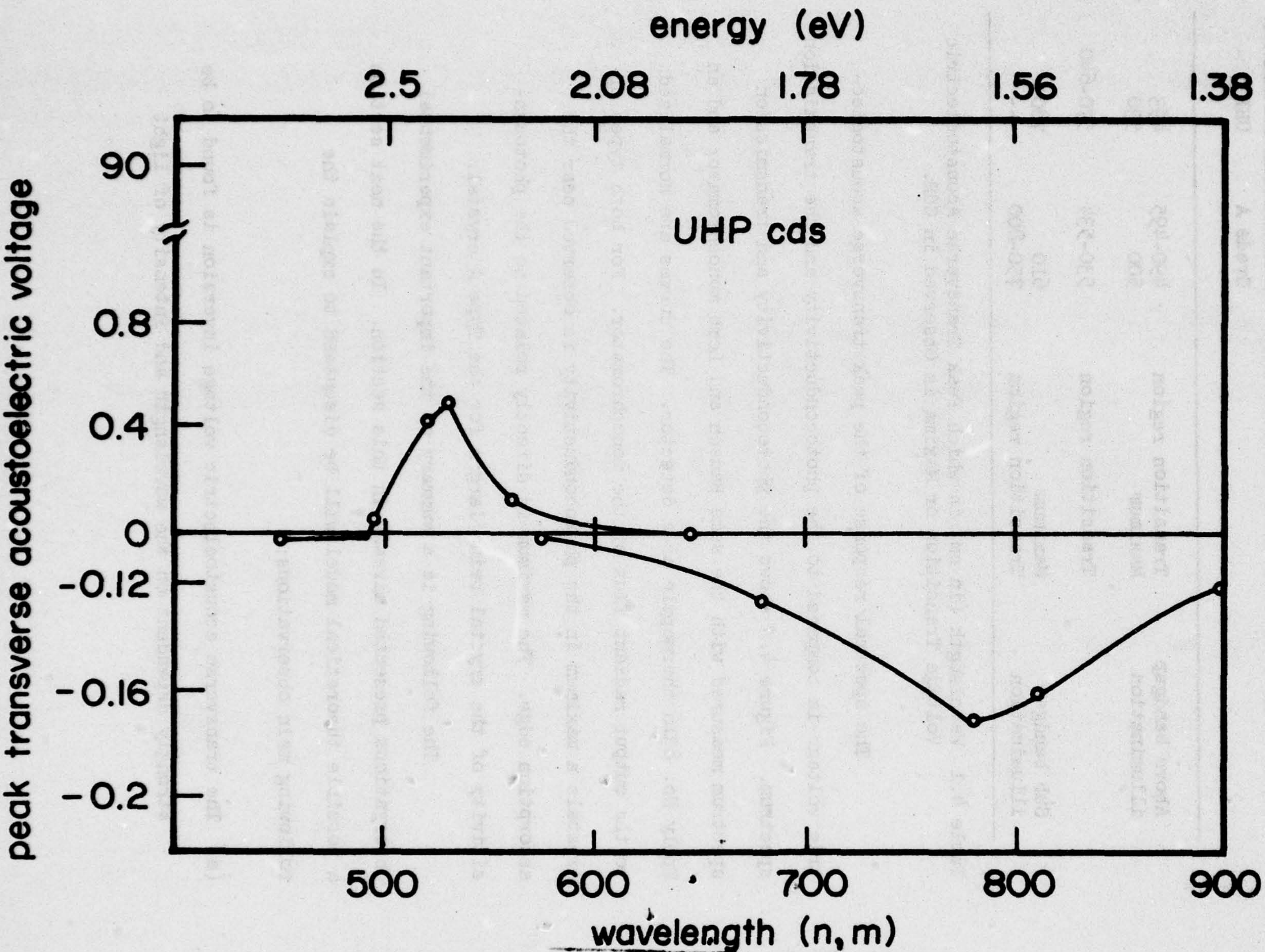

Fig. 4.6 The Spectral Response of the Peak Transverse Acoustoelectric Voltage, Measured at the Beginning of the rf Pulse in UHP CdS. The Transition Region is Shown by Double Value of Peak Voltages Associated with the Negative and Positive Peak Voltages Appear at the Beginning of the rf Pulse. The Vertical Scale is Normalized to the Radiant Flux Output of

		Grade A	UHP
Above bandgap illumination	Transition region	490-495	493
	Maximum	500	530
	Transition region	530-534	570-640
Sub bandgap illumination	Maximum	610	780
	Transition region	750-800	---

Table 4.1 Wavelength (in nm) in which Peak Transverse Acoustoelectric Voltage Transition or Maxima is Observed in CdS.

The spectral response of the peak transverse acoustoelectric voltage is compared to the photoconductivity and the transmission spectrum. Figure 4.7 shows the photoconductivity and transmission spectrum measured with the same Bausch and Lomb monochromator and an Epply No. 8316 thermopyle as a detector. The curves are normalized to the output radiant flux of the monochromator. For both types of crystals a maximum in the photoconductivity is observed near the absorption edge. The maximum is directly related to the photosensitivity of the crystal being larger for the Type A crystal.

The following is a summary of the important experimental observations presented already in this section. In the next section a possible theoretical model will be discussed to explain the following main observations:

(a) The transverse acoustoelectric voltage inversion is found to be strongly dependent on the wavelength and intensity of light

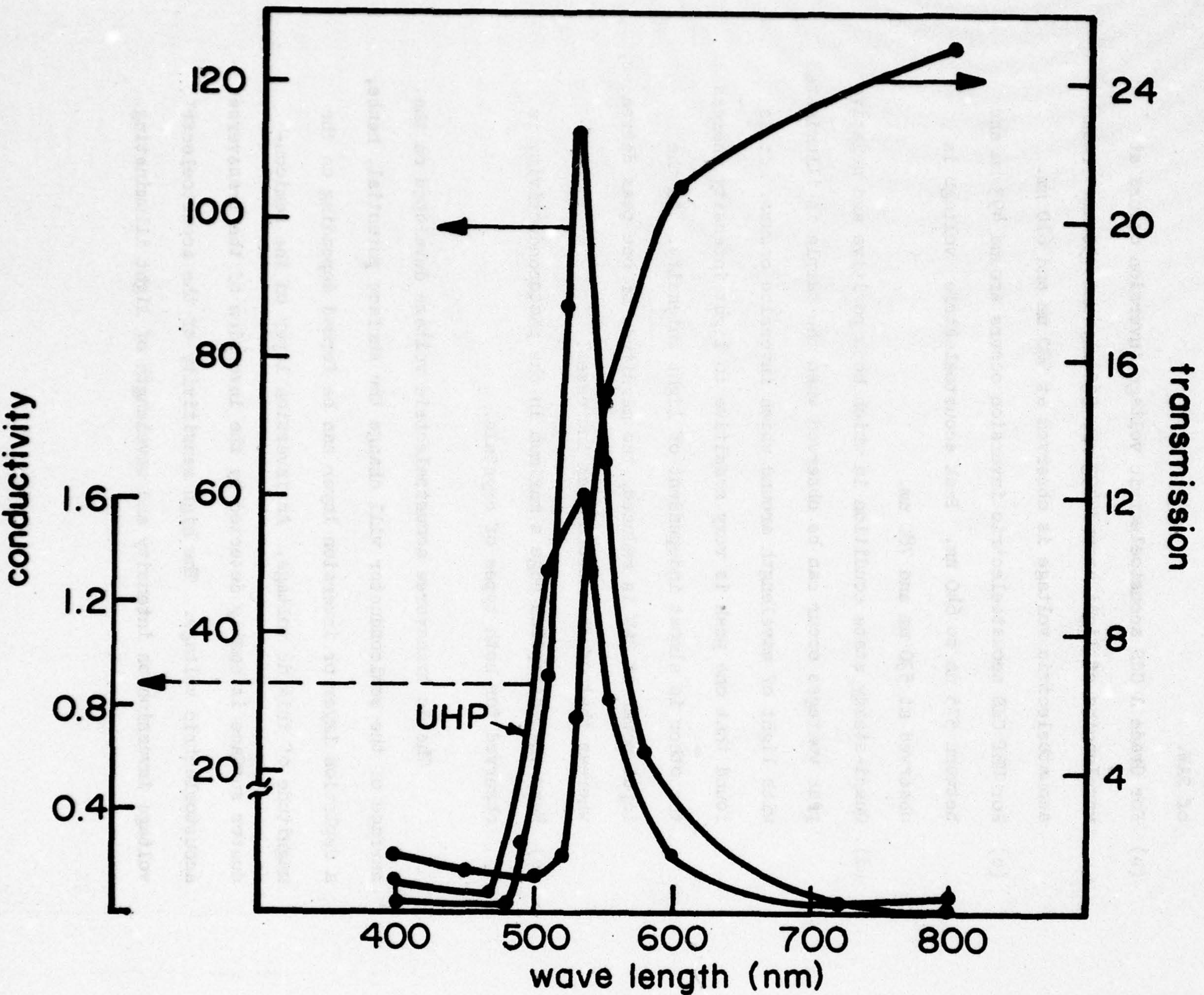

Fig. 4.7 Photoconductivity and Transmission Spectrum for Grade A and UHP CdS

illuminating the semiconductor surface, and on the input power of SAW.

(b) For Grade A CdS acoustoelectric voltage inversion occurs at wavelengths of light around 493 nm, 530 nm, and 790 nm. Peak acoustoelectric voltage is observed at 500 nm and 610 nm.

(c) For UHP CdS acoustoelectric inversion occurs around 493 nm and between 575 nm to 640 nm. Peak acoustoelectric voltage is observed at 530 nm and 780 nm.

(d) Quasi-steady state condition in which both positive and negative peak voltages occur can be observed when the sample is illuminated with light of wavelength around which inversion occurs. It is found that one peak is very sensitive to light intensity whereas the other is almost independent of light intensity. As the input power of SAW is reduced, the magnitude of one peak decreases, whereas that of the second peak increases.

(e) Near the absorption edge a maximum in the photoconductivity is observed for both types of crystals.

The dc transverse acoustoelectric voltage developed on the surface of the semiconductor will change the surface potential, hence, a depletion layer or inversion layer can be formed depending on the magnitude of this dc voltage. An inversion layer on the semiconductor surface is easily detected by the inversion of the transverse acoustoelectric voltage. The high sensitivity of the acoustoelectric voltage inversion on intensity and wavelength of light illuminating

the semiconductor surface, and on power input of the SAW can be explained as follows: The power input of SAW determines the magnitude of the dc acoustoelectric voltage hence, for low input power no inversion is observed. The semiconductor photoconductivity of both the bulk and the surface, depends on (a) the wavelength of incident light, and (b) the intensity of incident light. As the magnitude of the transverse acoustoelectric voltages is related to semiconductor conductivity, the inversion produced by this dc voltage is also dependent on the wavelength and intensity of light.

The spectral response of the peak transverse acousto-electric voltage was used to determine the energy band and surface state location in the energy band of GaAs.[55] This method becomes even more sensitive for CdS due to large photoconductivity which results in the acoustoelectric voltage inversion phenomena. The spectral response of the peak acoustoelectric voltage shows that almost no absorption of photons occurs for photon energy smaller than 1.5 eV. It is reasonably to assume that for very high resistivity material the dc acoustoelectric voltage which develops right on the surface of the semiconductor causes deep depletion to the semiconductor surface, thus very low positive voltage associated with an n-type surface appears for energy smaller than 1.5 eV. For low resistivity material (UHP) optical generation still exists at this range, thus, negative peak voltage associated with a p-type surface appears for energy smaller than 1.5 eV.

The sub bandgap spectrum is very similar to the sub bandgap spectrum of the surface photovoltage reported for CdS.[56,57] Incident photons with an energy $h\nu = E_t - E_v$ excite electrons from the valence band into the unoccupied surface states. Thus, the net negative charge located in the surface increases. The free holes created in the valence band rapidly recombine in the bulk, as the minority carrier lifetime in CdS is extremely small. Conservation of charge requires a corresponding increase in the barrier height. This mechanism together with the dc acoustoelectric voltage which tends to deplete the semiconductor surface will cause an inversion layer on the semiconductor surface. The threshold photon energy of the acousto-electric inversion is $E_c - E_t = 1.61$ eV, accordingly the number of thermally activated transitions from or into the conduction and valence bands is negligible.

The second deep level surface states at $E_c - E_t = 2.05$ eV is found to be deep level oxygen level, hence, this is an extrinsic level whereas the first one is an intrinsic level. Although the traps are located below the Fermi level they are not completely filled. This type of non equilibrium configuration can exist provided the rate of trapping of free electrons from the conduction band is very small. Another possibibility for the increase in the surface potential is that the excitation takes place from the surface states to the conduction band. Due to the electric fields existing in the space charge and the dc acoustoelectric field, these electrons will be removed from the surface. The deep acceptor level will immediately

capture electrons from the valence band, causing a net positive charge on the surface. Conservation of charge requires a corresponding increase in the surface potential, hence, an inversion layer will occur. It is reasonable to assume that direct excitation from surface state to conduction band occurs for $E_c - E_t = 2.05$ eV, whereas direct excitation from the valence band to surface state occurs for $E_c - E_t = 1.61$ eV ($E_t - E_v = 0.8$ eV).

The maximum near the absorption edge in the photoconductivity response measured as a function of the illuminating wavelength is due to the difference between surface and volume absorption.[57] For both types of crystals we can assume that the surface recombination and hence, the lifetime for surface excited carriers is independent of the bulk condition, and that the surface lifetime is much smaller than the bulk lifetime. The maximum in the photoconductivity spectral response occurs when a transition is made from surface to volume absorption with increasing wavelength. The magnitude of the maximum is directly related to the photosensitivity of the crystal. Thus, for Grade A crystal we observe a very large peak in the photoconductivity, two orders of magnitude greater than that for the UHP. In agreement with photoconductivity spectrum, the acoustoelectric voltage spectrum near the absorption edge shows zero voltage for Grade A and maximum for the UHP around light wavelength of 530 nm or 2.36 eV.

The appearance of the zero acoustoelectric voltage when band to band transition occurs, is due to a large increase in

photoconductivity whereas the zero voltage at 800 nm, where transition from the band to surface states occurs, is due to an increase in surface conductivity, which is not observed in the photoconductivity spectrum. Comparison of the peak voltage maximum for UHP at 530 nm and at 780 nm shows that for direct excitation of electrons from the valence band to the surface states, only minority carrier concentration increases, and very small dc transverse acoustoelectric voltage is developed, whereas near the absorption edge, generation of free electrons and holes occurs and much higher dc acoustoelectric voltage is developed right on the surface.

The spectral response of the peak voltage with photons of above bandgap energy results from the dependence of the penetration depth of light on photon energy.[56] On going from 530 nm to 490 nm the magnitude of the absorption length decreases by a factor of approximately three, thereby increasing the free carrier generation rate near the surface. Thus, even though the photoconductivity is decreasing as shown in Fig. 4.7, surface conductivity is increasing for very high photon energy and very small constant acoustoelectric voltage appears. At photon energy of 2.53 eV ($\sim$493 nm) the light starts to penetrate inside the semiconductor, and a very high dc acoustoelectric voltage starts to be developed right on the surface of the semiconductor. The transition between very high photoconductivity near the absorption edge to very high surface conductivity at photon energy well above the energy band accompanies two nulls of acoustoelectric voltage. This, in turn, produces a very high positive

maximum peak voltage at 2.5 eV for Grade A CdS.

Table 4.2 summarizes the observed surface states and absorption edge for Grade A and UHP CdS.

	Grade A	UHP
Surface absorption (eV)	2.55	2.53
Absorption edge (eV)	2.35	2.36
Energy position of surface state $E_c - E_t$ (eV)	2.05, 1.61	1.6

Table 4.2 Observed Surface States, Absorption Edge and Surface Absorption in CdS

4.3 Determination of Absorption Edge and Surface-State Locations in GaAs using the SAW Convolver

In Sections 4.3 and 4.4 we present experimental results for semiconductor spectroscopy using a 2 μm epitaxial layer of GaAs n on n^+. The epitaxial layer resistivity is 0.7 ohm-cm ($n \cong 5\ 10^{15}$). The extrinsic Debye length is of the order of 0.06 μm. The semi-infinite approximation cannot be used in this case as the SAW wavelength is larger than the epitaxial layer thickness (λ = 70 μm). The exact solution for the finite thickness semiconductor is presented in Section 2.2.4. Due to the large difference between the SAW wavelength (~ 70 μm) and the extrinsic Debye length, the main contribution to the electric fields inside the semiconducor is from the last

two terms in the linear combination (A_3 and A_4) of Equation (2.2-23a). The first one is an exponential decay with very short decay constant ($(\gamma k)^{-1} = L_D$), the second one increases exponentially with distance away from the semiconductor surface, with the same decay constant. However, for extrinsic semiconductor A_3 is several orders of magnitude larger than A_4 ($A_3/A_4 >> 1$), as seen in Equation (2.2-23b). Hence, we shall ignore the contribution of the last term to the electric field, and assume that the interaction region is of the order of a Debye length. In order to check the validity of this assumption, we shall repeat the spectral response of this thin epitaxial layer under accumulation condition in Section 4.4 and compare the results to those obtained under no external dc bias presented in Section 4.3.

Figure 4.8a shows an oscilloscope trace of the dark transverse acoustoelectric voltage for a 1 msec rf pulse. The time constant associated with the acoustoelectric voltage pulse is approximately 20 μsec. The wavelength of sample illumination is increased monotonically for successive traces. Figure 4.8 b shows the acoustoelectric voltage for light of 0.9 μm wavelength, shining vertically on the bottom of the delay line. It is noted that the acoustoelectric voltage increases and that the time constant increases to a value of 1 msec. The spectral response of the peak transverse acoustoelectric voltage is shown in Fig. 4.9. The acoustoelectric voltage is normalized to the radiant flux output of the monochromator. It is noted that there are three distinct peaks labeled A, B, and C

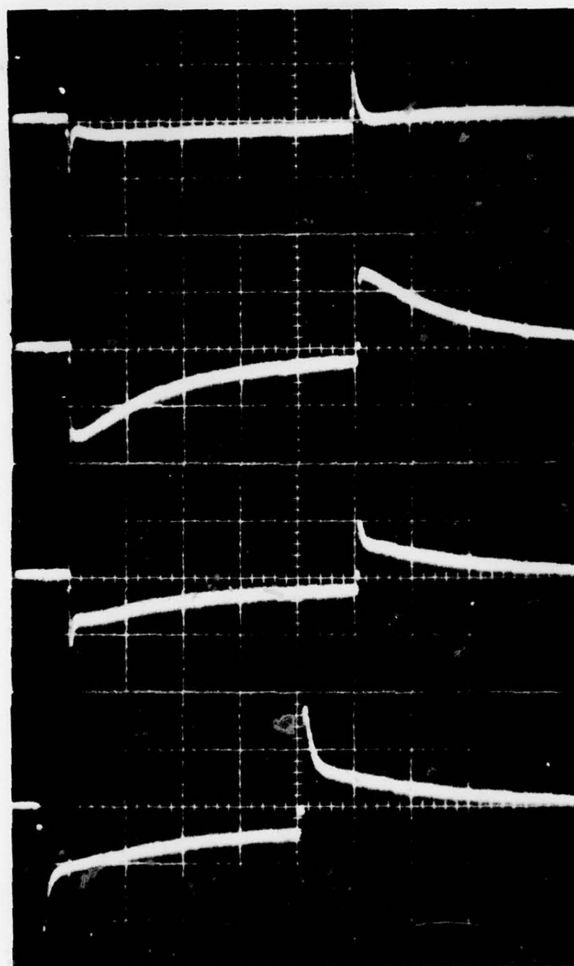

Fig. 4.8 Acoustoelectric Voltage for Various Wavelengths of Light. Horizontal Scale: 0.2 msec/div., Vertical Scale: 0.1 mV/div. (a) No Light; (b) Wavelength 0.9 μm; (c) Wavelength 1.26 μm; (d) Wavelength 1.74 μm (Horizontal Scale: 0.1 msec/div.).

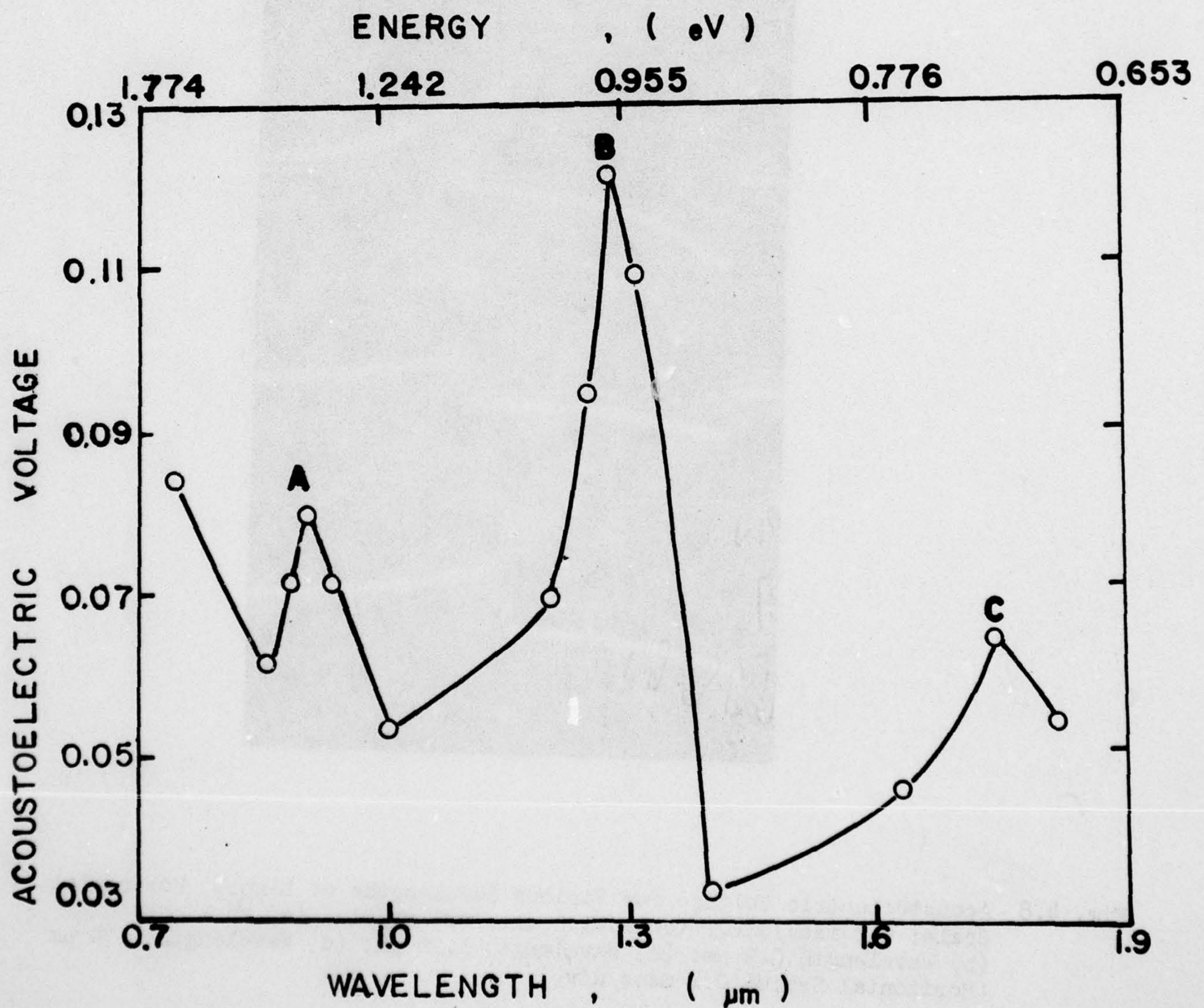

Fig. 4.9 Plot of Peak Acoustoelectric Voltage as a Function of the Wavelength of Light. Peaks Labeled A, B, and C are at 0.9, 1.26, and 1.74 μm, Respectively. The Vertical Scale is Normalized to the Radiant Flux Output of the Monochromator.

at 0.9, 1.26, and 1.74 μm, or 1.38, 0.98, and 0.71 eV, respectively. Figures 4.9c and 4.9d show the other two maxima in the acoustoelectric voltage. It is obvious that these two maxima are different from the first one. They have two different time constants, the first one is short, approximately 20 μsec, which is very similar to the time constant of dark condition, followed by a very long time constant, approximately 1 msec. Figure 4.10 is the attenuation of the delay line as the wavelength of the light is varied. Zero attenuation corresponds to the output of the delay line in dark condition. The attenuation is normalized to the radiant flux output of the monochromator. The peaks labeled A, B, and C are at the same wavelengths as in Fig. 4.9.

The experimental results suggest that the peak A in the acoustoelectric voltage is associated with band-to-band transitions leading to generation of free carriers. Under subband-gap illumination there is discrete electron transition from the surface states to the conduction band leading to an increase in free-carrier concentration, which gives rise to peaks labeled B and C.

The acoustoelectric current is the time average of the product of the surface conductivity and the electric field; thus, the maxima of the transverse acoustoelectric voltage occur when the photon energy is such that there is transition of electrons from surface state to conduction band. Although the contributions of electrons and holes to the acoustoelectric voltage are of opposite

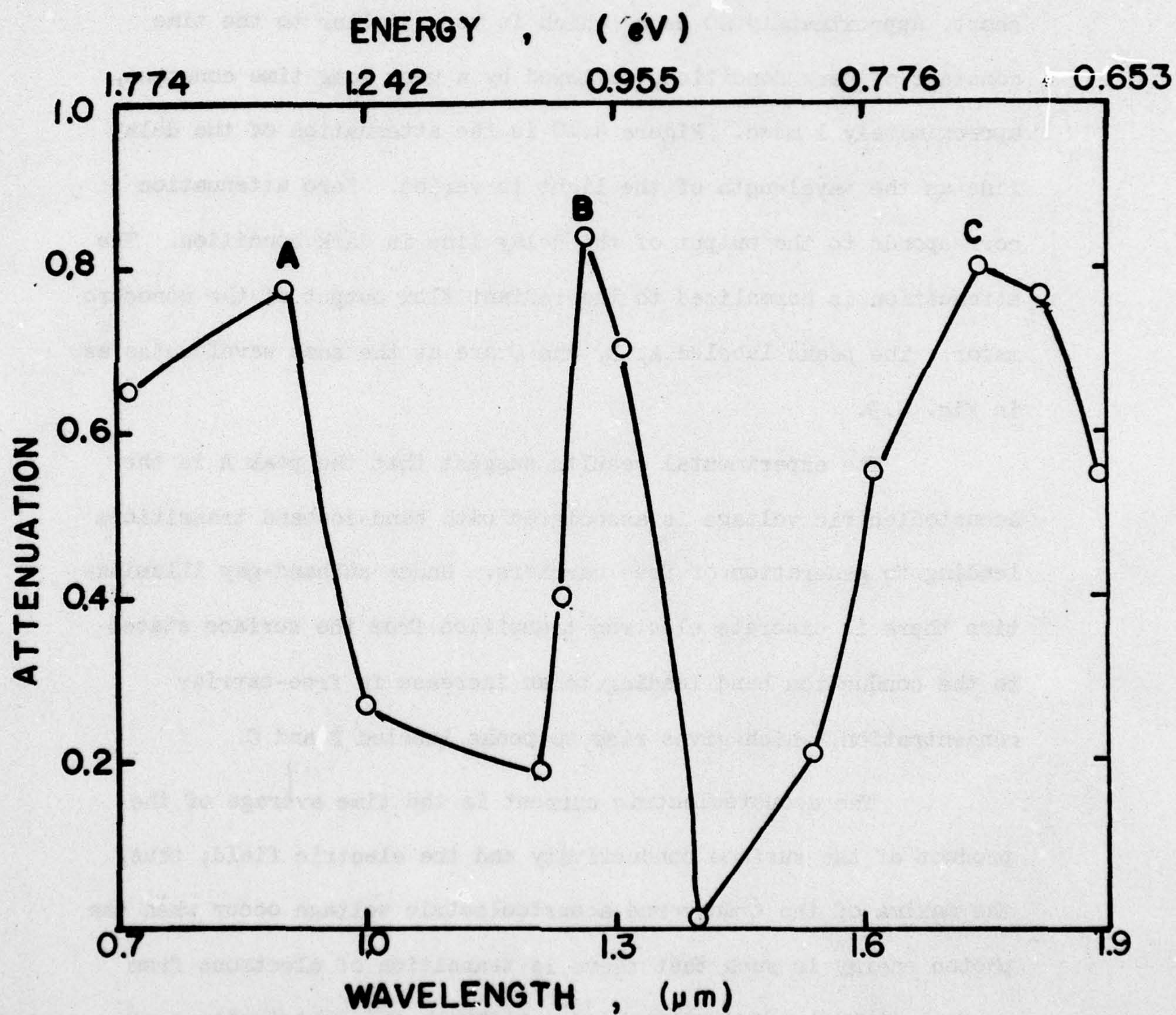

Fig. 4.10 Plot of Delay Line Attenuation as a Function of Wavelength of the Light. Peaks Labeled A, B, and C are at 0.9, 1.26, and 1.74 μm Respectively. The Vertical Scale is Arbitrary and is Normalized to the Radiant Flux of the Monochromator.

polarity. The contribution of holes can be ignored due to their small mobility compared to the electron mobility.

The attenuation is a function of the semiconductor surface conductivity. It increases to a maximum value and then decreases as the semiconductor surface conductivity is increased. Thus, as we follow the increasing part of this curve we get maxima of attenuation whenever the semiconductor conductivity increases. The transverse acoustoelectric voltage and the attenuation dependence on the semiconductor conductivity is very similar, hence, we get the peaks of their response curve at the same wavelength of light.

The time constant of the transverse acoustoelectric voltage is short ($\sim$20 μsec) for the dark condition and becomes longer ($\sim$ 1 msec) when the sample is illuminated. Still there is a definite difference between the time constants of the band-to-band transition and the surface-state-to-conduction-band transition. The possible reason for the long time constant of the band-to-band transition is that the recombination process involves two deep-level recombination centers below the Fermi level which are filled with electrons. This gives short lifetime for minority carriers but long lifetime for majority carriers. The over-all time constant also includes the time constant of the external circuit which remains constant for various light illuminations. Thus, only the relative time constant to dark condition was measured, not the absolute value.

The surface-state-to-conduction-band transition has two different time constants. The first time constant is very short possibly due to fast recombination centers. After the fast recombination centers reach the steady-state condition the process continues with a long time constant, because it involves generation and recombination of carriers from deep-level centers in which the extrinsic generation rate is much larger than the thermal generation rate and recombination rate. Thus, the population and depopulation processes of surface states are exponential with time and are characterized by very large time constants. Measurement of surface-state locations in GaAs was reported previously[59,60] by measuring the photovoltage under subband-gap illumination and the capacitance of Schottky barrier diodes; surface-state locations are in excellent agreement with the results reported here. The absorption edge obtained here is 1.38 eV compared to 1.43 eV in the literature. This may be due to the large bandwidth of the monochromator (15 nm). When the bandwidth is reduced the peaks become very narrow and the position of the peaks can be measured more accurately.

4.4 Semiconductor Spectroscopy using the Transient Delay Line Attenuation

Semiconductor spectroscopy using the SAW convolver output as a detector has an important advantage, that it is possible to apply an external dc bias during the spectroscopy. The dc bias will determine the semiconductor surface potential prior to the applica-

tion of the light. Thus, it is possible to fill or empty traps prior to the application of the light. When optical absorption occurs the interaction is dominated by a small region in the energy band which is determined by the external dc bias.

An oscilloscope trace of the delay line output for different wavelengths is shown in Fig. 4.11. The semiconductor is GaAs 0.7 ohm-cm (2 μm epitaxial layer) and the external dc bias is such that the semiconductor surface is depleted. It is observed that the thermal relaxation of deep level surface states is much faster when direct optical excitation from surface states to conduction band occurs. In addition, the steady state attenuation varies with the photon energy as observed in Fig. 4.12. The three maxima A, B. and C are at 0.86, 13 μm, and 1.74 μm, or at 1.45 eV, 0.95 eV and 0.71 eV respectively. These values are very similar to the maxima obtained in the transverse acoustoelectric spectroscopy. Thus, the absorption edge and the deep level surface states can be detected also by the delay line attenuation during an external applied dc bias. The dc bias improves very much the sensitivity of the detection system, even though no new results appear compared to the detection by the delay line output without an external dc bias.

In order to be able to detect shallow traps which are usually empty and hence, do not contribute to the optical generation, the dc bias will be such that the semiconductor surface is accumulated

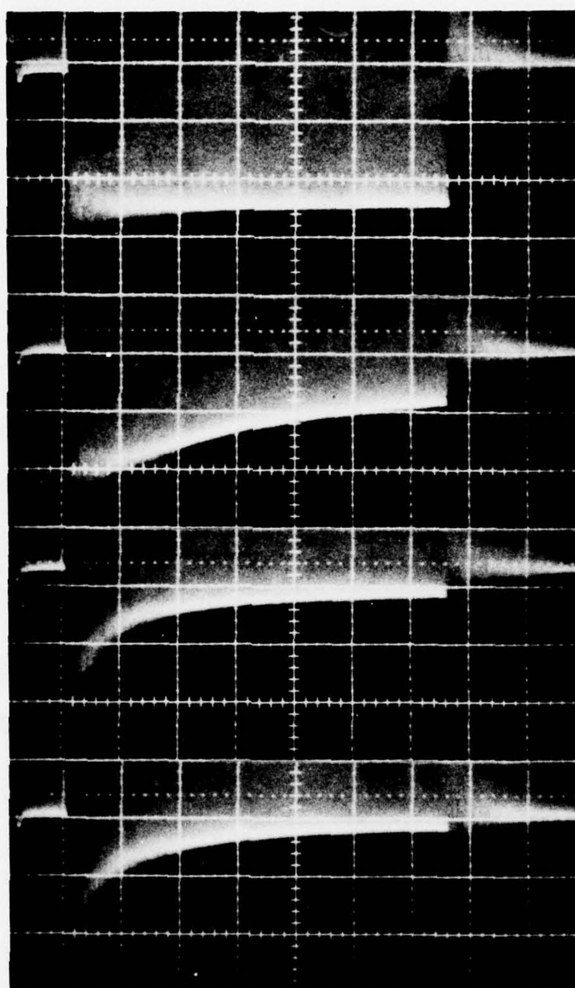

Fig. 4.11 Attenuated Delay Line Output for n on n^+ GaAs, when an External dc Voltage is applied Across the Semiconductor and $LiNbO_3$ such that the Semiconductor Surface is Depleted. Vertical scale: 5 mV/div. Horizontal scale: 0.2 ms/div. V_{dc} = 250 V. (a) No Light; (b) Wavelength of Light 0.86 μm; (c) Wavelength of Light 1.3 μm; (d) Wavelength of Light 1.74 μm.

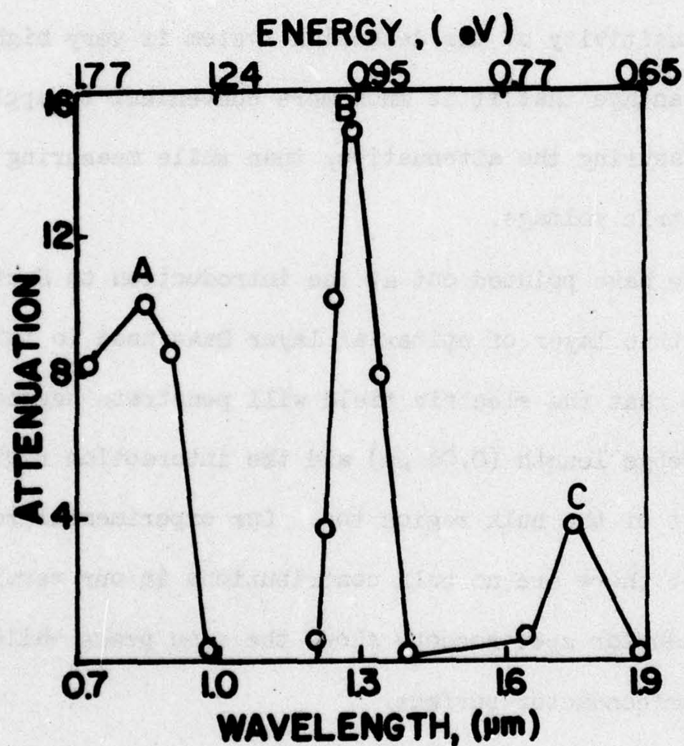

Fig. 4.12 Plot of the Attenuation of Delay Line Output for n on n^+ GaAs, as a Function of the Wavelength of Light. The Attenuation is Measured at the End of the External dc Pulse. Peaks Labeled A, B, and C are at 0.86 μm, 1.3 μm, and 1.74 μm respectively. The Vertical Scale is Normalized to the Radiant Flux Output of the Monochromator.

and we observe the relaxation in the delay line output after the dc bias is removed. Figure 4.13 shows the relaxation for different wavelengths. As can be observed from the spectral response of the decay time, (Fig. 4.14) only the deep level and the absorption edge can be detected with very high sensitivity.

Although no new information appears from the transient delay line attenuation spectroscopy, it is important to emphasize that the sensitivity of the detection system is very high, and it has the advantage that it is much more convenient to apply an external dc while measuring the attenuation, than while measuring the dc acoustoelectric voltage.

We have pointed out at the introduction to Section 4.3, that due to the thin layer of epitaxial layer GaAs used in this study, it is possible that the electric field will penetrate beyond the extrinsic Debye length (0.06 μm) and the interaction region may include part of the bulk region too. Our experimental results suggest that there are no bulk contributions in our results, since the semiconductor spectroscopy shows the same peaks while accumulating the semiconductor surface.

4.5 The Spectral Response of the Convolution Voltage

Similar to the delay line attenuation it is possible to apply an external dc bias to the semiconductor-delay line structure

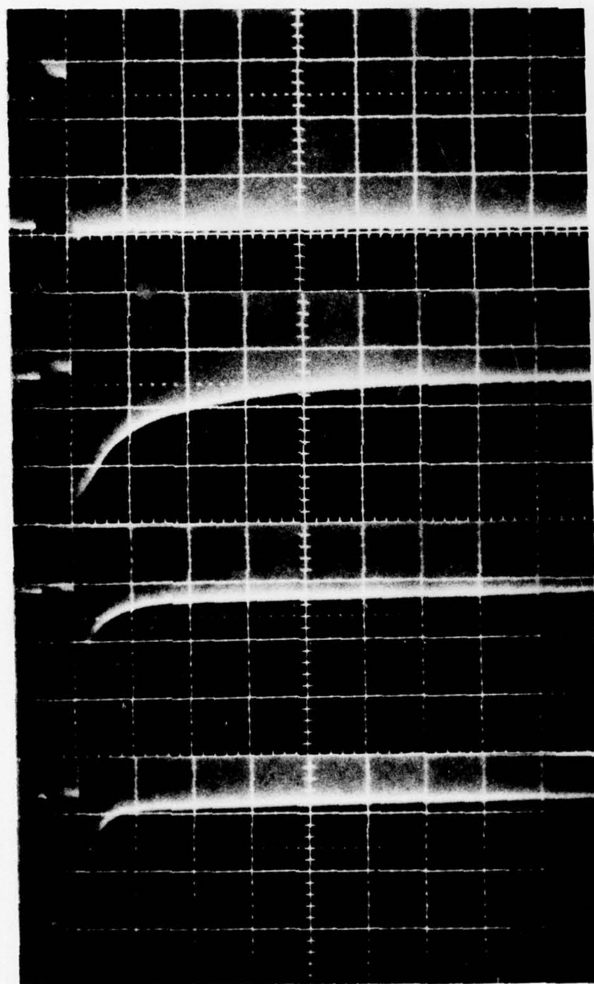

Fig. 4.13 Attenuated Delay Line Output for n on n^+ GaAs, when External dc Voltage is Applied Across the Semiconductor and $LiNbO_3$ such that the Semiconductor Surface is Accumulated. Vertical scale: 5 mV/div. Horizontal scale: 1 ms/div. V_{dc} = 250 V. (a) No Light; (b) Wavelength of Light 0.86 μm; (c) Wavelength of Light 1.3 μm; (d) Wavelength of Light 1.74 μm.

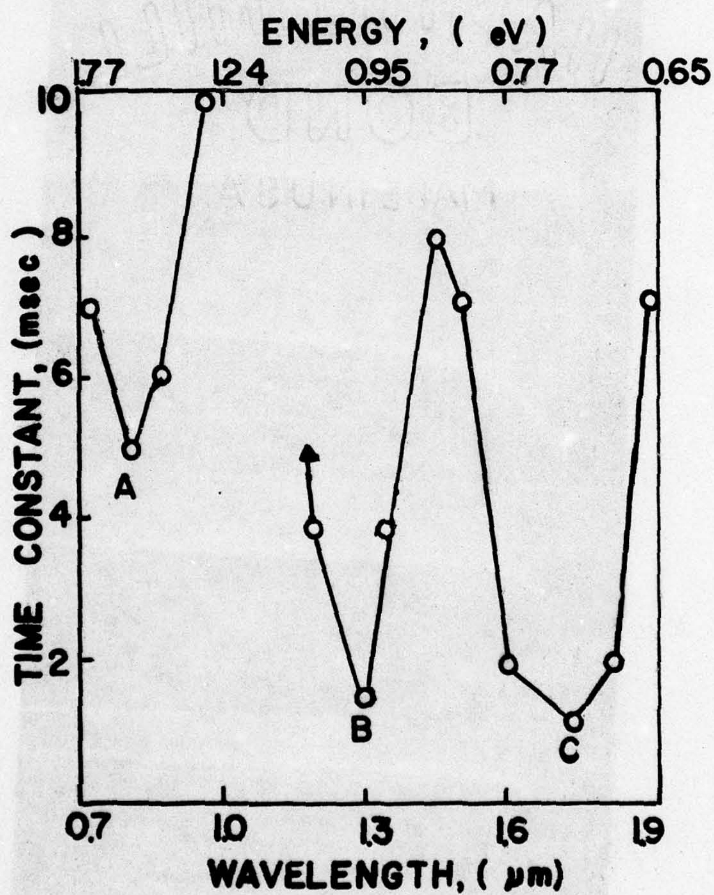

Fig. 4.14 Plot of the Time Constant Associated with the Return to Steady State in Delay Line Output for n on n^+ GaAs, as a Function of the Wavelength of Light. Peaks Labeled A, B, and C are at 0.86 μm, 1.3 μm, 1.74 μm.

while measuring the convolution voltage. Although the output port of the convolution voltage is the same as the input port for the external dc bias, it is easy to separate them due to the large difference in the frequency range. Whereas it is much more difficult to apply the dc bias while measuring the dc transverse acoustoelectric voltage.

The schematic of the experimental set-up for observing the spectral response of the convolution voltage is shown in Fig. 4.15. Adding the splitter to the system, results in the autoconvolution of the input modulations with twice the input frequency. Figure 4.16 is the spectral response of the delay line attenuation, acoustoelectric voltage, and the convolution voltage for Grade A CdS. All three parameters show maximum near the absorption edge, but it is observed that only the acoustoelectric voltage is sensitive enough to the subband-gap illumination. This is due to the difference in the output impedance of the measuring system. The acoustoelectric voltage is measured on 2 M-ohm output impedance, whereas the convolution voltage and the delay line attenuation have 50 ohm output impedance.

We can conclude that the transverse acoustoelectric voltage has the best sensitivity for detecting optical generation in a semiconductor. By applying an external dc bias to the SAW-semiconductor structure the transient delay line output also can be used with very good sensitivity to optical generation in a semiconductor.

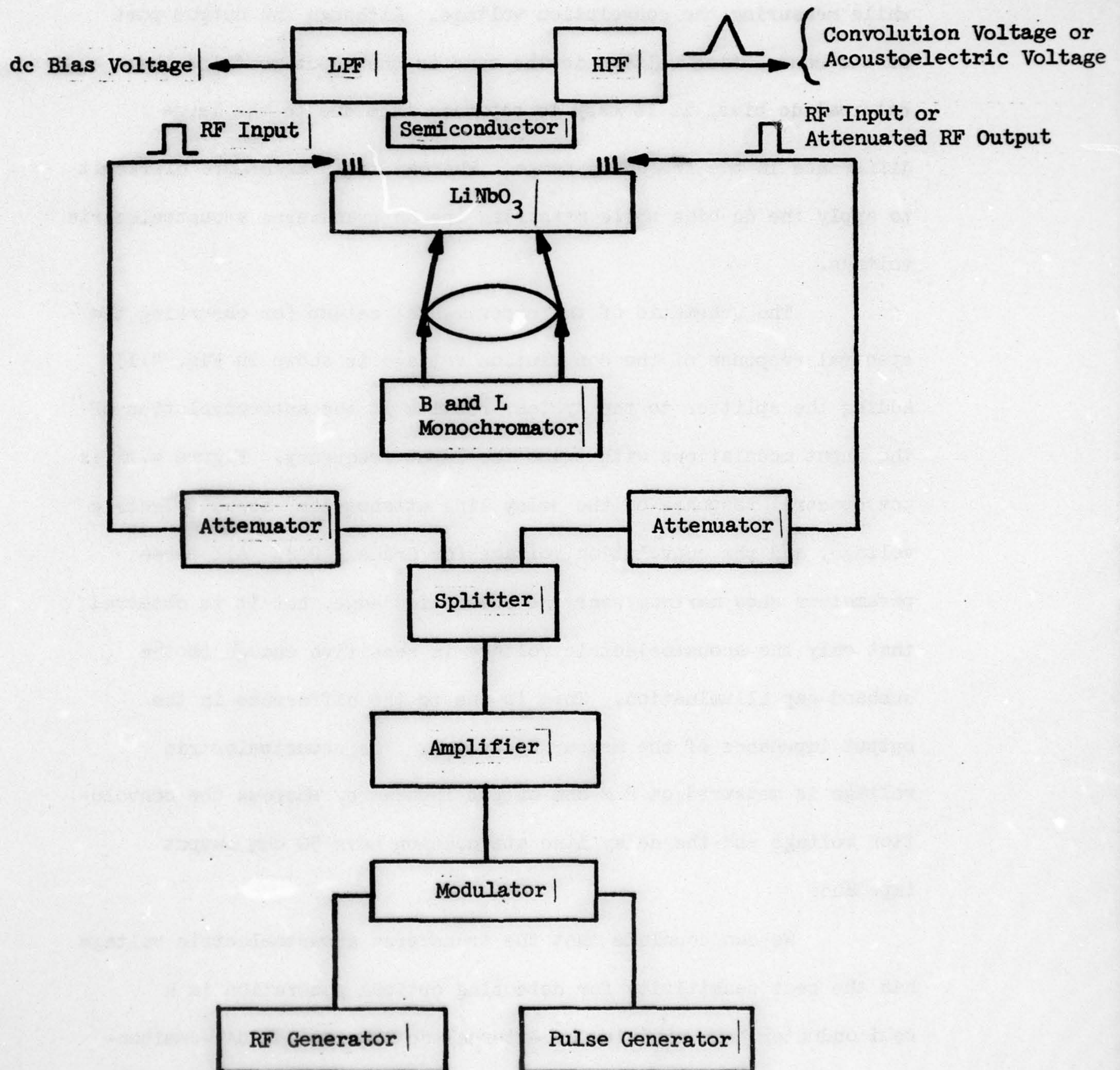

Fig. 4.15 Experimental Arrangement for Measuring the SAW Convolution, Transverse Acoustoelectric Voltage and Attenuation.

AD-A045 324 RENSSELAER POLYTECHNIC INST TROY NY MICROWAVE ACOUST--ETC F/G 20/12
NONDESTRUCTIVE EVALUATION OF ELECTRICAL PROPERTIES OF SEMICONDU--ETC(U)
JUL 77 H GILBOA, P DAS N00014-75-C-0772

UNCLASSIFIED RPI-MA-ONR-15 NL

3 OF 3
AD
A045 324

END
DATE
FILMED
11-77
DDC

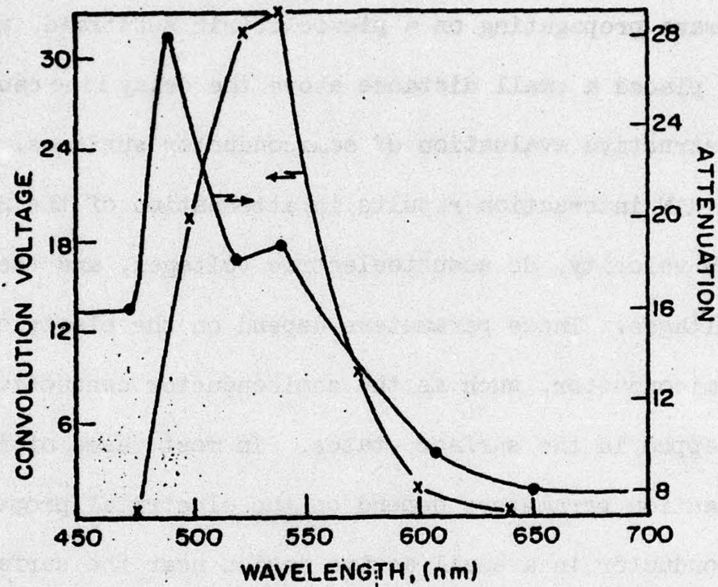

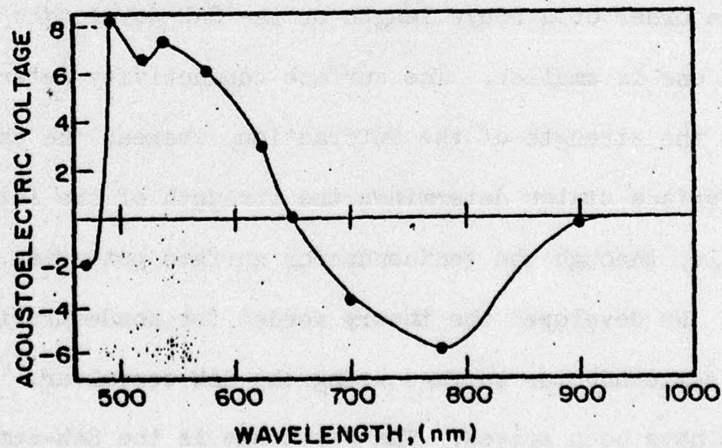

Fig. 4.16 The Spectral Response of (a) the Convolution Voltage, and SAW Attenuation; (b) the Peak Transverse Acoustoelectric Voltage. The Vertical scale is Normalized to the Radiant Flux Output of the Monochromator.

CHAPTER V

SUMMARY

The space charge coupled interaction between surface acoustic wave propagating on a piezoelectric substrate, and a semiconductor placed a small distance above the delay line can be used for nondestructive evaluation of semiconductor surfaces. The semiconductor-SAW interaction results in attenuation of the SAW, changes in the SAW velocity, dc acoustoelectric voltages, and the ac convolution voltages. These parameters depend on the electrical properties of the semiconductor, such as the semiconductor conductivity, and charge trapped in the surface states. In most cases of interest, the interaction parameters depend on the electrical properties of the semiconductor in a small active region near the surface, which is of the order of a Debye length or the SAW wavelength depending on which one is smaller. The surface conductivity determines directly the strength of the interaction, whereas the charge trapped in the surface states determines the strength of the interaction indirectly, through the semiconductor surface potential.

We developed the theory needed for nondestructive evaluation of semiconductor surface using the SAW convolver. Two main problems have been solved. The first one is the SAW-semiconductor interaction for high resistivity materials in near flatband condition (i.e., the carrier density near the semiconductor surface is considered constant and equal to the bulk density). For this case, majority and minority carrier interaction is considered. We have

shown that for the infinite thickness approximation ($d >> \lambda$, where d is the semiconductor thickness, and λ is the SAW wavelength) simple analytical expressions can be obtained for the propagation loss, change in SAW velocity, dc transverse acoustoelectric voltage, and convolution voltage. The analytical expressions are valid for frequencies smaller than 200 MHz and semiconductor resistivities smaller than 100 ohm-cm. For resistivities higher than 100 ohm-cm, the analytical expression becomes very complicated, especially if one considers the case where the surface recombination is not negligible. The carrier lifetime has to be considered only for those materials where the lifetime is very short compared to the SAW frequency. The surface recombination velocity in addition to its effect on the surface effective lifetime, determines the perpendicular current density on the semiconductor surface and for materials of very high surface recombination velocity (above 100 cm/sec) it reduces both the attenuation and the voltages developed in the semiconductor. For finite semiconductor thickness an exact numerical solution is used to obtain the SAW-semiconductor interaction parameters.

When the semiconductor is biased externally such that band bending occurs, and the semiconductor surface is in off flatband condition (i.e., the carrier density near the surface is not constant), the bulk conductivity is replaced by an effective surface conductivity. The effective surface conductivity for a known

semiconductor surface potential is found by averaging the excess carrier density over the space charge region, and multiplying it by the carrier surface mobility. In the case of depletion the space charge region is the depletion layer width, in the case of accumulation or inversion, the space charge region is equal to twice the center of mass defined by Equation (2.3-12). Computer plots of the SAW-semiconductor interaction parameter as a function of the semiconductor surface potential are shown. For the propagation loss and the convolution voltage we observe two maxima, one in the accumulation region, and the second in deep depletion. For the acousto-electric voltages, in addition to the two maxima, an inversion in the sign of the voltages is observed. The exact solution for the off flatband condition is also presented. The fourth-order linear differential equation with non-constant coefficient which is obtained, requires a very difficult numerical solution. However, it is clear that the exact solution should include the dc field caused by the band bending. For accumulation and shallow depletion, the average surface conductivity is a good approximation to the off flatband interaction.

The SAW convolver is used to determine the distribution of the density of surface states (cm^{-2} eV^{-1}), and majority carriers capture cross section (cm^2) in the energy gap. By applying an external dc bias across the semiconductor delay line structure, we can observe the transient response of the delay line output. This transient response is due to the relaxation of surface states which

result in a relaxation effect in the semiconductor surface conductance. The results obtained agree with the already known distribution of surface states in the energy gap; it is constant at the middle of the gap, and it increases toward the conduction band. The capture cross section is constant in the middle of the gap and it decreases toward the conduction band.

Photoconductivity measurements using the SAW convolver to monitor the semiconductor conductivity decay, after a flash of light is applied to the semiconductor, is also presented. For low-level generation we can assume that the delay line attenuation varies linearly with the semiconductor conductivity, hence the photoconductivity response time can be obtained by the delay line output decay. Experimental results of Si, CdS, GaAs are presented; their response times agree very well with the known lifetimes of these materials.

Semiconductor spectroscopy using the SAW convolver as a detector for optical absorption by a semiconductor is presented. In this case we use both the delay line attenuation and the transverse acoustoelectric voltage to monitor changes in the semiconductor conductivity, or the charge trapped in the surface states, due to optical excitaion. For GaAs we were able to detect two deep level surface states, and the absorption edge. For high resistivity CdS, the detection system is much more sensitive as we observed not only maxima and minima in the spectral response of the delay line attenuation and transverse acoustoelectric voltage, but in addition,

transverse acoustoelectric voltage inversion is obtained at certain photon energy.

In conclusion, this report presents the basic physical understanding for the SAW-semiconductor interaction, needed for non-destructive evaluation of semiconductor surfaces and demonstrates it by several experiments in which the SAW convolver is used to obtain electrical properties of semiconductor surfaces.

CHAPTER VI

REFERENCES

1. H. D. Nine, "Photosensitive Ultrasonic Attenuation in CdS," Phys. Rev. Letters, 4, 359-361 (1960).

2. A. R. Hutson, J. H. McFee, and D. L. White, "Ultrasonic Amplification in CdS," Phys. Rev. Letters, 7, 237-239 (1961).

3. A. R. Hutson and D. L. White, "Elastic Wave Propagation in Piezoelectric Semiconductor," J. of Appl. Phys., 33, 1, 40-47, (1962).

4. D. L. White, "Amplification of Ultrasonic Wave in Piezoelectric Semiconductor," J. of Appl. Phys., 33, 8, 2547-2554 (1962).

5. R. M. White and F. W. Voltmer, "Direct Piezoelectric Coupling to Surface Elastic Waves," Appl. Phys. Letters, 7, 314-316 (1965).

6. B. T. Khari-Yakub and G. S. Kino, "A Monolithic Zinc-Oxide-on-Silicon Convolver," Appl. Phys. Letters, 25, 188-190 (1974).

7. L. A. Coldren, "Effect of Bias Field in a Zinc-Oxide-on-Silicon Acoustic Convolver," Appl. Phys. Letters, 25, 473 (1974).

8. M. Lubkkala and P. Merilainen, "Image Scanning by Acousto-Electro-optic Interaction," Electronic Letters, 10, 6, 80-81 (1974).

9a. W. C. Wang, "Signal Generation via Nonlinear Interaction of Oppositely Directed Sonic Waves in Piezoelectric Semiconductor," Appl. Phys. Letters, 18, 337-338 (1971).

b. W. C. Wang and P. Das, "Surface Wave Convolution in Piezoelectric Semiconductors," Proc. IEEE, 60, 1109 (1972).

c. W. C. Wang, "Convolution of Surface Waves in a Structure of Semiconductor on $LiNbO_3$," Appl. Phys. Letters, 20, 15, 389-392 (1972).

10. T. Grudkowski and C. F. Quate, "Acoustic Readout of Charge Storage in GaAs," Appl. Phys. Letters, 25, 99-101 (1974).

11. J. J. Campbell and W. R. Jones, "A Method for Estimating Optimal Crystal Cuts and Propagation Directions for Excitation of Piezoelectric Surface Waves," IEEE Sonics and Ultrasonics, 15, 4, 209-217 (1968).

12. K. A. Ingebrigtsen, "Linear and Nonlinear Attenuation of Acoustic Surface Wave in a Piezoelectric Coated with a Semiconducting Film," J. of Appl. Phys., 41, 2, 454-459 (1970).

13. K. A. Ingebrigtsen, "Surface Wave in Piezoelectric," J. of Appl. Phys., 40, 7, 2681-2686 (1969).

14. K. M. Lakin and H. J. Shaw, "Surface Wave Delay Line Amplifiers," IEEE MTT-17, 11, 912-920 (1969).

15. K. M. Lakin, "Perturbation Theory for Electromagnetic Coupling to Elastic Surface Waves on Piezoelectric Substrates," J. Appl. Phys., 42, 3, 899-906 (1971).

16a. W. C. Wang and P. Das, "On the Theory of the Normal Component Separate Media Space Charge Charge Convolver," Proceedings of the IEEE, 61, p. 1054 (July 1973).

b. W. C. Wang and P. Das, "Surface Wave Convolver via Space Charge Nonlinearity," Proceedings of the IEEE Ultrasonics Symposium, p. 316 (1972).

17. M. Yamanishi and T. Kawamura, "Surface Wave Convolver and Correlator using Nonlinear Electron Interaction in Coupled Semiconductor Piezoelectric Systems," Supplement to the J. of Japan, Appl. Phys., 42 (1973).

18. G. S. Kino and T. M. Reeder, "A Normal Mode Theory for the Rayleigh Wave Amplifier," IEEE ED, 18, 10, 909-120 (1971).

19. W. W. Otto "Theory for Nonlinear Coupling between a Piezoelectric Surface and an Adjacent Semiconductor," J. of Appl. Phys., 45, 10 4373-4383 (1974).

20. S. Takada, K. Hok, H. Hayakawa, and N. Mikoshiba, "Controllable Nonlinear Interactions between Elastic Surface Waves and Carriers in Si-$LiNbO_3$ MIS Structure," Supplement to the J. of Japan Appl. Phys., 42, 21-29 (1973).

21a. G. S. Kino and H. Gautier, "Convolution and Parametric Interaction with Semiconductors," J. Appl. Phys., 44, 12 5219-5221 (1973).

b. H. Gautier and G. S. Kino, "A Detailed Theory of the Acoustic Wave Semiconductor Convolver," IEEE Sonic and Ultrasonic, 24, 1 23-33 (1977).

22. J. D. Maines and E. G. Paige, "Surface Acoustic Wave Devices for Signal Processing Applications," Proceedings of the IEEE, May 1976.

23. R. M. Hays and C. S. Hartman, "Surface Acoustic Wave Devices for Communications," Proceedings of the IEEE, May 1976.

24. C. F. Quate, "Optical Image Scanning with Acoustic Surface Wave," IEEE Trans. Sonics and Ultrasonics, SU-21, 283-288 (1974).

25. A. Bers and J. H. Cafarella, "Surface Wave Correlator-Convolver with Memory," 1974 Ultrasonics Symposium Proceedings.

26. H. Hayakawa and G. S. Kino, "Storage of Acoustic Signals in Surface State in Silicon," Appl. Phys. Letters, 25, 4, 178-180 (1974).

27. Ph. Defranould, H. Gautier, C. Maefeld and P. Tournois, "P-N Diode Memory Correlators," 1976 Ultrasonics Symposium Proceedings.

28. A. Bers, J. H. Cafarella and B. E. Burke, "Surface Mobility Measurement using Acoustic Surface Wave," Appl. Phys. Letters, 22, 8, 399-401 (1973).

29. P. Bierbaum, "Determination of Electron Mobilities in Thin Metal Film frcm the Attenuation of Elastic Surface Wave," J. Acoust. Soc. Am., 55, 4, 766-774 (1974).

30. T. C. Lim, T. Wolfram, E. A. Kraut, and S. K. Sinha, "Wavelength Dependence of the Photoenhancement of Nonlinear Surface Wave Convolution," Appl. Phys. Letters, 22, 8, 421-423 (1973).

31. T. C. Lim, E. A. Kraut, F. J. Morin, and J. R. Oliver, "Temperature and Wavelength Dependence of the Photoenhancement of Nonlinear Surface Wave Convolution," Appl. Phys. Letters, 29, 4, 229-231 (1976).

32. K. Hoh, H. Hayakawa, and N. Mikoshiba, "Photoenhancement of Surface Wave Convolution on GaAs," Japan J. of Appl. Phys., 13, 2, 363-364 (1974).

33. Z. Ueda, J. Shirafeiji, and Y. Inuishi, "Effect of Light Illumination on CdS-$LiNbO_3$ Convolver and Relation to the Photoconductivity Spectrum", Appl. Phys. Letters, 28, 8, 418-419 (1976)

34. T. Shiosaki, T. Kuroda, and A. Kawabata, "Application of Surface Waves to the Study of Semiconductor Surface State using the Separated Medium Acoustoelectric Effect," Appl. Phys. Letters, 26, 7, 360-362 (1975).

35. A. Many, Y. Goldstein and W. B. Grover, Semiconductor Surface, North Holland Publishing Co., 1965.

36. J. Bardeen, "Surface States and Rectification at a Metal Semiconductor Contact," Physical Review, 71, 10, 717-727 (1947).

37. W. Shockley and W. T. Read, Jr.,. "Statistics of the Recombination of Holes and Electrons," Physical Review, 87, 5, 835-843 (1952).

38. E. H. Nicollian and A. Goetzberger, "The Si-SiO_2 Electrical Properties as Determined by the Metal-Insulator Silicon Conductance Technique," Bell System Tech. J., 46, 1055 (1967).

39. P. V. Gray and D. M. Brown, "Density of SiO_2-Si Interface States," Appl. Phys. Letters, 8, 2, 31-33 (1966).

40. W. Fahrner and A. Goetzberger, "Energy Dependence of Electrical Properties of Interface States in Si-SiO_2 Interfaces," Appl. Phys. Letters, 17, 1, 16-18 (1970).

41. D. V. Lang, "Deep Level Transient Spectroscopy: A New Method to Characterize Traps in Semiconductors," J. of Appl. Phys., 45, 7, 3023-3032 (1974).

42. J. C. Carballes, J. Varon, and T. Ceva, "Capacitive Methods of Determination of the Energy Distribution of Electron Traps in Semiconductors," Solid State Commun., 9, 1627-1631 (1971).

43. C. T. Sah, W. W. Chan, H. S. Fu, and J. W. Walker, "Thermally Stimulated Capacitance (TSCAP) in p-n Junctions," Appl. Phys. Letters, 20, 193-195 (1972).

44. D. L. Losee, "Admittance Spectroscopy of Deep Impurity Levels: ZnTe Schottky Barriers," Appl. Phys. Letters, 21, 54- (1972).

45. H. Kukimoto, C. H. Henry and F. R. Merrit, "Photocapacitance Studies of the Oxygen Donor in GaP Capture Cross Sections," Physical Review, B7, 2499 (1973).

46. B. A. Auld, Acoustic Fields and Waves in Solids, John Wiley and Sons, New York, 1973.

47. A. J. Slobodnik, Jr., "Surface Acoustic Waves and SAW Materials," Proceedings of the IEEE, May 1976.

48. R. H. Kingston and S. F. Neustader, "Calculation of the Space Charge, Electric Field, and Free Carrier Concentration at the Surface of a Semiconductor," J. of Appl. Phys., 26, 2, 718-720 (1955).

49. H. C. Nathanson, C. Jund and J. Grosvalet, "Temperature Dependence of Apparent Threshold Voltage of Silicon MOS Transistors at Cryogenic Temperature," IEEE Trans. ED-15, 362-368 (1968).

50. M. R. Boudry, "Theoretical Origins of N_{ss} Peaks Observed in Gray-Brown MOS Studies," Appl. Phys. Letters, 22, 530-531 (1973).

51a. O. Madelung, Physics of III-V Compounds, John Wiley and Sons, New York, 1964.

b. H. Hilsum and C. B. Holeman, Proceedings of the International Conference on Semiconductors, Prague, Publishing House of the Czechoslovakian Academy of Science, p. 962.

52. L. Jastrzebski, H. C. Gatos, and J. Lagowski, "Observation of Surface Recombination Variations in GaAs Surfaces," J. of Appl. Phys., 48, 4, 1730-1731 (1977).

53. J. I. Pankove, Optical Processes in Semiconductors, Prentice-Hall, 1971.

54. T. S. Moss, G. J. Burrell, and E. Ellis, Semiconductor Opto-Electronics, John Wiley and Sons, New York, 1973.

55. H. Gilboa, M. E. Motamedi and P. Das, "Determination of Energy Band and Surface State Location in GaAs using the Separated Medium Surface Acoustoelectric Effect," Appl. Phys. Letters, 27, 12, 641-643 (1975).

56. F. Steinrisser and R. E. Hetrick, "Wwavelength Dependence of the Surface Photovoltage in Vacuum Cleaved CdS," Surface Science, 28, 607-620 (1971).

57. J. Logowski, C. L. Balestra and H. C. Gatos, "Photovoltage Inversion Effect and Its Application to Semiconductor Surface Studies," Surface Science, 27, 547-558 (1971).

58. R. H. Bube, "Surface Photoconductivity in Cadmium Sulfide Crystals," J. Chem Phys., 21, 1409 (1953).

59. J. Lagowski, I. Baltov and H. C. Gatos, "Surface Photovoltage Spectroscopy and Surface Piezoelectric Effect in GaAs," Surface Science, 40, 216-226 (1973).

60. Y. Fureikawa, "Trap Levels in Gallium Arsenide," Japan. J. of Appl. Phys., 6, 675-679 (1967).

61. P. Das, M. E. Motamedi, R. T. Webster, "Semiconductor Surface Study by Transverse Acousto-electric Voltage using Surface Acoustic Wave," Solid State Electronics, 19, pp. 121-123 (1976).

62. M. E. Motamedi, R. T. Webster and P. Das, "Application of SAW Delay Line Attenuation and Transverse Acoustoelectric Voltage for Determination of Semiconductor Surface Properties," 1975 IEEE Ultrasonics Symposium Proceedings, pp. 668-671.

63. H. Gilboa, M. E. Motamedi and P. Das, "Study of GaAs Epitaxial Layer using the Separated Medium Acousto-electric Effects," 1975 IEEE Ultrasonics Symposium, pp. 663-667.

64. P. Das, M. E. Motamedi, H. Gilboa and R. T. Webster, "Determination of Electrical Surface Properties of Si, GaAs and CdS using Acoustic Surface Wave," J. Vacuum Science and Tech., 13, pp. 948-953 (1976).

65a. P. Das and H. Gilboa, "CdS Surface Study using Acoustic Surface Wave," APS Meeting, Atlanta, Georgia, March 1976.

b. Abstract of above-mentioned paper published in Bull. Am. Phys. Soc., Series II, 21, p. 342 (1976).

66. H. Gilboa and P. Das, "Semiconductor Surface Spectroscopy using Acoustic Surface Wave," presented at the International Conference on Recent Developments in Optical Spectroscopy of Solids, Taormina, Italy, September 1976.

67. M. E. Motamedi and P. Das, "Study of Ion-Implanted Silicon Surface using Acousto-electric Voltage," presented at the 1976 Ultrasonics Symposium, Annapolis, Maryland, September, October 1976.

68a. H. Gilboa and P. Das, "Semiconductor Surface State Time Constant Study using SAW Interaction," APS Meeting, San Diego, California, March 1977.

b. Abstract of the above-mentioned paper published in Bull. Am. Phys. Soc., Series II, 22, 3, p. 365 (1977).

69. H. Gilboa and P. Das, "Transverse Acoustoelectric Voltage Inversion and its Application to Semiconductor Surface Study: CdS," Surface Science, 62, 536-550 (1977).

70. M. E. Motamedi and P. Das, "Study of Semiconductor Surface Space Charge Layer using SAW Convolver," IEEE Trans. Sonics and Ultrasonics, to be published.

71. M. E. Nokali and E. L. Adler, "A Simplified Theory for Semiconductor Coupled Surface Wave Convolver," IEEE Sonics and Ultrasonics, 24, 3, 218-221 (1977).

72. P. Das, M. N. Araghi and W. C. Wang, "Convolution of Signals using Surface Wave Delay Lines," Appl. Phys. Letters, 21, p. 152 (1972).

73. R. H. Bube, Photoconductivity in Solids, John Wiley and Sons, New York, 1960.

74. A. G. Milnes, Deep Impurity in Semiconductors, John Wiley and Sons, New York, 1973.